Topology study for an inductive power transmitter in cordless kitchen system

Mahesh Itraj

Master of Science Thesis

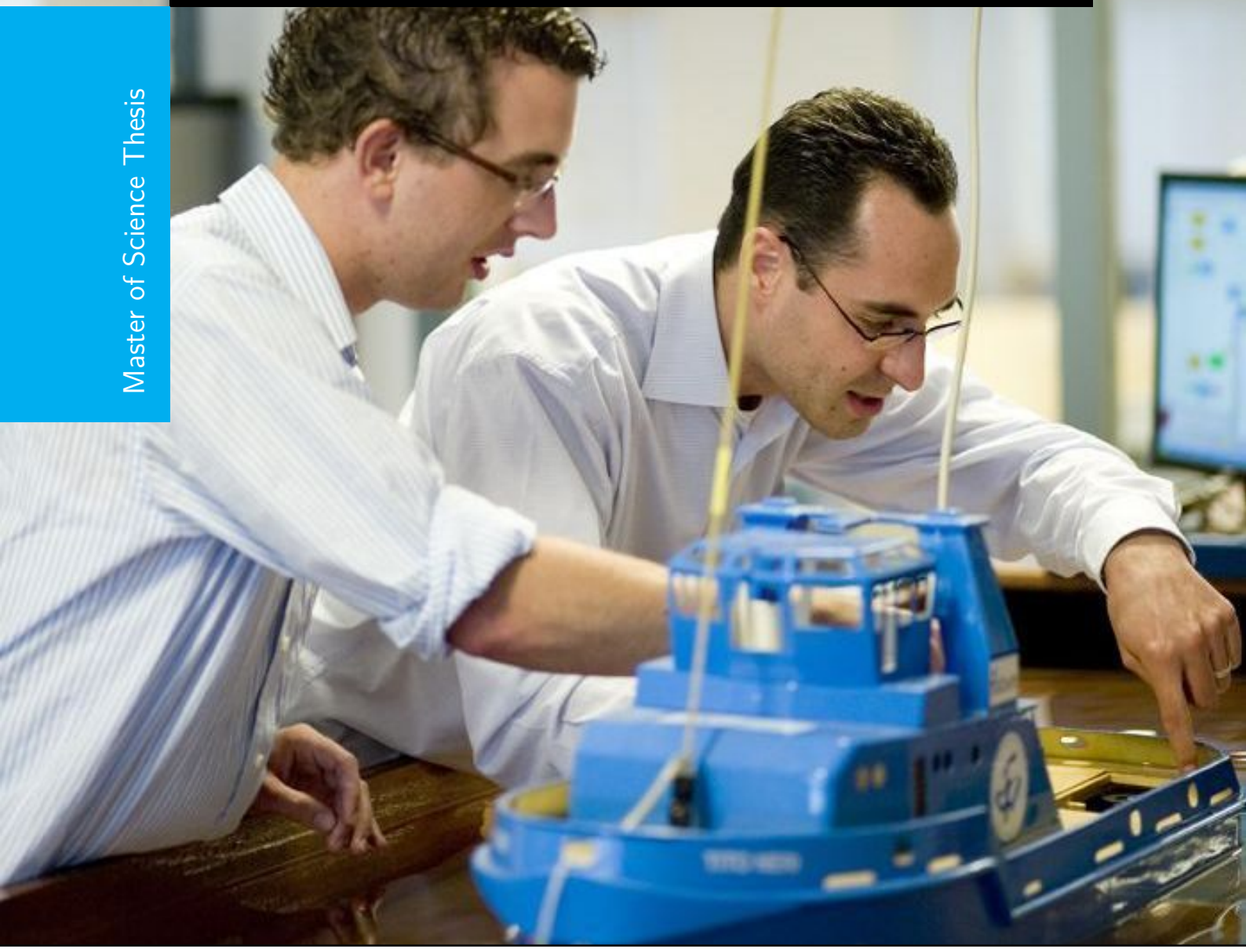

TU Delft Delft University of Technology

DC systems, Energy conversion & Storage

Topology study for an inductive power transmitter in cordless kitchen system

Master of Science Thesis

For the degree of Master of Science in Electrical Power Engineering at Delft University of Technology

Mahesh Itraj

26^{th} July 2017

Faculty of Electrical Engineering, Mathematics and Computer Science (EEMCS) · Delft University of Technology

Delft University of Technology
Department of
DC systems, Energy conversion & Storage (dces)

The undersigned hereby certify that they have read and recommend to the Faculty of Electrical Engineering, Mathematics and Computer Science (EEMCS) for acceptance a thesis entitled

Topology study for an inductive power transmitter in cordless kitchen system

by

Mahesh Itraj

in partial fulfillment of the requirements for the degree of

Master of Science Electrical Power Engineering

Dated: 26^{th} July 2017

Supervisor(s):

Prof.Dr.ir. J.A. Ferreira

Ing. Will Ettes

Reader(s):

Dr. J. Dong

Dr.ir. M. Cvetkovic

Abstract

In a cordless kitchen system, the appliances do not make use of a power cord. The system consists of a power channel and a communication channel. There are various resonant topologies which can be implemented in the power channel[9]. The chosen topology should meet the functional as well as non-functional requirements of the system. Presently, a series resonant topology is used in the system. The topology is easy to understand, to implement and could meet the functional requirements like the amount of power and high efficiency of the system easily. But, it is difficult to meet the non-functional requirements like overvoltage protection, EMI and simple control of the system. This master's thesis is mainly focused on design and realization an inductive power transmitter which addresses the following research questions:

- EMI: The present inductive power transmitter is based on a series resonant inverter which has a disadvantage of high dV/dt's across the inverter bridge and the transmitter coil. Furthermore, ZVS of the power switches can be lost at low duty cycles or low loads. Both mechanisms causes high dV/dt's in the system, which results in increase in common mode noise problems.
- Overvoltage: The present series resonant topology with the calculated circuit components and given load conditions (coupling factor (k) and load resistance (R_L)), is observed to be operating in the capacitive mode of operation, when the load is disconnected/removed. Therefore, disconnection of the load causes overvoltage on the transmitter as well as the receiver coil. The overvoltage, in the absence of 'expensive' protective means, can damage the system components and the system may fail to operate.
- Simple control: The present system is a 4^{th} order system. Due to weak coupling between the transmitter and the receiver coils, there exists multiple operating points where the voltage gain is the same. Therefore, it is difficult to find an optimal operating point for the control loop. Also, as mentioned in previous point, the load disconnection results in capacitive mode of operation of the system. To protect the system the control loop should take care that the system operates in the desired inductive mode of operation, as fast as possible and without causing significant losses.

Table of Contents

List of Figures

List of Tables

Preface

In July 2016, I started working in Philips Consumer Lifestyle B.V., Drachten, as an intern. During first three months I did my internship and later on I started with my master's thesis. A few things which inspired me to continue my master's thesis in the same organisation are: deep technical knowledge, friendly nature, result oriented approach and independent working.

The master's thesis and hence this report is all about the cordless kitchen system. The power transfer in a cordless kitchen system is done with the help of an inductive power system, consisting of an inductive power transmitter and an inductive power receiver. Philips has already built a demo inductive power system which can meet the functional requirements of the system (like the amount of power transferred and high efficiency) but the system requires, expensive means to meet the non-functional requirements (like EMI, over voltage protection, simplicity in control etc.). The thesis describes the problems associated with the present demo system and suggests an alternative topology for the inductive power transmitter which can meet the functional as well as the non-functional requirements of the system. A new demo model with the new transmitter topology is analyzed, simulated and proven to be a possible alternative to the present transmitter.

During my one year in Philips Consumer Lifestyle B.V., I have received an enormous amount of support from number of people. I would especially thank my supervisors, Mr. Will Ettes and Prof. J.A. Ferreira for being a continuous source of motivation and support. I would like to thank Mr. Will Ettes and the whole cordless kitchen team for believing in me and giving this opportunity. I would also like to thank the whole Technical Expert Group (TEG) of Philips, Drachten, for providing me a friendly environment and all kinds of help, if needed. Last but not the least, I would like to express my gratitude towards my family in India and The Netherlands who are my inner strength. Thank you!

The report proceeds with an introduction about the cordless kitchen project. It is followed by the description and the analysis of the present system. Next, the detailed analysis of other possible topologies and selection of the alternative topology is described. It is followed by the description about the new proposed model. The report concludes with the conclusion and a paper publication. The paper is published during the Wireless Power Congress arranged by WEKA FACHMEDIEN GmbH in July-2017.

Mahesh Itraj
Drachten, July 2017

Chapter 1

Introduction

The Wireless Power Consortium (WPC) develops standards for the appliances and devices which make use of the cordless power transfer. The development of the Qi standard for the cordless mobile charging system has been already developed and implemented in practice. A cordless kitchen system is one of the projects for which the standardization development is in progress. As an active member of the WPC and a consumer appliance developer, Philips is also working on the standardization process of the cordless kitchen system. A cordless kitchen system operates with the help of an inductive power transfer system. It is based on the operating principle of an inductive coupler. An alternating current flowing through a coil produces its own alternating magnetic field. If another coil is placed near the first one then this alternating magnetic field gets linked to it. It induces a voltage at the terminals of the second coil. Such an arrangement of coils is called as an inductive coupler. The inductive coupler in a cordless kitchen system consists of a transmitter coil and a mutually coupled receiver coil. The transmitter coil is situated beneath the counter-top of the kitchen table whereas the receiver coil is situated in the appliance itself, as shown in Figure 1-1.

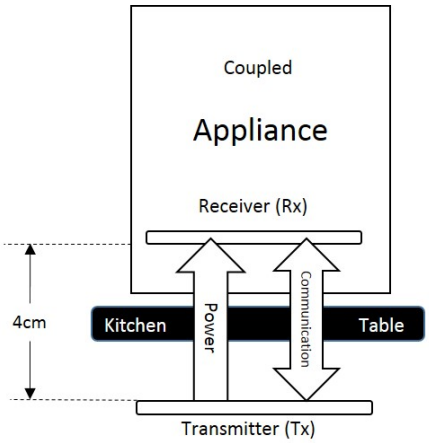

Figure 1-1: Introduction to the cordless kitchen appliance

The transmitter coil and the receiver coil along with the power processing units (AC-AC or AC-DC conversion stages) forms the power channel of the cordless kitchen system. The power has to be transferred from the transmitter side to the receiver side at a coil to coil distance of 4 cm, with high efficiency. The resonance principle is used to achieve maximum power transfer efficiency. Next to the power channel, the system is also equipped with a bidirectional communication channel. The transmitter needs to provide only the requested amount of power to the load. Therefore, the communication channel offers a mean to communicate between the transmitter and the receiver. It is based on the operating principle of the near field communication (NFC). The information such as the type of appliance, required amount of power can be exchanged via the communication channel. The basic operation of the cordless kitchen system can be explained with the help of a flowchart as shown in the Appendix A-1.

As the transmitter is powered, it goes into 'low power ping' mode. In this mode, the transmitter checks for the presence of a receiver on the kitchen table top. If a receiver is detected, the communication channel is turned ON and the information exchange takes place. During this interval, information about receiver type, amount of power required is exchanged between the transmitter and the receiver. If a request for power transfer is sent from the receiver to the transmitter then the power channel is turned ON and power transfer (over 2.4kW) from the transmitter to the receiver can take place. If the receiver does not send a request for the power transfer then the communication channel is turned OFF and the transmitter goes back to low power ping mode.

1-1 Cordless power technologies

There are two types of operating principles for the power channel: Inductive Power Transfer (IPT) and Induction Heating (IH). An appliance equipped with a motor or a resistive heating element operates according to the IPT principle. A food processor or a hot air oven are good examples of the appliances operating according to the IPT. On the other hand, an appliance equipped with a metal pan sole where the eddy currents are used to heat the appliance, operates on the IH principle. A simple rice cookware is a good example of an appliance operating on the IH principle. The block diagrams for the IPT and the IH are shown in Figure 1-2 and Figure 1-3, respectively.

1-1-1 Inductive Power Transfer

From Figure 1-2 one can observe that for the appliances operating on IPT principle, the power channel consists of an AC-AC conversion stage, a resonant inductive coupler, an optional AC-DC conversion stage and a load. The AC-AC conversion stage consists of a full bridge diode rectifier and a full bridge IGBT inverter. This stage converts the mains voltage (V_{mains}) to a high frequency AC voltage ($V_{ac_{HF}}$). The resonant inductive coupler consists of a resonant tank on the transmitter side, a transmitter coil, a mutually coupled receiver coil and another resonant tank at the receiver side. The transmitter side is usually equipped with two coils. According to the power requirements, only one or both of the coils can be energized. The coupling factor (k) between the transmitter and the receiver coils varies from 0.25 to 0.35. Further the AC-DC conversion stage comprising of a full bridge fast reverse recovery diode rectifier can be used to convert the high frequency AC to DC voltage (V_{load}). In the appliances

which are equipped with a motor, the AC-DC conversion stage is always present. Some appliances which are equipped only with a resistive heating element, as shown in Figure 1-7, may not require this stage.

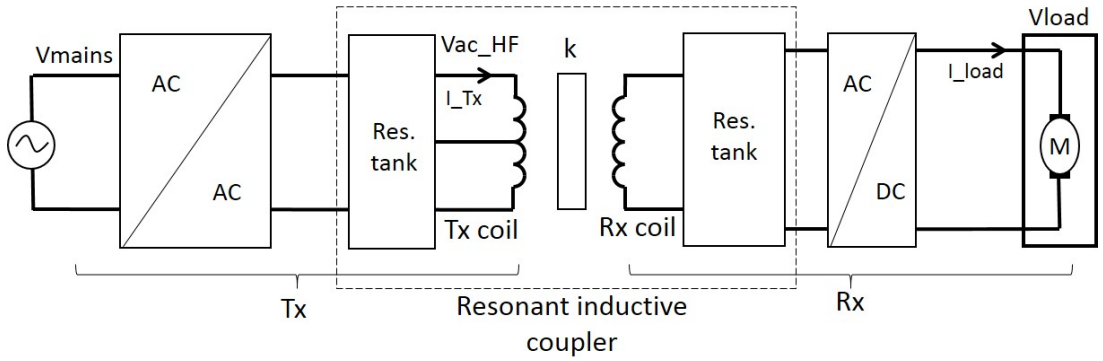

Figure 1-2: Block diagram of the power channel operating on Inductive Power Transfer (IPT)

1-1-2 Induction Heating

From Figure 1-3 one can observe that for the appliances operating according to the IH principle, the transmitter side remains the same. The receiver side consists of an metal pan sole as a load. An IH appliance makes use of the eddy currents to produce the heat required to cook the food. The coupling factor between transmitter and the metal pan sole (receiver coil) varies from 0.1 to 0.15. Therefore, a repeater coil is placed in between the transmitter coil and the metal pan sole. A repeater coil acts like a magnetic lens. It improves the effective coupling factor and therefore, improves the efficiency of the power transfer. Though the repeater circuit is placed in between the transmitter and metal pan sole, it is beneficial to place it in the appliance, close to the metal pan sole. The position of repeater coil can be optimized with the help of mathematical and experimental analysis[5][7].

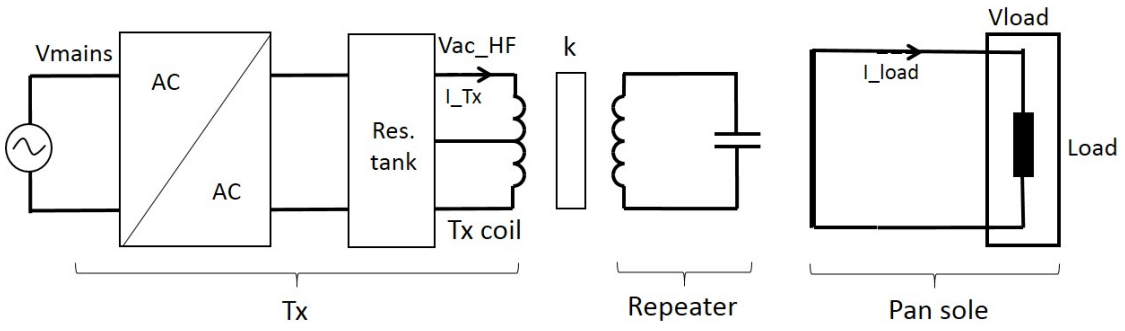

Figure 1-3: Block diagram of the power channel operating on Induction Heating (IH)

1-2 Generic architecture for cordless kitchen system-IPT

As mentioned earlier, next to the power channel the cordless kitchen system is equipped with the communication channel. As shown in Figure 1-2, for the power transfer a Tx coil and a mutually coupled Rx coil are in place. Similarly, for the communication there is a separate Tx coil and a separate mutually coupled Rx coil. Therefore, a generic architecture for the cordless kitchen system operating on the IPT principle can be represented as shown in Figure 1-4. The control units along with the communication coils forms an outer feedback loop. It can be observed from Figure 1-4 that the operation of the power channel can influence the operation of the communication channel. Therefore, to avoid the interference between the two channels, Time Division Multiplexing (TDM) technique is used [Appendix A-5].

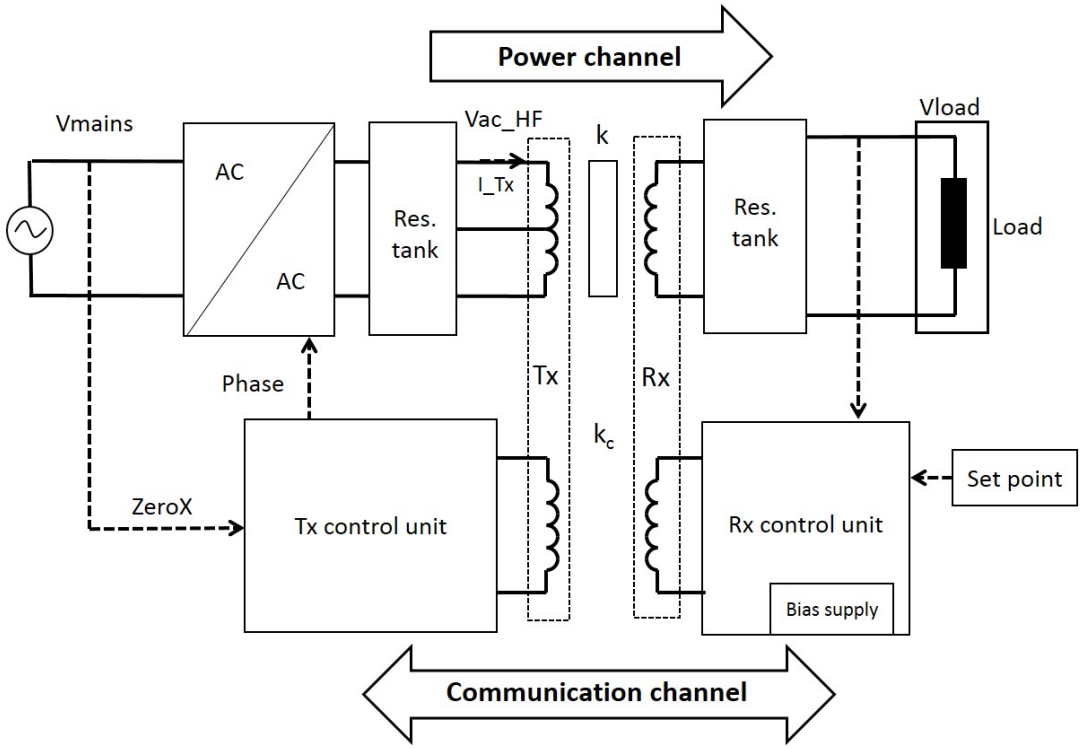

Figure 1-4: Generic architecture of cordless kitchen system- IPT

1-3 Simplified block diagrams for IPT

As explained in the previous section, both the power channel and the communication channel are the essential parts of the cordless kitchen system. Though both the channels are important, this thesis is dedicated to the power channel operating on the IPT principle. Therefore, in this section an attempt is made to understand the behaviour of the system on different loads and to derive the simplified block diagrams for the IPT power channel. As mentioned earlier, with IPT the load can be a motor or a simple resistive heating element. In case of a motor as the load, the load appears to be disconnected for some period of time. Figure 1-5 explains the load disconnection of a motor load with the help of conceptual diagram.

Figure 1-5a shows the ideal output voltage of the AC-DC conversion stage on the receiver side. However, when a motor is connected as a load, a back EMF (E_b) is developed in steady state as shown in Figure 1-5a. When the back EMF (E_b) is equal or higher than the output voltage of the AC-DC conversion stage (V_{load}), the current cannot flow through the receiver (Rx) and the load appears to be disconnected as shown in Figure 1-5c.

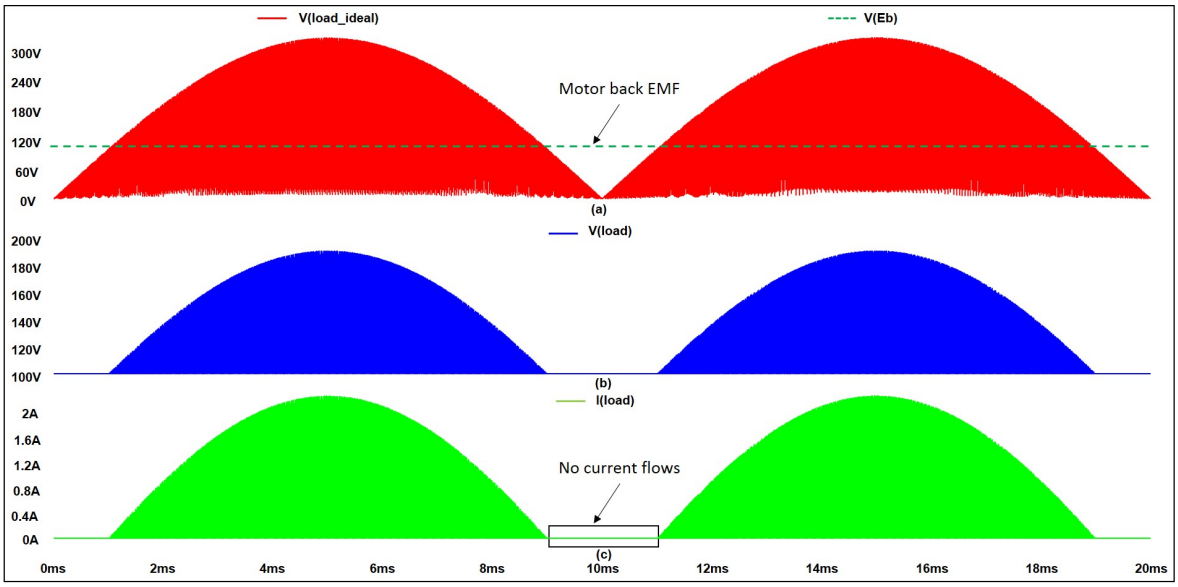

Figure 1-5: Conceptual representation of a motor load disconnection

Similarly, in case of a resistive heating element as the load, a temperature sensitive switch might be employed to control the heat produced in the appliance. When the switch is opened, the current cannot flow through the receiver (Rx). Thus, the reduced block diagrams from Figure 1-2 can be derived, as shown in Figure 1-6 and Figure 1-7.

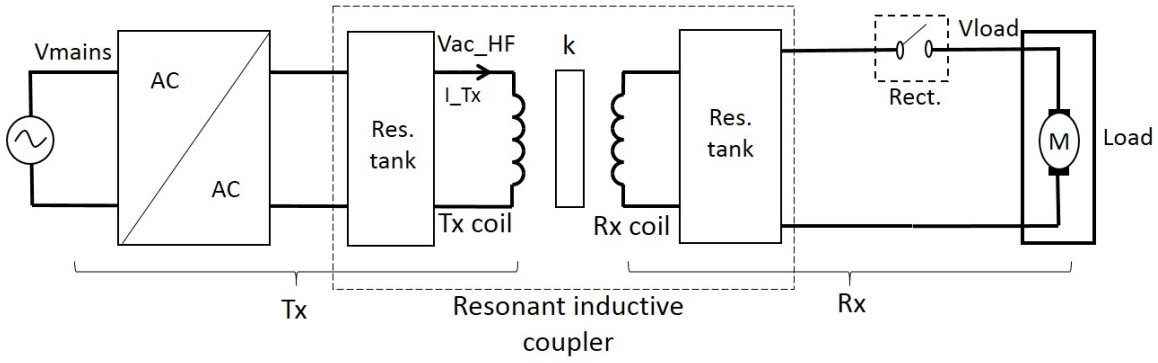

Figure 1-6: Simplified block diagram for IPT with motor

One can use these simplified block diagrams as a base for further detailed studies.

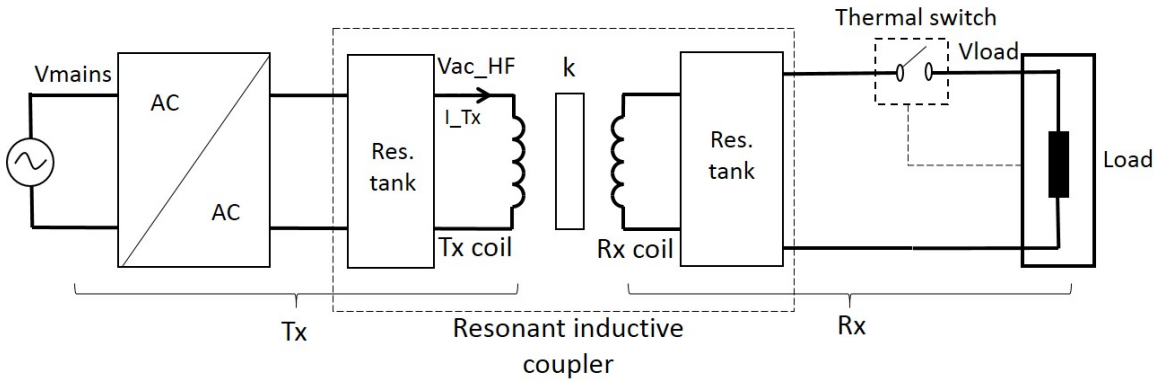

Figure 1-7: Simplified block diagram for IPT with resistor

Conclusion

This chapter provided an overview of the cordless kitchen system. An introduction to the power channel and the communication channel between the transmitter and the receiver is given. The chapter explained different operating principles of the power channel with the help of the block diagrams. These block diagrams are used as base to investigate different topologies for the cordless kitchen system. Present choice for the cordless kitchen system topology is described in the next chapter.

Chapter 2

Description of the present topology

2-1 Introduction

There are various resonant topologies which can meet the functional requirements of the system[9]. Amongst all the resonant topologies, the series resonant topology is the first choice for the designers because it is easy to understand and to implement. Figure 2-1 shows the present topology of the cordless kitchen system. It can be observed that the series resonance principle is used on the transmitter as well as on the receiver side.

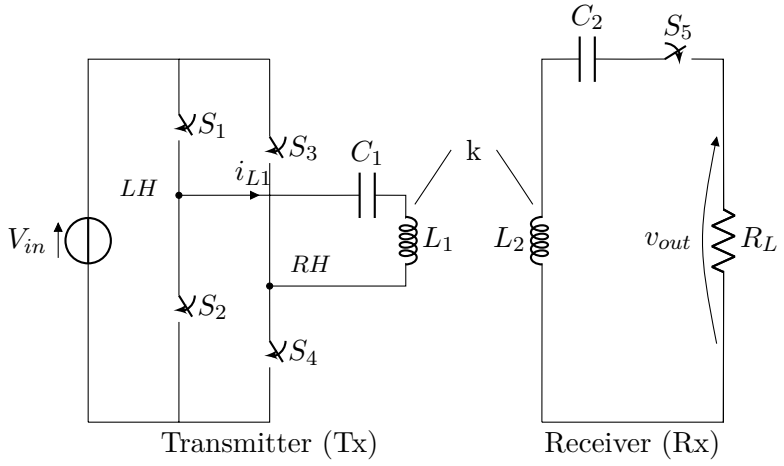

Figure 2-1: Series resonant topology

From Figure 2-1 it can be seen that a transmitter (Tx) consists of a voltage source (V_{in}) representing the rectified mains voltage, an inverter stage consisting of four power switches (S_1 to S_4), a transmitter coil (L_1) and a capacitor (C_1) connected in series with each other. On the other hand, a receiver (Rx) consists of a receiver coil (L_2), a capacitor (C_2) and a load (R_L) connected in series. The switch S_5 represent the AC-DC conversion stage or

the temperature sensitive switch as explained in previous chapter. The transmitter coil (L_1) and the receiver coil (L_2) are coupled to each other with the coupling factor (k). If the transmitter (Tx) is powered in the absence of the transmitter, it has its natural resonant frequency (f_{tx}). Similarly, in the absence of the coupling (k), the receiver (Rx) has its natural resonant frequency (f_{rx}). In practice, the f_{tx} and f_{rx} are chosen to be equal [3] and the coupling factor (k) is in the order of 0.3 to 0.35. Thus, the whole inductive power system has its natural resonant frequency or frequencies (f_{res}). The behaviour of such a coupled circuit is highly dependent on the coupling factor. For low coupling factors the f_{tx} and f_{rx} are merged into a single resonant frequency f_{res}. For higher coupling factors the f_{tx} and f_{rx} frequencies are moved away from each other, resulting in f_{res1} and f_{res2}[6]. With the help of frequency domain simulation of the circuit shown in Figure 2-3, effect of coupling factor on the resonant frequency of the system can be explained as shown in Figure 2-2.

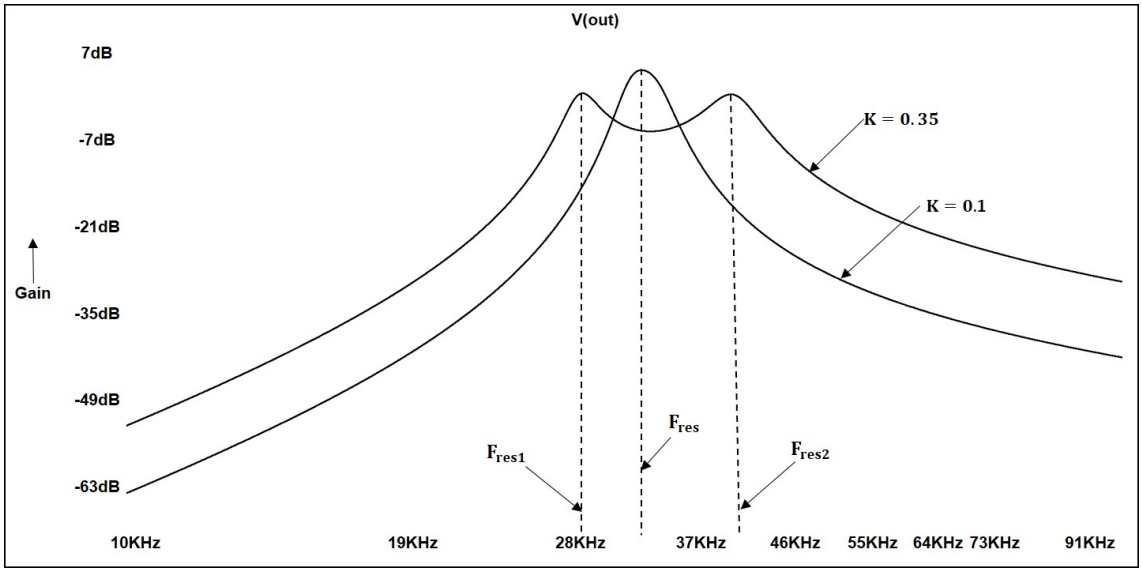

Figure 2-2: Effect of coupling factor (K) on resonance frequency of the system for L_1=L_2=290uH, C_1=C_2=80nF, R_L= 10Ω, K=0.35 and 0.1, $V_{ac} = 1V$

The inverter stage of the transmitter can be operated at different operating points (f_{op}). Choosing the optimal f_{op} for the inverter is an important task because the high frequency AC voltage is applied to the transmitter coil with the help of the power switches. Thus, one has to make sure that Zero Voltage Switching (ZVS) of the power switches is applied, avoiding high dV/dt's in the inverter stage. For the particular values of the circuit components one can determine the optimal operating frequency for the inverter stage of the transmitter with the help of the mathematical analysis as shown in Appendix A-2 and Appendix A-4. The conditions for the optimal operating point are:

- Inductive mode of operation: To make sure that Zero Voltage Switching (ZVS) for the power switches is applied, it is always desired to operate the system in the inductive mode of operation. Inductive mode of operation implies that the phase of the input current (I_{L1}) should be slightly negative with respect to inverter bridge voltage.
- Maximum output power: The operating point should be chosen such that the output power gain is maximum at that point.

- Maximum efficiency: The operating point should be chosen such that the efficiency of the system is maximum at that point.

The details about the optimal operating point (f_{op}) are mentioned in the next section.

The cordless kitchen system control loop consists of two kinds of controls: a frequency control and a duty cycle (D) control. The frequency control is used to vary the f_{op} to achieve the maximum efficiency for the power transfer. The duty cycle control is used to vary the amount of power transferred to the receiver side, at a particular f_{op}.

2-2 Mathematical analysis

The mathematical analysis along with time domain and frequency domain simulations of the series resonant topology is discussed in this section. The mathematical analysis can be used to derive the different transfer functions. The frequency domain simulations can be used to observe the bode plots of important parameters like impedance, input voltage (or current), output voltage (or current), etc. The time domain simulations can be used to observe the instantaneous voltages across and current through the different circuit components. To proceed with the analysis following (realistic) values are chosen:

- $f_{tx} = f_{rx} = 33$ kHz
- $L_1 = 290$ uH
- $L_2 = 290$ uH
- $C_1 = 1/(4\pi^2 f_{tx}^2 L_1)$ F
- $C_2 = 1/(4\pi^2 f_{rx}^2 L_2)$ F
- $k = 0.35$
- $M = k\sqrt[2]{L_1 L_2}$ H
- $R_1 = R_2 = 50$ mΩ
- $R_L = 10\ \Omega$
- $V_{in} = 325$ V DC (for time domain)
- $V_{ac} = 1$ V AC (for frequency domain)

From Figure 2-1, a simplified equivalent circuit can be derived for the mathematical analysis as shown in Figure 2-3.

In the circuit shown in Figure 2-3, R_1 represents the equivalent series resistance of the transmitter along with the reflected equivalent series resistance of the receiver. R_2 represents the load resistance. V_{12} represents the voltage induced in the transmitter coil (L_1) due to the

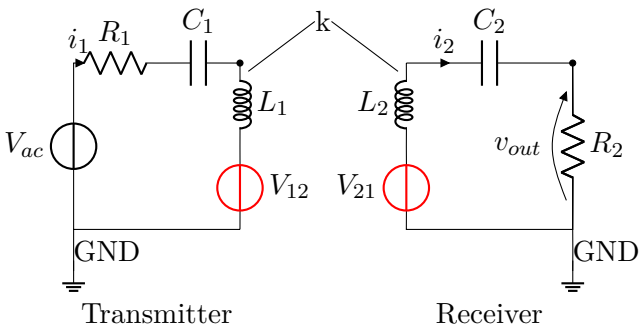

Figure 2-3: Simplified equivalent circuit of present topology

mutual inductance (say, M) and the current flowing through the receiver coil (i_2). V_{21} represents the voltage induced in the receiver coil (L_2) due to the mutual inductance and current flowing through the transmitter coil (i_1).

$$\frac{V_{out}}{V_{ac}} = \frac{s^3(C_1C_2MR_2)}{s^4(L_1L_2C_1C_2 - M^2C_1C_2) + s^3(R_2L_1C_1C_2 + R_1L_2C_1C_2) + s^2(L_2C_2 + L_1C_1 + R_1R_2C_1C_2) + s(R_1C_1 + R_2C_2) + 1} \tag{2-1}$$

With the help of Laplace transform and transformer theory, the voltage transfer function can be derived [Appendix A-2]. Similarly, one can also derive the current transfer functions [Appendix A-4]. From the Equation 2-1, it should be noted that the order of characteristic equation (denominator) is four. Consequently, it is called as 4^{th} order system. With the help of the derived transfer function, frequency domain simulations can be performed. Figure 2-4a shows the bode plot for the power delivered to R_2 whereas, Figure 2-4b shows the variation of the efficiency w.r.t. operating frequency. Figure 2-4a shows two resonant peaks. Thus, the transmitter can be operated at, or near two resonant frequencies for the maximum power transfer. There are two falling edges and two rising edges. The frequency control loop can operate either on the falling edge or on the rising edge. In any case, there are two operating points at which the gain is the same but the efficiency can be different.

One can also plot the efficiency variation of the system with respect to operating frequency. A simple equation for the efficiency of the system can be derived as shown in Equation 2-2 [Appendix A-4] and can be plotted as shown in Figure 2-4b.

$$\eta = \frac{P_L}{P_P} \tag{2-2}$$

From the marked crosses in Figure 2-4, it can be seen that the maximum power transfer operating point does not match the maximum efficiency operating point. The maximum efficiency point lies in between the two resonant peaks. With the given load conditions and the coupling factor, one can observe that maximum efficiency and maximum power gain occurs at different frequencies, as shown in Figure 2-4. Therefore, choosing the optimal operating point is comparatively harder.

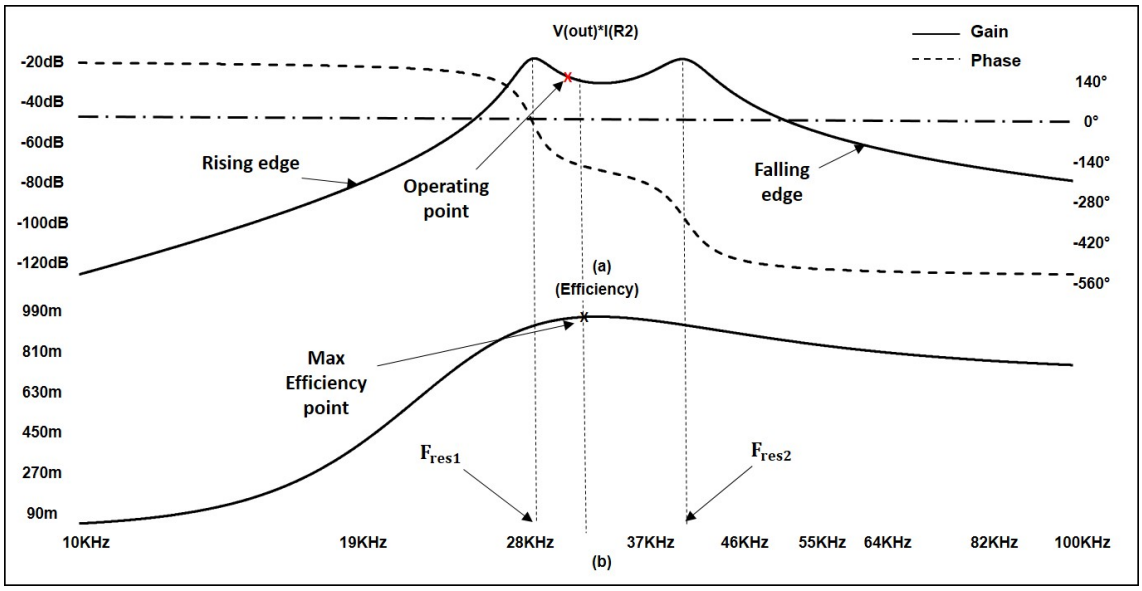

Figure 2-4: Relation between output power and efficiency of power channel

2-3 Time domain simulations

For this topology and the calculated values of circuit components, the optimal operating point (f_{op}) can be calculated to be 32.7kHz[2] and the frequency control loop operates on the falling edge of the power gain plot. To check the voltage at different circuit nodes and current through the circuit components at the calculated f_{op}, the time domain simulations of the circuit shown in Figure 2-1 can be performed.

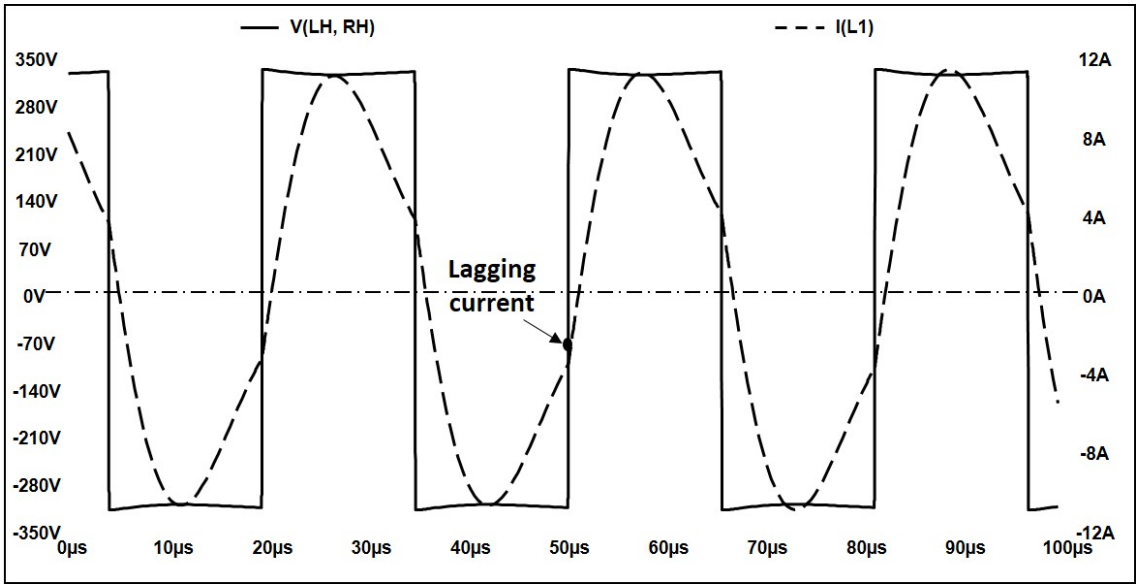

Figure 2-5: Operation of the system at the calculated f_{op}, D=100%

Figure 2-5 shows the voltage across the inverter stage of the transmitter (V(LH,RH)) and the input current (I(L_1)). The lagging current indicates the power channel operating in inductive mode. As mentioned earlier, the inductive mode of operation is always preferred to get the advantage of Zero Voltage Switching (ZVS) of the power switches. The ZVS of the power switches improves the efficiency of the system by reducing the switching losses. Due to ZVS the voltage across the switches rises steadily, (i.e. no high dV/dt's) minimizing the EMI problem. As mentioned earlier, at particular f_{op} the duty cycle (D) control is used to control the power delivered to the load. Figure 2-5 shows the waveforms for D=100%. Figure 2-6 shows the same waveforms but at D=50%. It can be observed from Figure 2-5 and Figure 2-6 that, introduction of duty cycle control results in loss of ZVS. The loss of ZVS causes high dV/dt on the corresponding node. The detailed description of ZVS technique and loss of ZVS at low duty cycles is given in Appendix A-9. Figure 2-7 shows the voltage across the

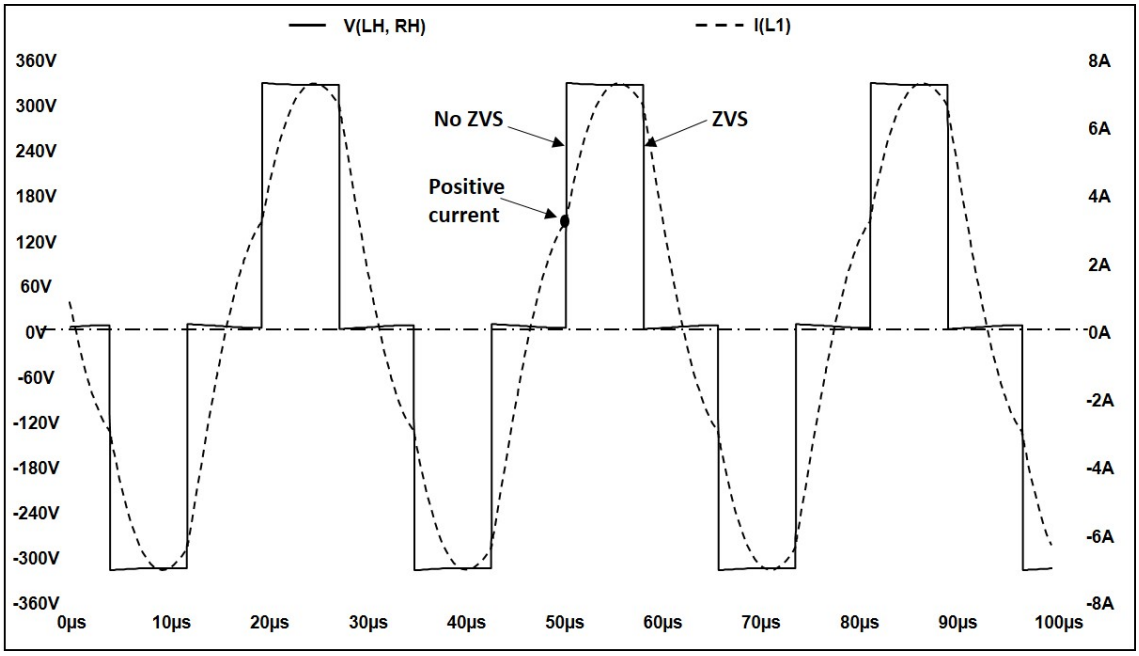

Figure 2-6: Operation of the system at the calculated f_{op}, D=50%

transmitter coil, when $f_{op}<f_{res1}$, $f_{op}=f_{res1}$ and $f_{op}>f_{res1}$. It can be clearly noted that high dV/dt's are observed in all the three cases.

These high dV/dt's can create a changing electric field between the electric node which carries the dV/dt and the surrounding conducting components, tracks etc., which has a capacitive coupling to the environment. This causes common mode currents to flow from the system to the environment and back to source via capacitive coupling, causing common mode noise emission from the system. On other hand, large dI/dt (may occur) may result into a changing magnetic field which can get coupled with surrounding conductors via induction, producing differential mode noise. The flow of the common mode currents can be represented as shown in Figure 2-8.

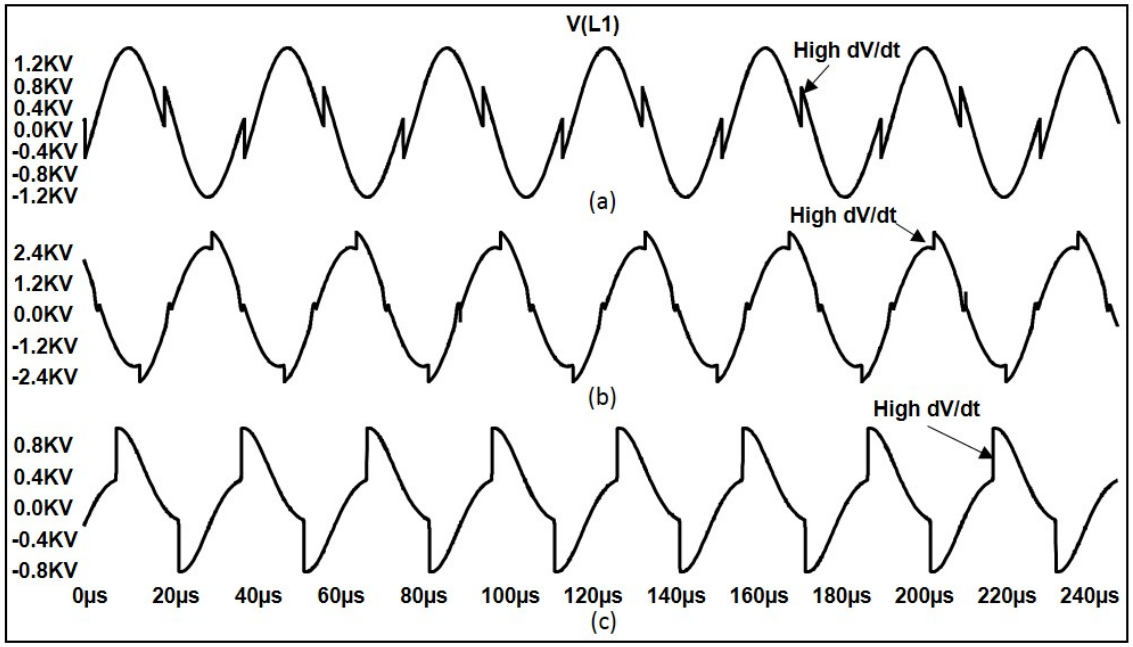

Figure 2-7: Voltage across transmitter coil (a)$f_{op}<f_{res1}$, (b)$f_{op}=f_{res1}$ and (c)$f_{op}>f_{res1}$, D=100%

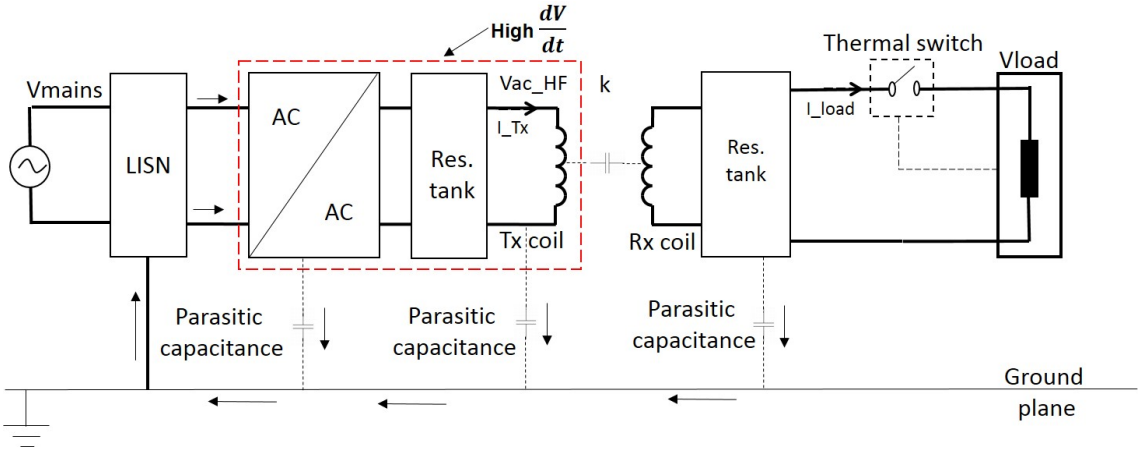

Figure 2-8: Representation of flow of common mode currents

2-4 Frequency domain simulations

As explained in Chapter 1-3, a motor load appears to be disconnected when the back EMF (E_b) is equal or higher than the output voltage (V_{load}) and a resistive heating element can get disconnected if the temperature sensitive switch is opened. Therefore, the load can get disconnected for a short time or for a long time. If the load is disconnected, the receiver circuit is no longer observed by the transmitter circuit. In the absence of the receiver circuit, the order of the system reduces from 4 to 2. The system instantly goes from the inductive mode to the capacitive mode of operation. One can observe this transition with the help of frequency domain simulations. Figure 2-9 explains the load disconnection case in detail with

the help of frequency domain simulations performed on equivalent circuit shown in Figure 2-3.

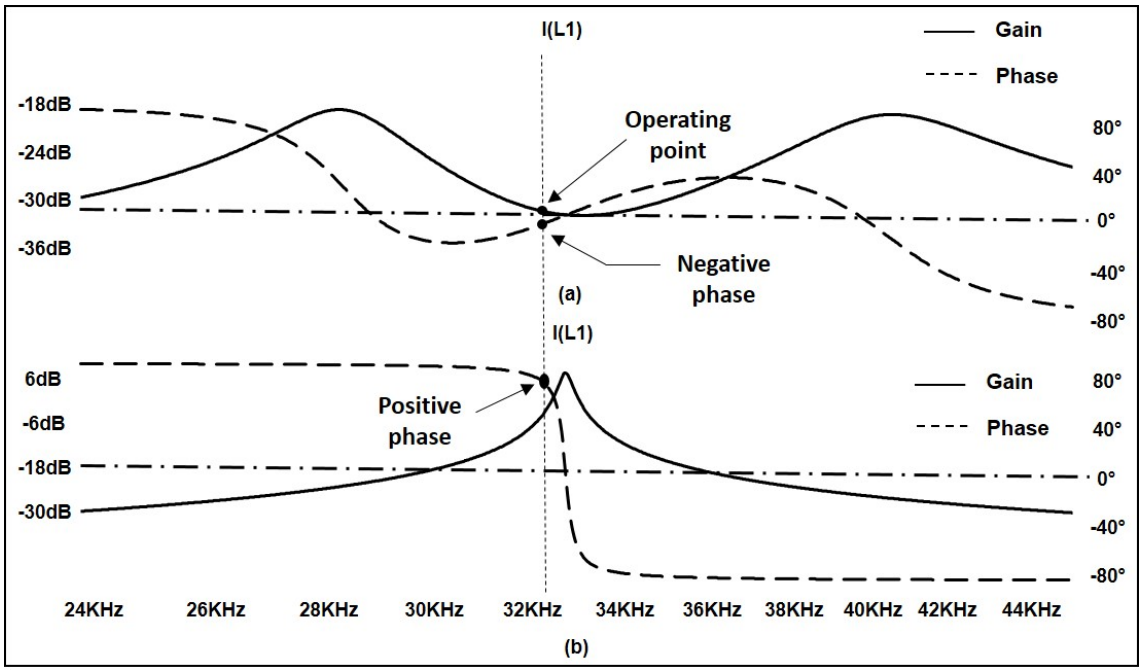

Figure 2-9: Frequency domain simulations of the input current (a) with load connected, (b) with load disconnected, D=100%

Figure 2-9a shows the frequency domain simulation of the input current ($I(L_1)$) when load is connected. As the load is connected, the order of the system is 4. It can be observed that, at the operating point, the phase of the current is negative for the given load. In practice, a small change in load can cause the system to move slightly in the capacitive mode. Therefore, the frequency control loop has to shift the operating point such that the system can again operate at the maximum efficiency point in the desired inductive mode. Figure 2-9b shows the frequency domain simulation of the input current when the load is disconnected. It can be observed that the phase of the current is positive. Therefore, in this case, the load disconnection can be characterized by an instantaneous transition of the system from the inductive to the capacitive mode of operation. The instantaneous transition of the system results in very high voltage across the transmitter coil, high dV/dt's at the bridge nodes and reverse recovery losses in the power switches. The high dV/dt's at the bridge nodes in the system causes common mode noise which could disturb the surrounding systems. Thus, to avoid such high dV/dt's, the system has to shift to a new operating point, as fast as possible. As the transmitter and the receiver coils are mutually coupled to each other, a very high voltage is induced in the receiver coil as well. Figure 2-10 shows the voltage across the receiver coil at the operating point, when the load is connected (Figure 2-10a) and disconnected (Figure 2-10b).

To avoid the high input current and overvoltage on both the transmitter and the receiver coil, the frequency control loop has to increase the f_{op} such that the system operates on the falling edge, in the desired inductive mode. As it can be seen from the Figure 2-9 and Figure 2-10,

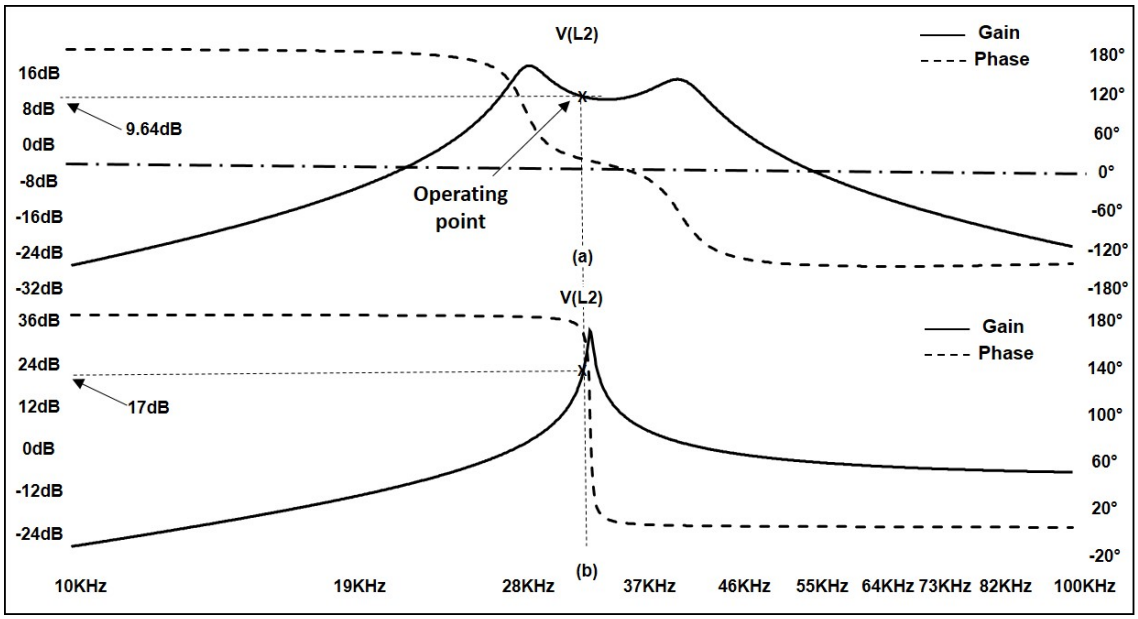

Figure 2-10: Receiver coil voltage gain when (a)load is connected, (b)load is disconnected, D=100%

increasing the frequency in the absence of the protective means can cause a very high input current and receiver coil voltage, resulting in system failure. Therefore, while the frequency is increased, the inner loop of the control system controls the input current cycle-by-cycle to a safe limit with the help of duty cycle control. Consequently, it also reduces the overvoltage on the transmitter and receiver coil. The outer loop of the control system, by means of the communication channel, ensures that the average load voltage does not exceed the safe limits, as shown in Figure 2-11

In this case, the duty cycle of the power switches is reduced to reduce the magnitude of the input current as well as the transmitter and receiver coil voltages. The communication channel in the present cordless kitchen system has a sample time equal to the half of the mains frequency (10msec @ 50Hz). Therefore, getting a feedback from the receiver side is not a cycle-by-cycle process. Thus, the frequency control loop requires more time to find a new optimal operating point. As the sampling rate of the communication channel cannot be changed, it is highly difficult to make a fast frequency control loop in practice.

Another important point to note is the voltage across the inverter power switches. From Figure 2-1, the peak amplitude of V_{in} can be expected and observed across the inverter power switches, irrespective of the load changes. Figure 2-12 shows the voltage across the switch S_2.

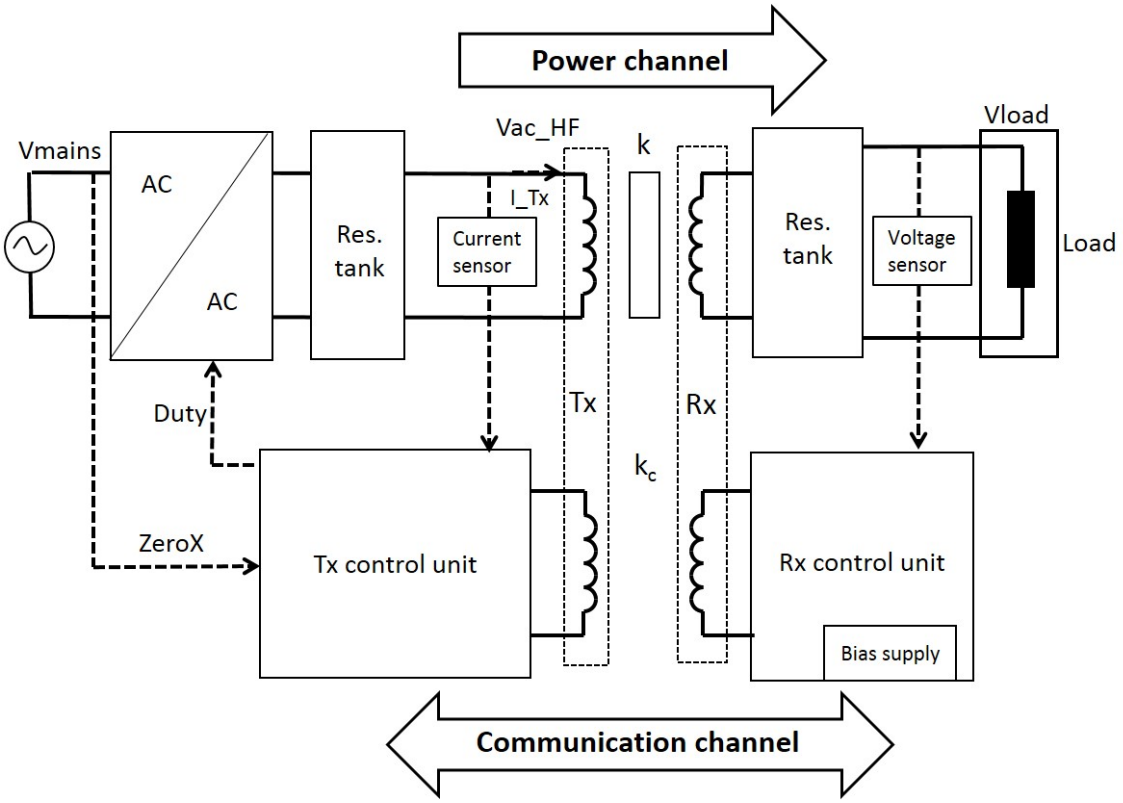

Figure 2-11: Basic block diagram for control mechanism in cordless kitchen system

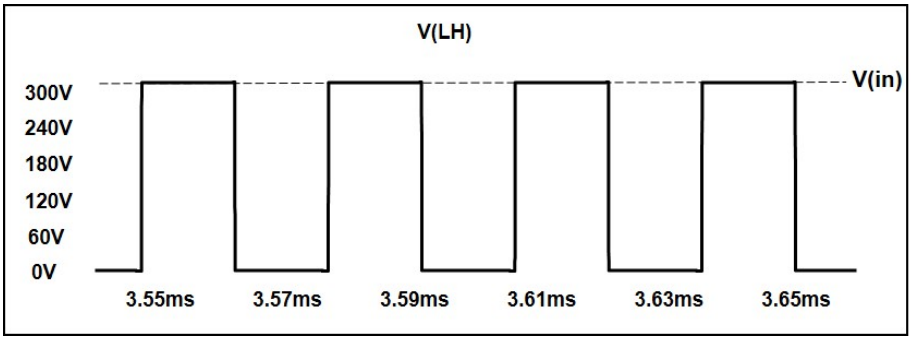

Figure 2-12: Voltage across the switch S_2

2-5 Operation of the communication channel

As described in the introduction, the data or information exchange between the transmitter and the receiver takes place with the help of the communication channel. The communication channel operates comparatively on lower voltage levels as compared with the power channel. Therefore, the communication channel and the power channel should not interfere with each other. Such an interference may transfer false information through the communication channel. To avoid the interference Time Division Multiplexing (TDM) is used where, the inverter stage of the power channel is completely switched OFF for a time duration (so-called a communication window) near the mains voltage zero crossings. During this communica-

tion window, the communication channel is activated and information exchange between the transmitter and the receiver can take place. The details about TDM technique are provided in Appendix A-5.

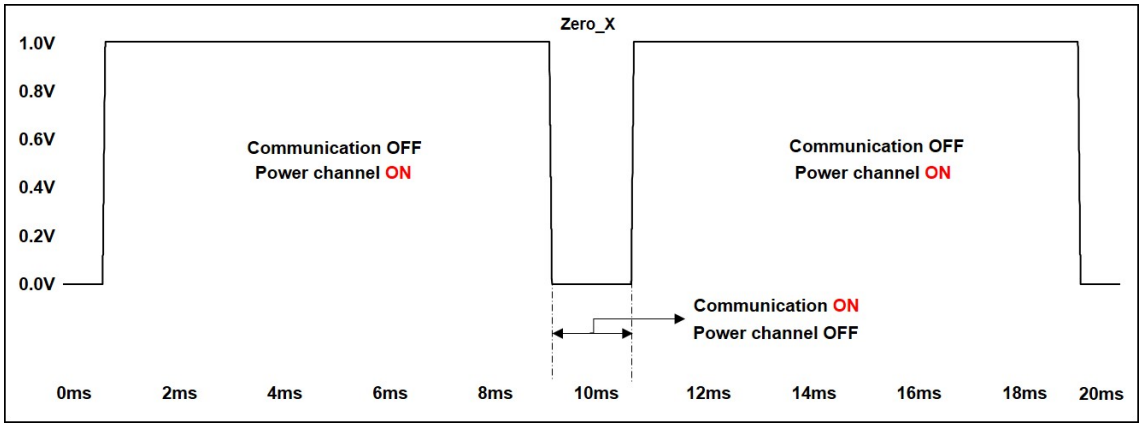

Figure 2-13: Example of a zero crossing signal

To provide this communication window, a zero crossing signal ($Zero\_X$) is used by the inverter stage. With the help of the zero crossing signal, mains voltage zero crossings are predicted and the power switches of the inverter stage are either completely opened (switched OFF) or operated at the desired duty cycle. An example of zero crossing signal is shown in Figure 2-13. Figure 2-14 shows a basic diagram of the series resonant topology equipped with zero crossing detection signal. The details about zero crossing detection signal are given in Appendix A-8.

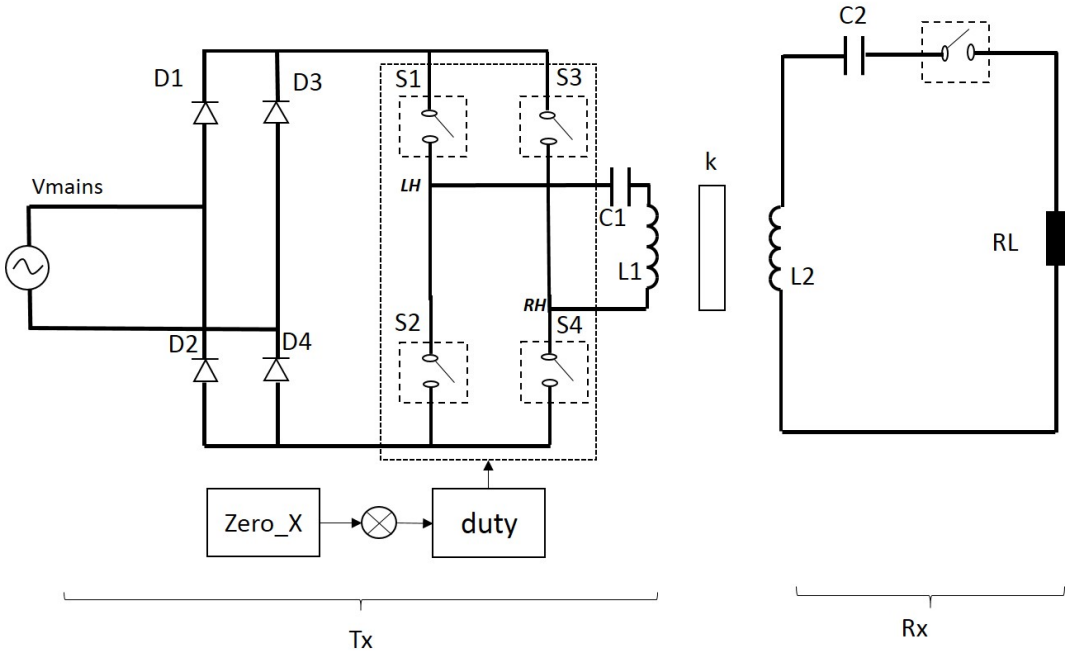

Figure 2-14: Block diagram of the present topology zero crossing signal

2-6 Requirements of the system

In the previous section, the presently used series resonant topology and its control was discussed in detail. It is capable of transferring the power at high levels (kW) with high efficiency but it is harder to meet the non-functional requirements of the system like EMI, overvoltages and simplicity in control.

As mentioned earlier, the introduction of duty cycle control might result in the loss of ZVS of the power switches resulting in high dV/dt's at the inverter bridge nodes. The change in the current w.r.t. time (dI/dt) as well as the change in the transmitter coil voltage w.r.t. time (dV/dt) may create electromagnetic interference (EMI) problems. This gives rise to the first requirement of the system: having a low EMI.

As explained in the introduction, the load disconnection can occur due to the back EMF (Eb) of a motor load or by opening a temperature sensitive switch. This abrupt change in the applied load causes severe overvoltages at the receiver side as well as at the transmitter side, as shown in Figure 2-10. The transmitter and the receiver can be protected against the overvoltages with the protective means, which are costly. Without these expensive protective means it may damage the system components and therefore the system may fail to operate. To avoid the expensive protective means and thus to keep the appliances cheap, the system should meet the second requirement : an intrinsic protection of the transmitter as well as receiver coils against the overvoltage.

As explained earlier, the communication channel has a sample time of 10msec. Therefore, in case of a load disconnection, the control loop cannot recognize the abrupt change in the load instantly. When it recognizes the load disconnection, the system is already operating in the capacitive mode and the control loop requires more time to find a new optimal operating point. It is desired that the system should always operate in the inductive mode and in any case, the control loop should be able to find the optimal operating point immediately and easily. As the sampling rate of the communication channel cannot be changed, it gives rise to the third requirement of the system: simplicity in the control system. Thus, one can summarize the non-functional requirements of the system as:

- Low EMI
- Protection against overvoltage
- Simple control system

Along with these non-functional requirements, the system must meet all the functional requirements also. One can summarize the most important functional requirements as:

- Power transfer over 2.4kW : As explained in the chapter-Introduction, the power transfer of over 2.4kW is required from the cordless kitchen system. An appliance from a food processor (about 700W) to a water kettle (about 2400W) must get powered and operate smoothly.
- Efficient power channel $> 90\%$: The efficiency of the power transfer should not be below 90%.

- Bidirectional communication at 13.56 MHz, bitrate 20Kbit/sec : As described in chapter 2-5, power channel and communication channel should not interfere with each other to avoid false information transfer between the transmitter and the receiver. Therefore, TDM technique is used to avoid the interference. To implement the TDM technique, a mains voltage zero crossing detector need to be realized.
- Transmitter coil - Receiver coil distance = 4cm : As explained in the introduction, the requested amount of the power should be transferred at a distance of 4cm between the transmitter coil and the receiver coil (placed in the appliance).

It is possible to meet the non-functional as well as functional requirements of the system with the present series resonant topology. To suppress the electromagnetic interference one can make use of an additional common mode choke coil or a bulky mains filter. To protect the system from the overvoltages during the load disconnection and to make the control system simpler, one can make use of an additional circuitry or operate the system on higher frequencies (for the same load conditions and system parameters). But, addition of a bulky mains filter or a circuitry are expensive means to compensate for the drawbacks of the present system. Whereas, by operating the system at higher frequencies one has to make a trade off between overvoltage protection and the maximum efficiency of the system. Therefore, it can be stated that the drawbacks of the present system can be minimized by modifying the transmitter part, the receiver part or the control part. In a cordless kitchen system, the transmitter (Tx) remains the same and the receiver (Rx) changes, depending on which appliance is located on the table top. Thus, it is beneficial if all the requirements of the cordless kitchen system are satisfied by modifying only the transmitter side. Thus, in the further studies different topologies for the transmitter part are analyzed keeping the receiver part the same[9]. The detail analysis of the two topologies: Voltage Source (VS) parallel resonant topology and Current Source (CS) parallel resonant topology is explained in the next Chapters. The basic requirement from the new transmitter topology is to meet all the non-functional requirements intrinsically without affecting the functional requirements.

Conclusion

This chapter provided a detailed description and operation of the present cordless kitchen system based upon the series resonant topology. The mathematical analysis gave the voltage transfer functions which can be used to observe the behaviour of the system over a broad range of operating frequencies. It can also be used to locate the resonant frequencies of the system. With the help of frequency and time simulations, drawbacks of the present topology are highlighted. This chapter also derived the most important functional as well as non-functional requirements of the cordless kitchen system from the previous sections. Based upon the requirements and practical conditions, the chapter provided two possible alternative topologies: VS parallel resonant topology and CS parallel resonant topology which may satisfy all the requirements stated in this chapter. The description and analysis of the VS parallel topology is given in the next chapter.

Chapter 3

Voltage Source parallel resonant topology

3-1 Introduction

Figure 3-1 shows the Voltage Source (VS) parallel resonant topology. It can be observed that the transmitter capacitor (C_1) is connected across the transmitter coil (L_1). This parallel resonant tank on the transmitter side is fed by constant current source formed by the input voltage source (V_{in}) and a choke coil (L_{choke}). To check the applicability of this topology in

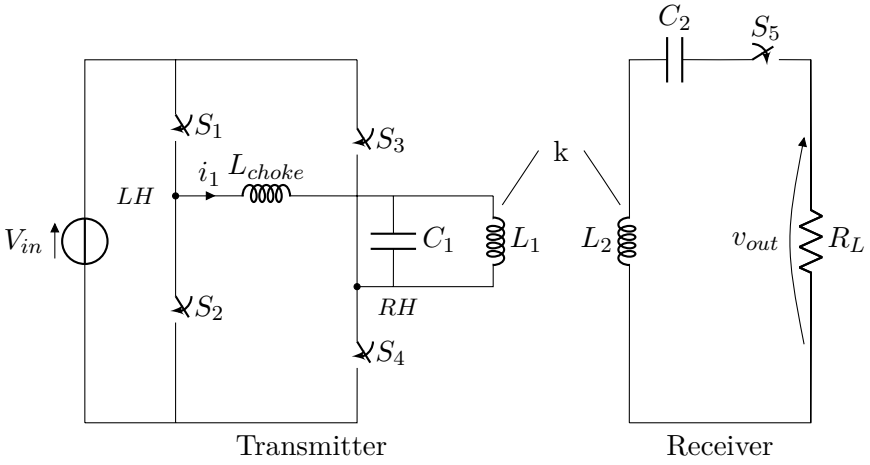

Figure 3-1: Voltage source parallel resonant topology

the cordless kitchen system, one must start with the mathematical analysis and simulations. For the mathematical analysis a simple equivalent circuit can be derived as shown in Figure 3-2 from Figure 3-1. As explained in previous chapters, the same mathematical analysis procedure can be followed for getting an optimal operating point (f_{op}) for calculated circuit component values and given load conditions. Based upon the requirements mentioned in the

previous section, the VS parallel resonant topology is analyzed with the help of mathematical analysis and simulations, in the further sections. To proceed with the simulations following (realistic) component values are used:

- $f_{tx} = f_{rx} = 33$ kHz
- $L_1 = 290$ uH
- $L_2 = 290$ uH
- $L_c = 1$ mH
- $C_1 = 1/(4\pi^2 f_{tx}^2 L_1)$ F
- $C_2 = 1/(4\pi^2 f_{rx}^2 L_2)$ F
- $k = 0.35$
- $M = k\sqrt[2]{L_1 L_2}$
- $R_1 = R_2 = 50$ mΩ
- $R_L = 10\ \Omega$
- $V_{in} = 325$ V DC (for time domain)
- $V_{ac} = 1$ V AC (for frequency domain)

3-2 Mathematical analysis

From Figure 3-1 an equivalent circuit can be derived, as shown in Figure 3-2.

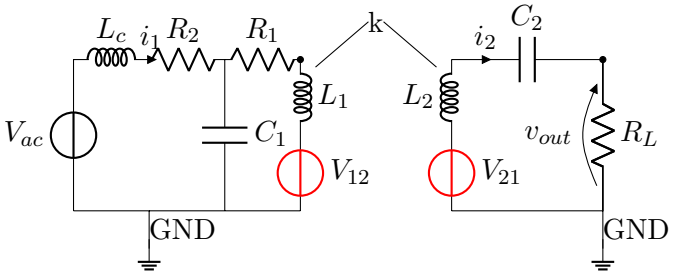

Figure 3-2: Simplified equivalent circuit for VS parallel resonant topology

In the above circuit, R_1 represents the equivalent series resistance of the transmitter along with the reflected equivalent series resistance of the receiver. R_2 represents the equivalent series resistance of the choke coil. R_L represents the load resistance. V_{12} represents the voltage induced in the transmitter coil (L_1) due to the mutual inductance (say, M) and the current flowing through the receiver coil (i_2). V_{21} represents the voltage induced in the receiver coil (L_2) due to the mutual inductance and current flowing through the transmitter coil (i_{L1}). As discussed earlier, to check the performance of the system at various operating frequencies

one can make use of the transfer function. With the help of suitable mathematical analysis a transfer function can be derived, as shown in Equation below [Appendix A-3]. The order of the characteristic equation (denominator) of the system transfer function is an indicator of the simplicity in the control system. The higher the order of the system, the more poles it has. And the more poles in the system, the more difficult it is to control. It can be seen from the Equation below that the order of the characteristic equation is 5. Consequently, it is called as 5^{th} order system. One can compare it with the present series resonant topology and can state that it is more difficult to control the VS parallel resonant topology.

$$\frac{V_{out}}{V_{ac}} = \frac{sMR_L(s^3L_1C_1C_2 + s^2R_2C_1C_2 + sC_2)}{\begin{aligned}&s^5(L_1L_2C_1C_2L_c - L_1C_1M^2C_2) + s^4(R_1L_1L_2C_1C_2 + R_2L_2C_2L_cC_1 + L_1C_1L_cR_LC_2 - R_2C_1C_2M^2)\\ &+s^3(R_1R_2C_1L_2C_2 + L_cL_2C_2 + L_1L_2C_2 + R_LC_2L_1C_1R_1 + R_2L_cC_1R_LC_2 + L_1C_1L_c - M^2C_2)\\ &+s^2(L_2C_2R_1 + L_2C_2R_2 + R_1R_2R_LC_1C_2 + R_LL_cC_2 + R_LL_1C_2 + L_1C_1R_1 + R_2L_cC_1)\\ &+s(R_1R_LC_2 + R_2R_LC_2 + R_1R_2C_1 + L_c + L_1) + (R_1 + R_2)\end{aligned}}$$

With the help of the derived voltage transfer function, one can plot a the behaviour of output voltage V_{out} over a wide range of operating frequencies. Figure 3-3 show the plot of output voltage against the operating frequency. It can be observed that the system possesses two resonance frequencies, f_{res1} and f_{res2}. The optimal operating point of the system can be calculated as done in chapter 2. For the realistic and calculated circuit component values, the optimal operating point for VS parallel topology is found to be 32.9kHz[2].

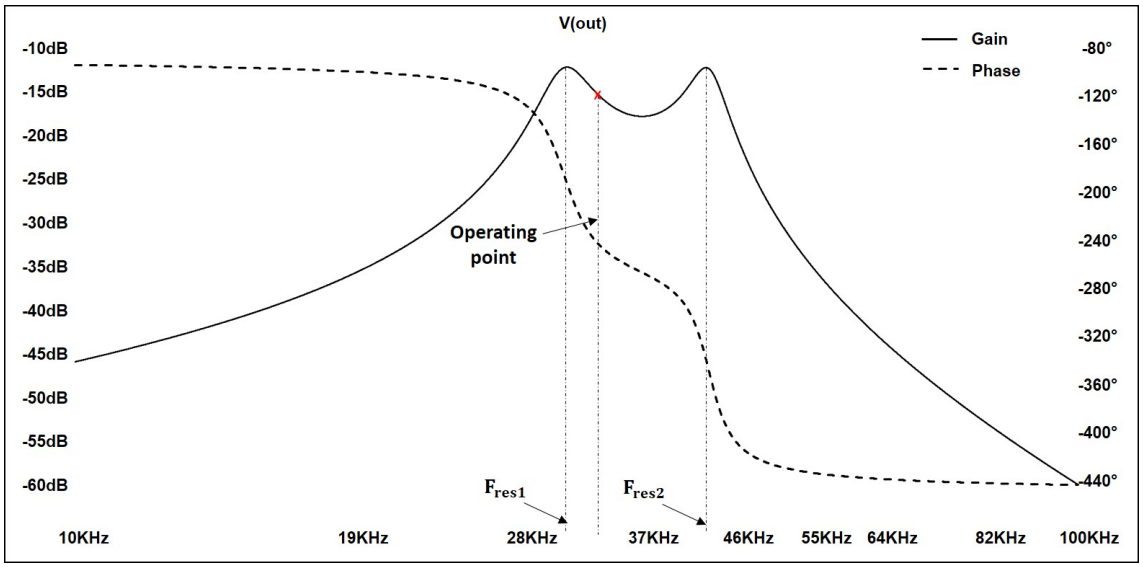

Figure 3-3: Behaviour of output voltage with respect to operating frequency

3-3 Time domain simulations

With the mathematical analysis the optimal operating point can be found out[2]. For the calculated component values and given load conditions the optimal operating point is 32.9kHz. As explained in earlier chapter, to check for the low EMI requirement one can perform time domain simulations of the circuit shown in Figure 3-1 at and near the calculated optimal operating point.

Figure 3-4 and Figure 3-5 shows the inverter bridge voltage and input current at operating frequency 32.9kHz and duty cycle (D) 100% and 50%, respectively.

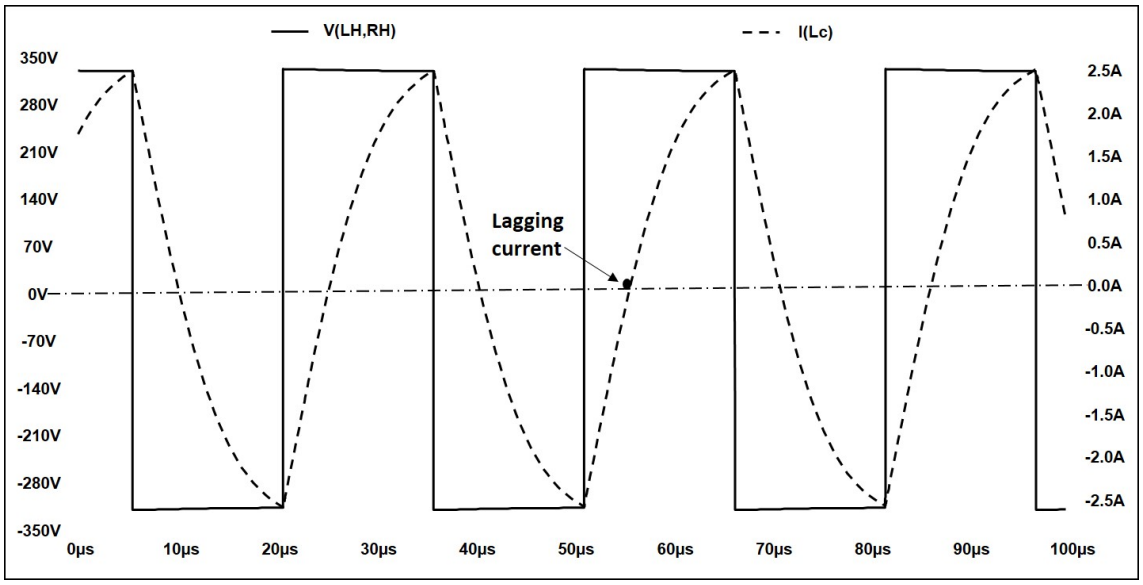

Figure 3-4: Operation of the VS parallel resonant topology at the calculated f_{op}, D=100%

It can be seen from Figure 3-4 that input current lags the inverter bridge voltage. The peak voltage across the inverter bridge is equal to the input voltage (V_{in}).

As seen in chapter 2, introduction of duty cycle control in series resonant topology, results in loss of ZVS. On the contrary, from Figure 3-5 it can be observed that introduction of duty cycle control does not result in loss of ZVS. The input current still lags the inverter bridge voltage. It can be considered as an advantage over the present topology.

Figure 3-6 shows the the transmitter coil (L_1) voltage when the inverter stage of the transmitter is operated below f_{res1}, at f_{res1} and above f_{res1}.

As described in chapter 2 with Figure 2-7, the series resonant topology shows the presence of high dV/dt's across the transmitter coil. On the contrary, Figure 3-6 shows that VS parallel resonant topology solves the issue of high dV/dt's for the transmitter coil (L_1). One can observe a sinusoidal voltage waveform across the transmitter coil. It is beneficial from EMI point of view. Therefore, it can be considered as another advantage over the present topology. To check for the satisfaction of other requirements of the system one can observe voltage across and current through the other circuit components. Figure 3-7 shows the voltage across the transmitter coil (L_1) and choke coil (L_{choke}). From Figure 3-6, one can observe the sinusoidal

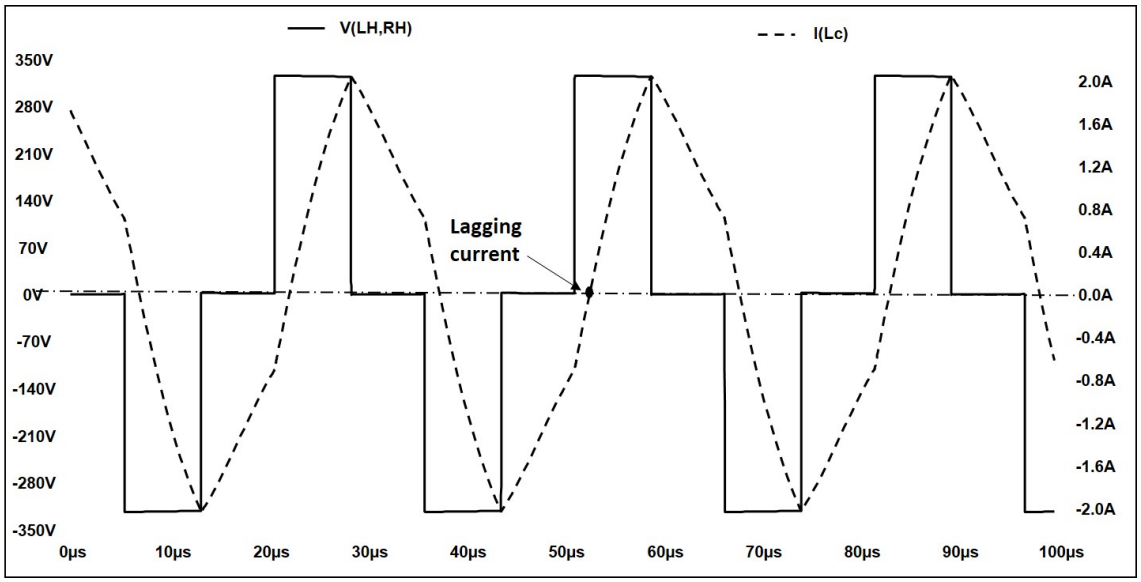

Figure 3-5: Operation of the VS parallel resonant topology at the calculated f_{op}, D=50%

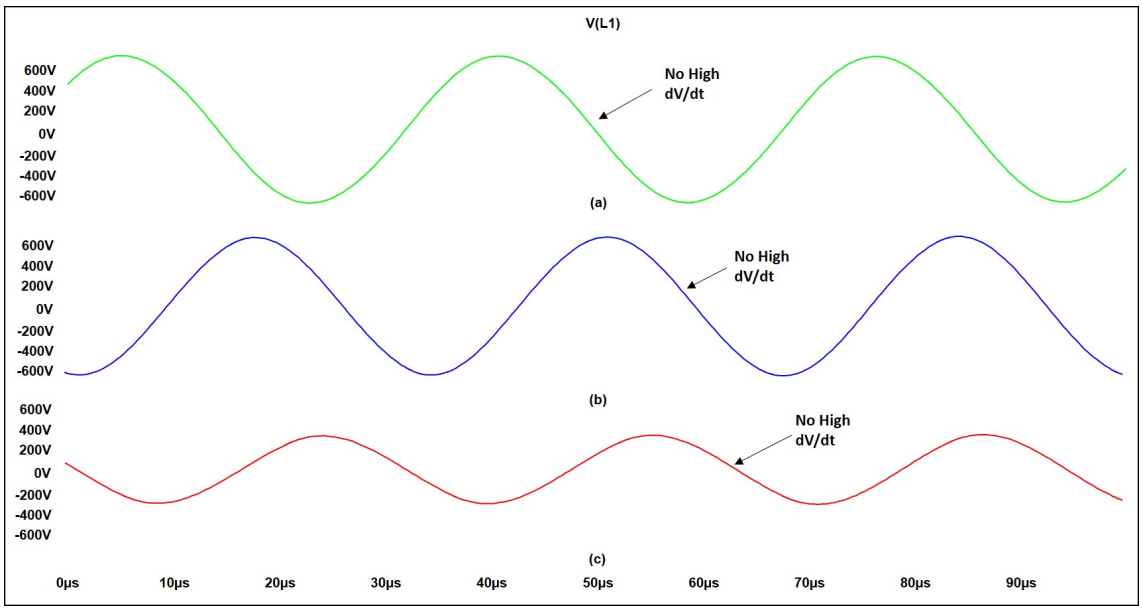

Figure 3-6: Voltage across transmitter coil (a)f_{op}<f_{res1}, (b)f_{op}=f_{res1} and (c)f_{op}>f_{res1}, D=100%

voltage waveform across the transmitter coil. However, Figure 3-7 also shows the presence of high dV/dt's across the choke coil. As explained in the chapter 2-6, high dV/dt's can cause EMI problems and thus are not desired. Therefore, VS parallel resonant topology solves the high dV/dt's issue for the transmitter coil (L_1) but it introduces high dV/dt's at atleast one of the nodes of the choke coil (L_{choke}).

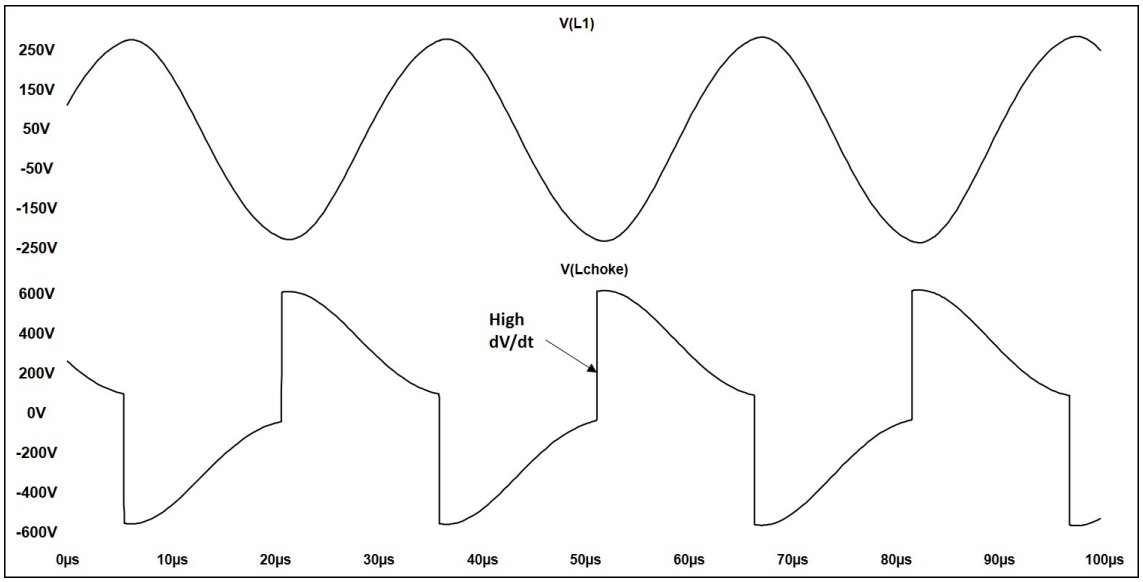

Figure 3-7: Voltage across the transmitter coil and choke coil at D=100%, f_{op}=32.9kHz

3-4 Frequency domain simulations

As explained in the introduction, the load (R_L) can get disconnected or appears to be disconnected for a short time. In case of the present topology, the load disconnection results in overvoltages across the transmitter as well as the receiver coil, as shown in Figure 2-10. For this topology, one can observe the behaviour of the receiver coil voltage when the load gets disconnected with the help of the frequency domain simulations. The frequency domain simulations can performed with the help of the equivalent circuit shown in Figure 3-2. Figure 3-8a shows the frequency domain simulation for receiver coil voltage when load is connected. Figure 3-8b shows the frequency domain simulation for receiver coil voltage when load is disconnected.

It can be seen from figure 3-8 that when the load is disconnected, the voltage level rises. Therefore one can state that, to avoid the damage due to overvoltage the system should be equipped with the protective circuitry and fast control loop.

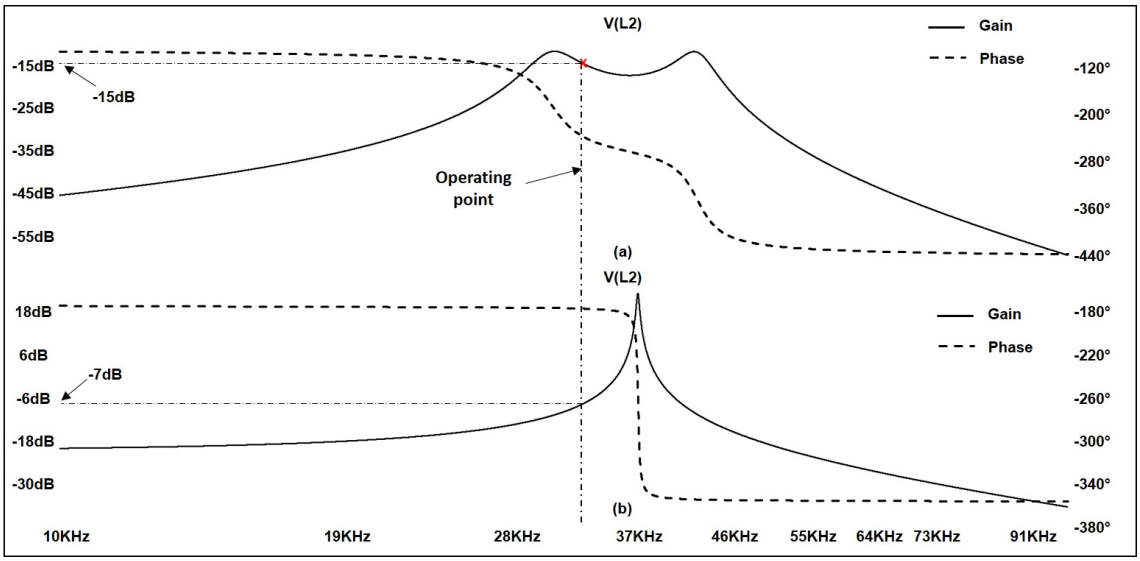

Figure 3-8: Receiver coil voltage gain when (a)load is connected, (b)load is disconnected, D=100%

Conclusion

The chapter provided the description along with the suitable analysis of the VS parallel resonant topology. It is observed that VS parallel resonant topology does have an advantages of duty cycle control without loss of ZVS, over the present topology. However, further simulations showed that it does have drawback of presence of high dV/dt's across the choke coil. The frequency domain simulation showed that in case of load disconnection the topology shows overvoltages in the system. To compensate for the overvoltage, the system should be equipped with the protective circuitry and fast control loop. Therefore, one can state that VS parallel resonant topology do not meet all the non-functional requirements of the cordless kitchen system and hence it can be discarded. The description and analysis of the Current Source (CS) topology is mentioned in the next chapter.

Chapter 4

Current Source parallel resonant topology

4-1 Introduction

Figure 4-1 shows the current source parallel resonant topology which might be easier to meet the non-functional requirements. There are more possible topologies but as mentioned earlier, the receiver side has not been modified. An attempt is made to meet the functional and non-functional requirements by modifying the transmitter side.

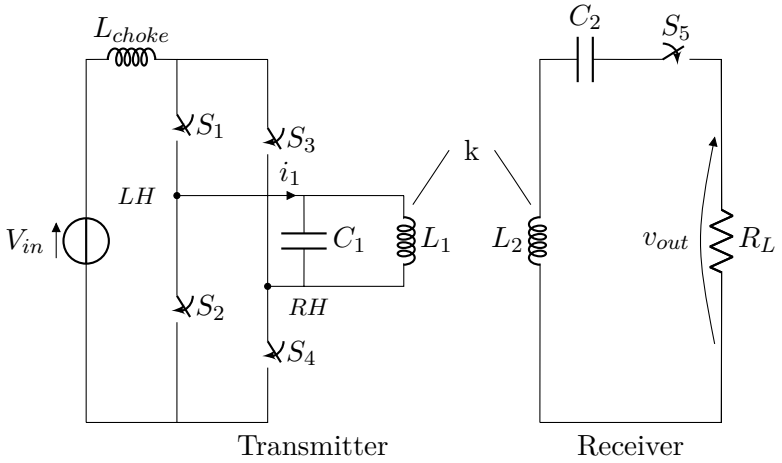

Figure 4-1: Current source parallel resonant topology

Figure 4-1 shows the current source (CS) parallel resonant topology. L_{choke} is placed on the DC side of the inverter stage to make a current source driven parallel resonant inductive coupler. It should be noted that, as it is a current source driven topology, there should be some 'overlap time' between the switches of the same bridge leg. To analyze the properties of

this topology, mathematical analysis together with the simulations in the time and frequency domain can be performed. Due to the presence of L_{choke} it is harder to perform the frequency domain simulations for this topology. Therefore, in this case a mathematical model for frequency domain analysis (voltage transfer function) is built with the help of simulations and then detailed analysis is performed.

One can reduce the circuit shown in Figure 4-1 to an equivalent circuit as shown in Figure 4-2 and proceed with the further evaluation. In this case, to proceed with the simulations following (realistic) values are chosen:

- $f_{tx} = f_{rx} = 33$ kHz
- $L_1 = 290$ uH
- $L_2 = 290$ uH
- $C_1 = 1/(4\pi^2 f_{tx}^2 L_{res})$ F
- $C_2 = 1/(4\pi^2 f_{rx}^2 L_2)$ F
- $L_{choke} = 1$ mH
- $L_{res} = L_1 || 2L_{choke}$ H
- $k = 0.35$
- $M = k\sqrt[2]{L_{res} L_2}$ H
- $R_1 = R_2 = 50$ mΩ
- $R_L = 10\ \Omega$
- $V_{in} = 325$ V DC (for time domain)
- $I_{ac} = 1$ A AC (for frequency domain)

4-2 Mathematical analysis

From Figure 4-1, a first order equivalent circuit for the frequency domain simulations can be derived, as shown in Figure 4-2. Figure 4-2 shows the pure parallel resonant converter in which the voltage source (V_{in}) and choke coil (L_{choke}) is replaced by a current source.

The topology is based on the principle of parallel resonance in which, the circuit offers maximum impedance at the resonant frequencies. Therefore, with the help of frequency domain simulations, an input impedance bode plot can be used to locate the resonance frequencies (f_{res1} and f_{res2}) of this system, as shown in Figure 4-3.

From Figure 4-3 it can be seen that the system always operates in the inductive mode of operation when it is operated below f_{res1} (as phase of the impedance is positive). Above f_{res1} it operates in capacitive mode up to a particular operating frequency above which, it again operates in the inductive mode. To completely avoid the capacitive mode of operation,

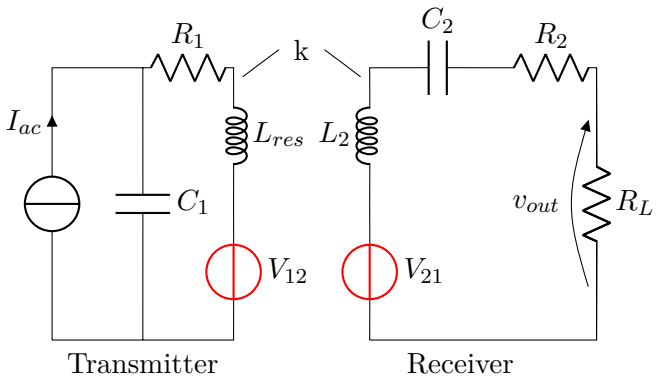

Figure 4-2: Equivalent circuit for frequency domain analysis

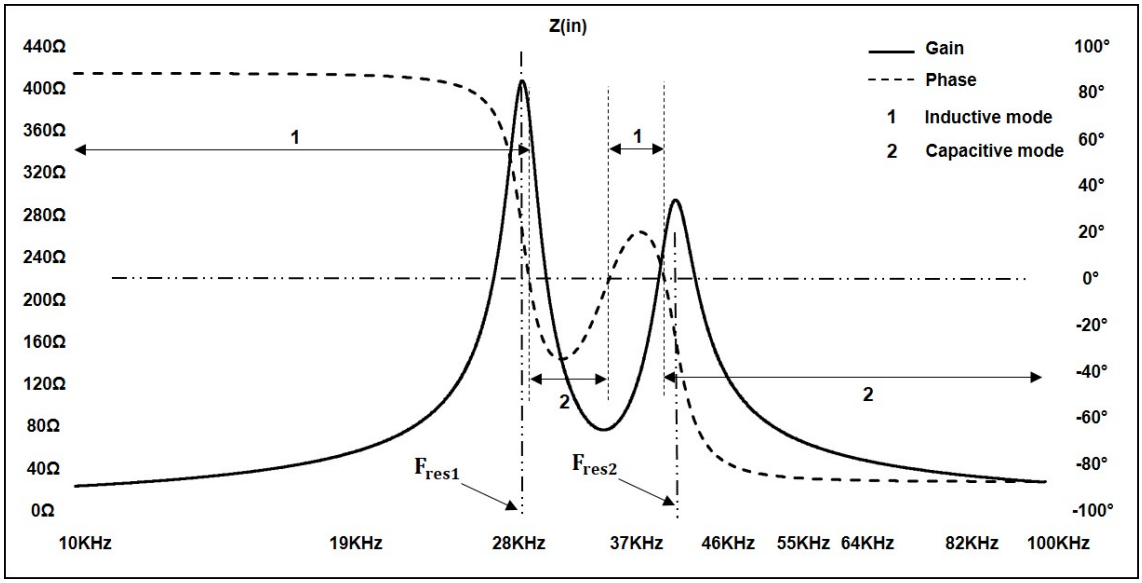

Figure 4-3: Input impedance bode plot

the resonant frequency of the whole system is chosen to be f_{res1}. For this topology and calculated circuit component values, this frequency (f_{res1}) is observed to be 28.2kHz. With the help of the information gathered from the input impedance plot and the calculated circuit component values, the time domain simulations of the circuit shown in Figure 4-1 can be performed. Figure 4-4 shows the voltage across the transmitter coil of the resonant inductive coupler when the inverter stage is operated at $f_{op}<f_{res1}$, $f_{op}=f_{res1}$ and $f_{op}>f_{res1}$.

Interestingly from Figure 4-4, it can be seen that when the inverter stage of the transmitter is operated at or below the f_{res1}, high dV/dt's are not observed. On the other hand, when the inverter stage is operated above the f_{res1}, high dV/dt's are observed. Thus, based upon the requirements stated in chapter 2-6, the operation of this topology at or below f_{res1} is preferred. When the system is operated below f_{res1}, the transmitter coil voltage waveform is almost a sine wave. It has an event near the zero crossing of the sinewave where the voltage is almost zero. Thus, for the analysis of the system operating at or below f_{res1}, First Harmonic Approximation (FHA) can be used [1]. With the help of FHA, a simplified equivalent circuit

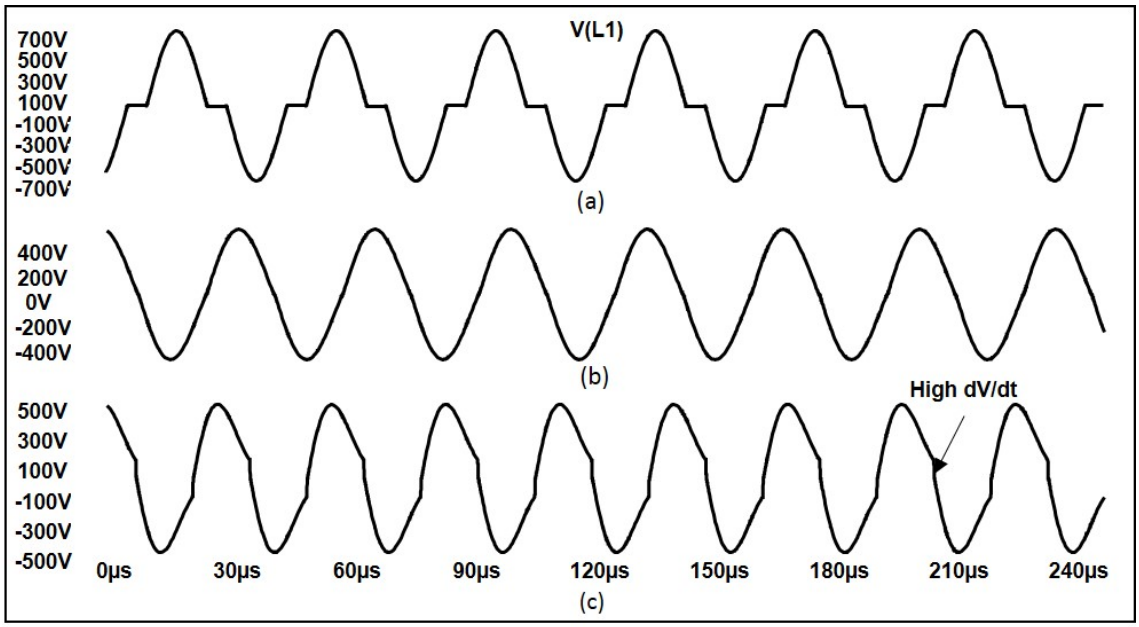

Figure 4-4: Voltage across transmitter coil (a)f_{op}<f_{res1}, (b)f_{op}=f_{res1} and (c)f_{op}>f_{res1}

of the system can be derived as shown in the Figure 4-5.

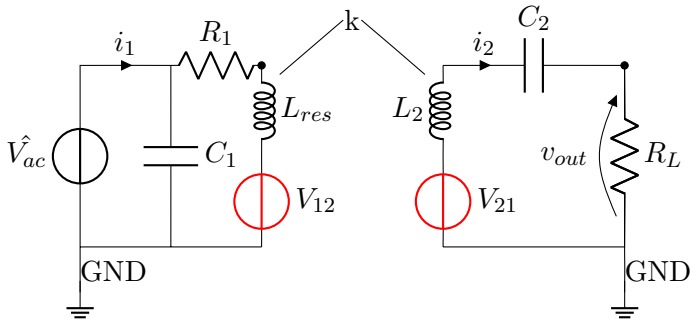

Figure 4-5: Simplified equivalent circuit for CS parallel resonant topology operated below f_{res1}

The FHA allows to replace the current source (I_{ac}) and capacitor (C_1) with an AC voltage source ($\hat{V_{ac}}$). In both the equivalent circuits shown in Figure 4-2 and Figure 4-5, R_1 represents the equivalent series resistance of the transmitter along with the reflected equivalent series resistance of the receiver. R_L represents the load resistance. V_{12} represents voltage induced in the transmitter coil (L_{res}) due to the mutual inductance (say, M) and the current flowing through the receiver coil (i_2). V_{21} represents the voltage induced in the receiver coil (L_2) due to the mutual inductance and the current flowing through the transmitter coil (i_1). By applying the Laplace transformation and the transformer theory, a voltage transfer function can be derived as shown below [Appendix B-1].

$$\frac{V_{L_2}}{\hat{V_{ac}}} = \frac{s^2(R_L M C_2) + sM}{s^3(L_{res}L_2C_2 - M^2C_2) + s^2(L_2R_1C_2 + L_{res}C_2R_L) + s(R_1R_LC_2 + L_{res}) + R_1} \quad (4\text{-}1)$$

From Equation 4-1 one can observe that the transmitter capacitor (C_1) does not influence

the receiver voltage gain but it is important to include C_1 in the model because it does affect the phase of the input current (i_1) with respect to the input voltage ($\hat{V_{ac}}$). It acts as a phase compensator. Equation 4-1 also shows that the order of the characteristic equation (denominator) is 3. The more poles in the system, more the difficult it is to control. Again interestingly, it implies that the CS parallel resonant topology is simpler to control than the present topology. Therefore, in the further analysis the operation of the current source parallel resonant topology above the f_{res1} is discarded and the operation at or below the f_{res1} is considered.

4-3 Time domain simulations

As mentioned earlier, for this topology and calculated circuit component values, the resonant frequency is observed to be 28.2kHz. Therefore the system is operated at or below 28.2kHz, and other parameters like the voltage across switches, behaviour on load disconnection etc. are examined in this section. The details of the simulation model are given in Appendix A-6 to A-8.

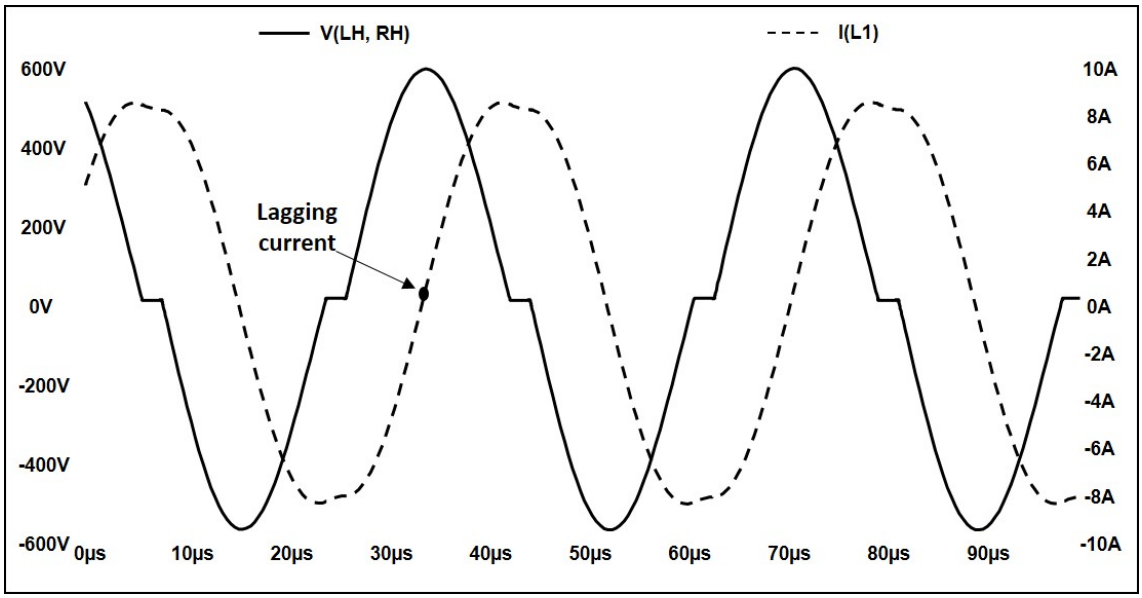

Figure 4-6: Voltage across and current through the transmitter coil L_1 at f_{op}=27kHz, and load connected

With the help of time domain simulations of the circuit shown in Figure 4-1, at f_{op} say 27kHz, the voltage across all the circuit components, in steady state conditions can be observed. Figure 4-6 shows the voltage observed across and the current through the transmitter coil (L_1). It can be observed from Figure 4-6 that transmitter coil current always lags the transmitter coil voltage which makes sure ZVS of the power switches. Figure 4-7 shows the voltage observed across the choke coil (L_{choke}) and the transmitter coil. It shows that there are no high dV/dt's present in any of the coils on transmitter side, under normal operating conditions. It is beneficial from the EMI point of view.

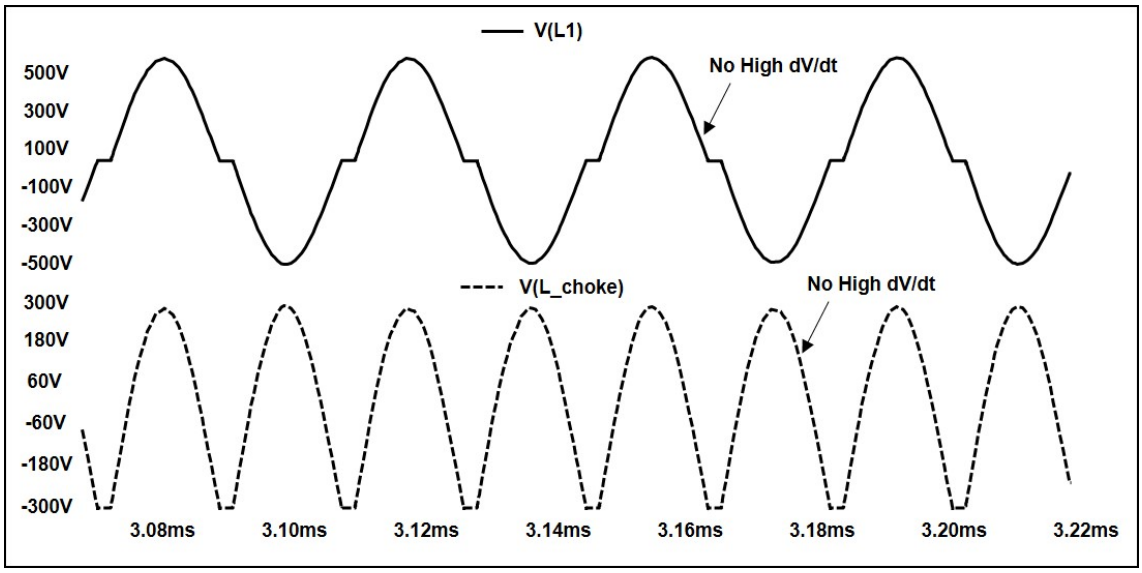

Figure 4-7: Voltage across L_1 and L_{choke} at f_{op}=27kHz

4-4 Frequency domain simulations

To observe the behaviour of this topology on load disconnection, frequency domain simulations can be performed. To proceed with the simulations one can use this equivalent circuit diagram as shown in Figure 4-5. However, to get accurate results one should model the source $\hat{V_{ac}}$ correctly. Therefore, the detailed frequency domain analysis of this topology is performed and described in the next chapter.

Conclusion

This chapter provided the description, mathematical analysis and time domain simulations of CS parallel resonant topology. Mathematical analysis showed that the order of the characteristic equation (denominator of voltage transfer function) is 3, which is lowest as compared to the present and the VS parallel topology. Time domain simulations showed that high dV/dt's do not occur when the system is operated at or below the resonance frequency (f_{res1}). One can observe that, CS parallel resonant topology possesses the advantages of simple control system, no high dV/dt's and no loss ZVS for the power switches intrinsically, when it is operated at or below (f_{res1}). To observe the behaviour of the system on load disconnection, one must perform the frequency domain simulations. However, it is not possible to get correct results from frequency domain 'simulations' because the voltage source ($\hat{V_{ac}}$) is not modeled accurately. The behaviour and mathematical modeling of the voltage source ($\hat{V_{ac}}$) is explained in the next chapter. Frequency domain 'analysis' of the CS parallel resonant topology is also explained in the next chapter.

Chapter 5

Proposed topology

5-1 Introduction

From the earlier chapters, one can understand the operation of the series resonant topology, VS parallel resonant topology and CS parallel resonant topology. The mathematical analysis with the time domain simulation results of all the topologies showed that CS parallel resonant topology has some advantages over the series resonant and VS parallel topologies when applied in the cordless kitchen system. The advantages can be listed as:

- Absence of high dV/dt's: From Figure 2-7 one can observe the presence of high dV/dt's in the series resonant topology. At low duty cycles, the series resonant topology loses the ZVS for the power switches causing additional high dV/dt's and hence an EMI issue. From Figure 3-7 one can observe that, in VS parallel resonant topology, voltage across the transmitter coil (L_1) is observed to be sinusoidal but it introduces high dV/dt's on atleast one of the nodes of choke coil (L_{choke}). And from Figure 4-7, it is evident that high dV/dt's are not observed in CS parallel resonant topology when it is operated at or below f_{res1}.
- The order of characteristic equation: CS parallel resonant topology results in a 3^{rd} order system whereas the series resonant topology and VS parallel resonant topology results in a 4^{th} and 5^{th} order system, respectively. As mentioned earlier, the higher the order of the system, the more difficult it is to control. Therefore, it is comparatively easier to control the CS parallel resonant topology.

Besides the advantages, CS parallel topology also has some disadvantages over other topologies. The disadvantages are:

- Loss of control over power: As explained in the introduction, duty cycle (D) control is used to control the power delivered to the load. Present series resonant topology and VS parallel resonant topology are voltage source driven topologies and therefore it

is easier to employ duty cycle control for the inverter power switches. As mentioned earlier, the series resonant topology facilitates the duty cycle control but at the expense of loss of ZVS. The current source driven topologies cannot make use of duty cycle (D) control and hence cannot control the power delivered to the load at a particular operating frequency (f_{op}).

- Communication window: As mentioned in chapter introduction and Appendix A-5, for the communication between the transmitter and the receiver, Time Division Multiplexing (TDM) is used. In TDM, the power channel is completely turned-OFF and communication channel is turn-ON, near the mains voltage zero crossings. In case of voltage source driven topologies, one can open all the inverter power switches to turn-OFF the power channel. But, one cannot make use of the same technique in case of a current source driven topology. In that case, one has to use alternative techniques to make the current source equal to zero for a short period of time. Therefore, it is comparatively harder to achieve a communication window in case of CS parallel resonant topology .

Considering the non-functional requirements of the cordless kitchen system and advantages of the CS parallel resonant topology, one can propose CS parallel topology (operation below f_{res1}) as an alternative topology. Therefore in this chapter, CS parallel resonant topology is stated as *proposed topology* and detailed analysis regarding load disconnection and control of the topology is discussed. Furthermore, a simulation model with alternatives to compensate for the disadvantages of this topology is provided.

5-2 Detailed analysis of the CS parallel resonant topology

In the previous chapter, one can see the behaviour of the voltage across the transmitter coil (L_1) when the system is operated below f_{res1}, at f_{res1} and above f_{res1}. When the system is operated below f_{res1}, one can model the system as shown in Figure 4-5 and Equation 4-1. However, the behaviour of the voltage source $\hat{V_{ac}}$ is not like an ideal frequency domain voltage source. For accurate analysis, one should model the source $\hat{V_{ac}}$ correctly.

5-2-1 Modeling of Voltage Source $\hat{Vac}$

As shown in Figure 4-4a, when the inverter stage of the transmitter is operated below f_{res1}, voltage across the transmitter coil appears to be a discontinuous function. Figure 5-1 shows the transmitter coil voltage at various operating frequencies below the f_{res1}.

It can be observed that as the operating frequency decreases, the peak voltage across the transmitter coil (V_{tx}) and time for which the voltage remains zero (T_{freeze}), increases. Therefore, the amplitude of the first harmonic ($V_{ac_{FHA}}$) changes with the operating frequency (f_{op}). Thus, it is difficult to perform the frequency domain simulations for the equivalent circuit shown in Figure 4-5. For better results from the frequency domain simulations, one has to model the source $\hat{V_{ac}}$ such that the amplitude of the first harmonic is a function of the operating frequency. The relation between the amplitude of the first harmonic ($V_{ac_{FHA}}$) and the operating frequency (f_{op}) can be derived with the help Fourier analysis of the transmitter coil voltage waveform shown in Figure 5-2.

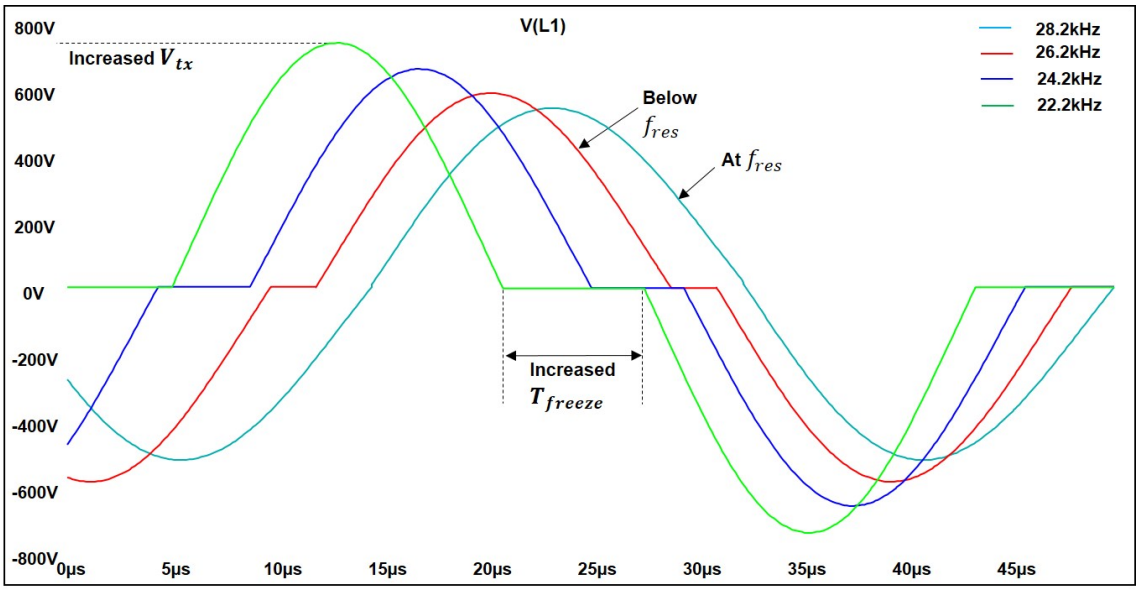

Figure 5-1: Variation of Tx coil voltage with the operating frequency

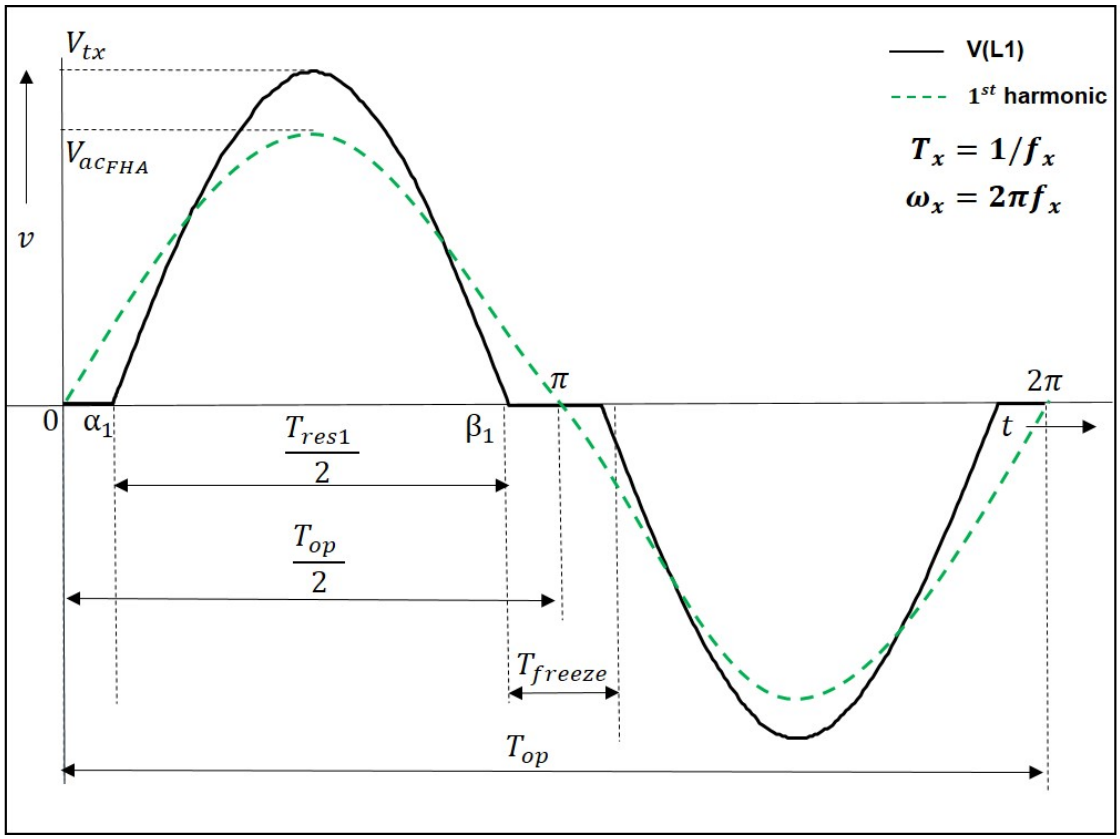

Figure 5-2: Transmitter coil voltage waveform for detailed analysis

From Figure 5-2 the relation between the peak amplitude (V_{tx}) and operating frequency (f_{op})

can be derived [Appendix B-4] and is as shown in the equation below:

$$V_{tx} = \frac{V_{in}\pi \dfrac{T_{op}}{T_{res1}}}{2}$$

At f_{op}=f_{res1}

$$V_{tx_{res}} = \frac{V_{in}\pi}{2}$$

And therefore the amplitude of the first harmonic ($V_{ac_{FHA}}$) can be calculated by Fourier analysis of the waveform shown in Figure 5-2 [Appendix B-3]:

$$V_{ac_{FHA}} = \frac{4V_{tx}}{T_{op}} \int_{\alpha_1}^{\beta_1} sin\ \omega_{res}(t-\alpha_1) sin\ n\omega_{op}t\ dt \tag{5-1}$$

$$= \frac{4V_{tx}}{T_{op}} \int_{\alpha_1}^{\beta_1} \frac{1}{2} cos(\omega_{res_1} - \omega_{res_1}\alpha_1 - \omega_{op}t) - \frac{1}{2} cos(\omega_{res_1} - \omega_{res_1}\alpha_1 + \omega_{op}t)\ dt$$

$$= \frac{-8V_{tx}}{T_{op}} cos\left(\frac{\pi}{2}\frac{\omega_{op}}{\omega_{res1}}\right) \frac{\omega_{res1}}{\omega_{op}^2 - \omega_{res1}^2} \tag{5-2}$$

$$\therefore \hat{V_{ac_{FHA}}} = \frac{V_{ac_{FHA}}}{V_{tx_{res}}} \tag{5-3}$$

The normalized value of the derived $V_{ac_{FHA}}$ can be used in Equation 4-1 for the frequency domain simulations. Figure 5-3 shows the equivalent circuit for CS parallel resonant topology with normalized fundamental harmonic. One can also observe the change in normalized fundamental harmonic with respect to operating frequency (f_{op}). With the help of such a mathematical model, one can proceed with the frequency domain analysis for this topology. To preserve the confidentiality, frequency domain analysis is described Appendix B-5.

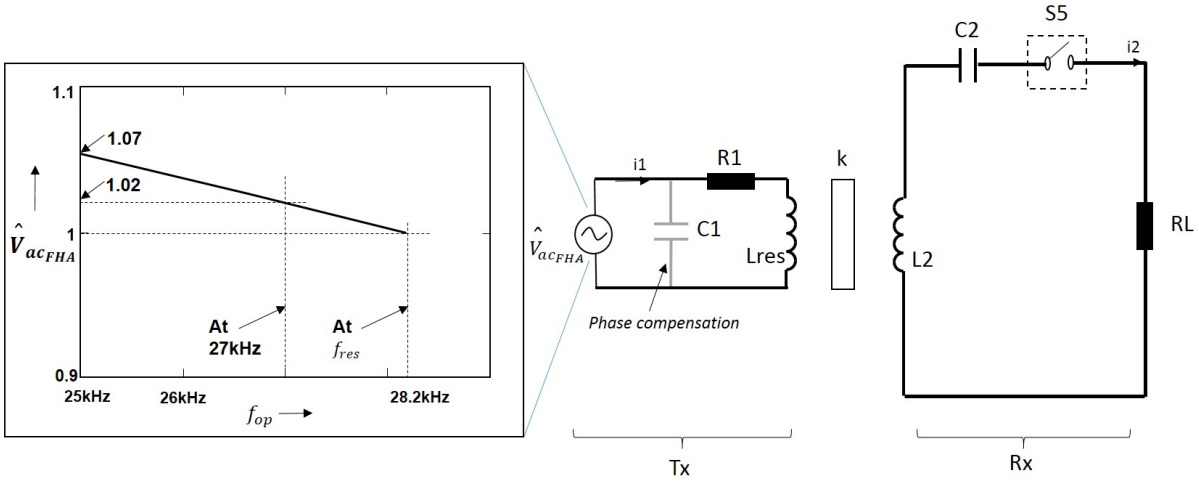

Figure 5-3: Equivalent circuit for CS parallel resonant topology with varying fundamental harmonic source

Another important point to observe is the switch voltage. It can be seen from Figure 5-4 that, the peak voltage ($V_{sw_{peak}}$) appearing across the switches is more than V_{in}. With the help of previously derived relation of the peak amplitude (V_{tx}), it can be calculated that $V_{sw_{peak}}$ is $\pi/2$ times the V_{in} at resonance and it increases further with decrease in the f_{op}, as shown in Figure 5-4.

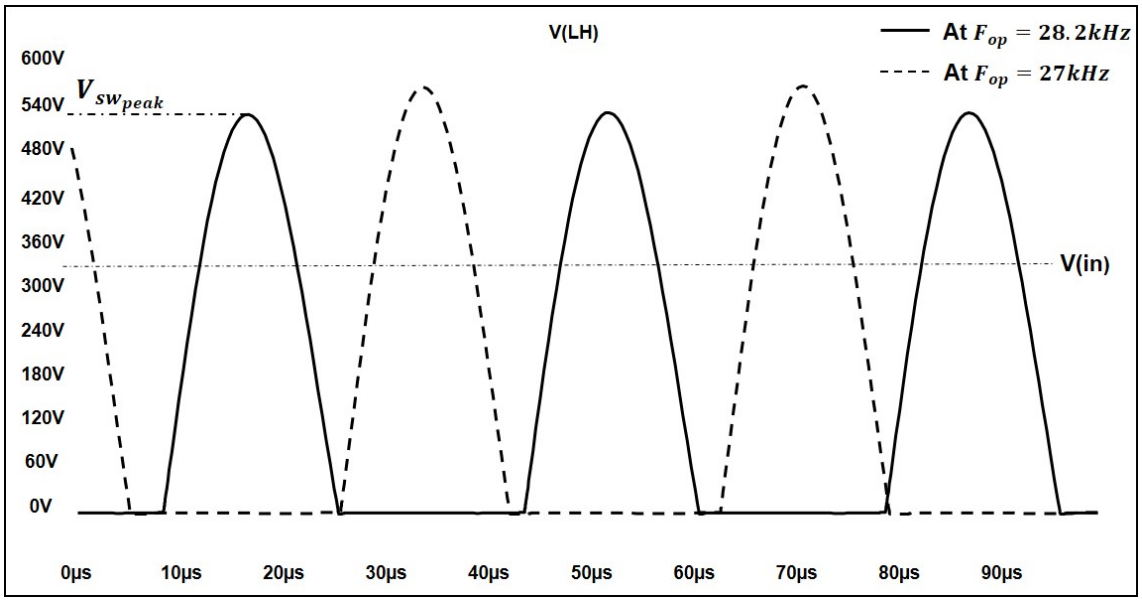

Figure 5-4: Voltage across the switch S_2

5-3 Introducing the communication window

As mentioned earlier in this chapter, it is comparatively difficult to make a communication window in case of the proposed topology. However, one can introduce the communication window with the help of a pre-power stage.

5-3-1 Detailed simulation model

One can perform the time domain simulations of the schematic shown in Figure 5-5 with calculated circuit component values, at operating frequency f_{op}=28.2kHz to observe the transmitter coil voltage. Figure 5-6 shows the time domain simulation for one mains cycle (20ms).

From Figure 5-6 it can be observed that at a particular operating frequency, the power delivered to the load cannot be varied as the proposed inverter topology cannot make use of the duty cycle (D) control. It can also be observed that the transmitter coil voltage varies according to the mains voltage. As discussed in earlier chapters and Appendix I, the cordless kitchen system makes use of 'Time Division Multiplexing' (TDM) for the communication between the transmitter and the receiver. That implies, the voltage across and current through the transmitter coil should be zero when the communication channel is active. Therefore, one

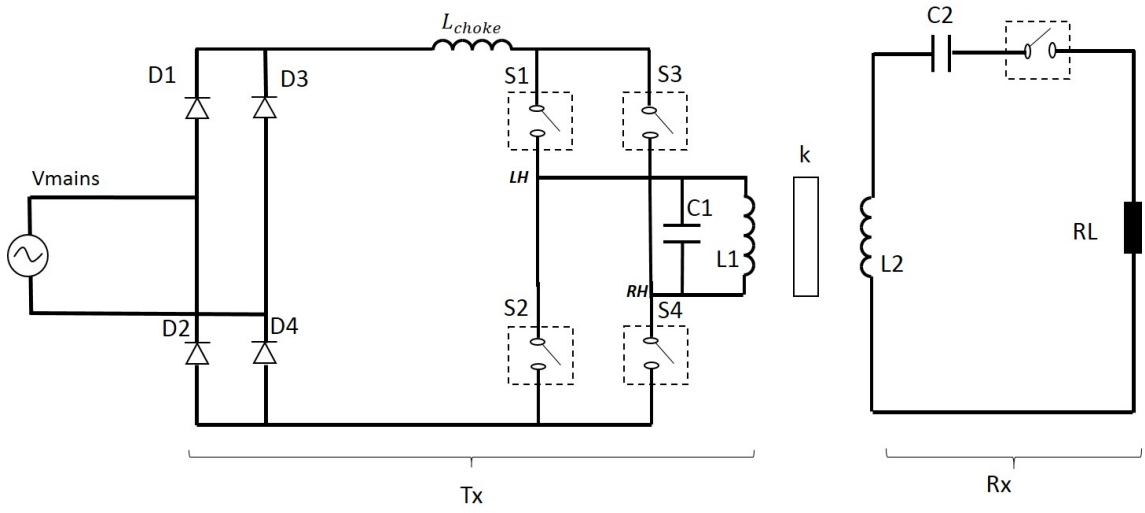

Figure 5-5: CS parallel resonant inverter topology

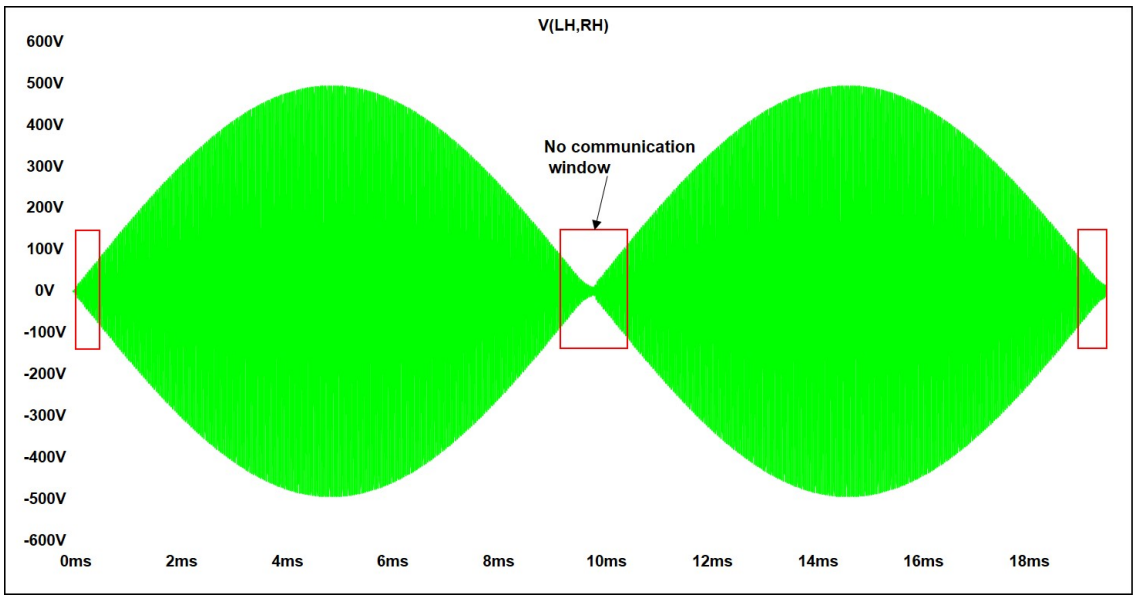

Figure 5-6: Transmitter coil voltage for one mains cycle, L_1=L_2=290uH, L_c=1mH,C_1 = $1/(4\pi^2 f_{tx}^2 L_{res})$ F, $C_2 = 1/(4\pi^2 f_{rx}^2 L_2)$ F R_L= 10Ω, K=0.35, $V_{mains} = 325V50Hz$

has to make sure that the communication window is always present in the power channel near the zero crossings of the mains voltage. To make it possible, one can introduce a buck stage in front of the proposed topology, as shown in Figure 5-7. The detailed schematic is shown in Appendix M.

As shown in the block diagram (Figure 5-7), a PWM signal can be used for the buck power stage operation. The duty cycle (D_{buck}) of this PWM signal can be varied. Therefore, one can get control over the power transferred at a particular operating frequency as well as a communication window near the zero crossing of the mains voltage by employing such a power stage.

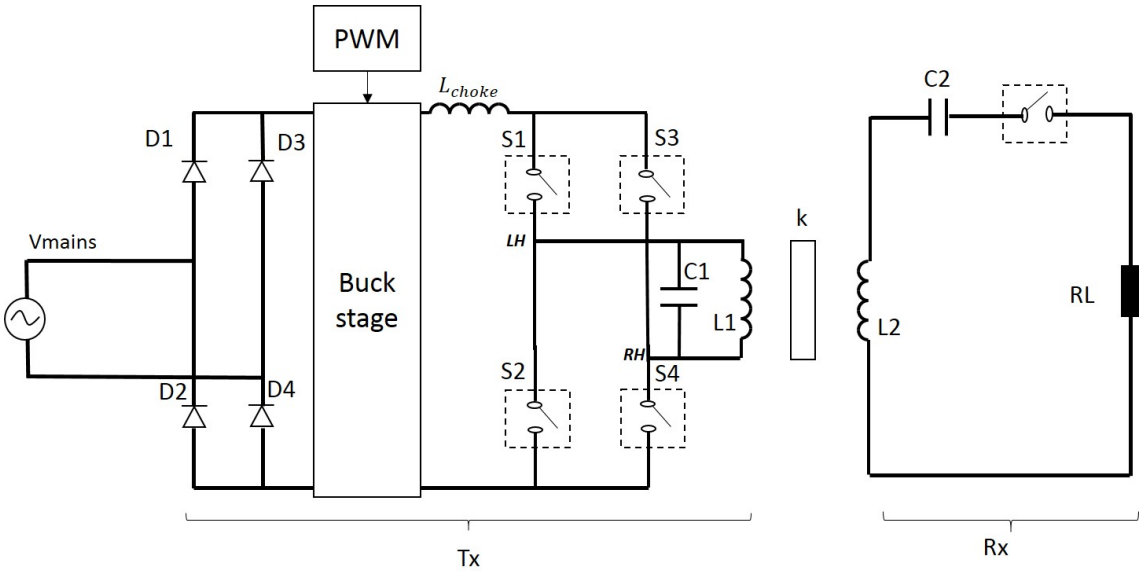

Figure 5-7: Proposed topology with Buck converter stage

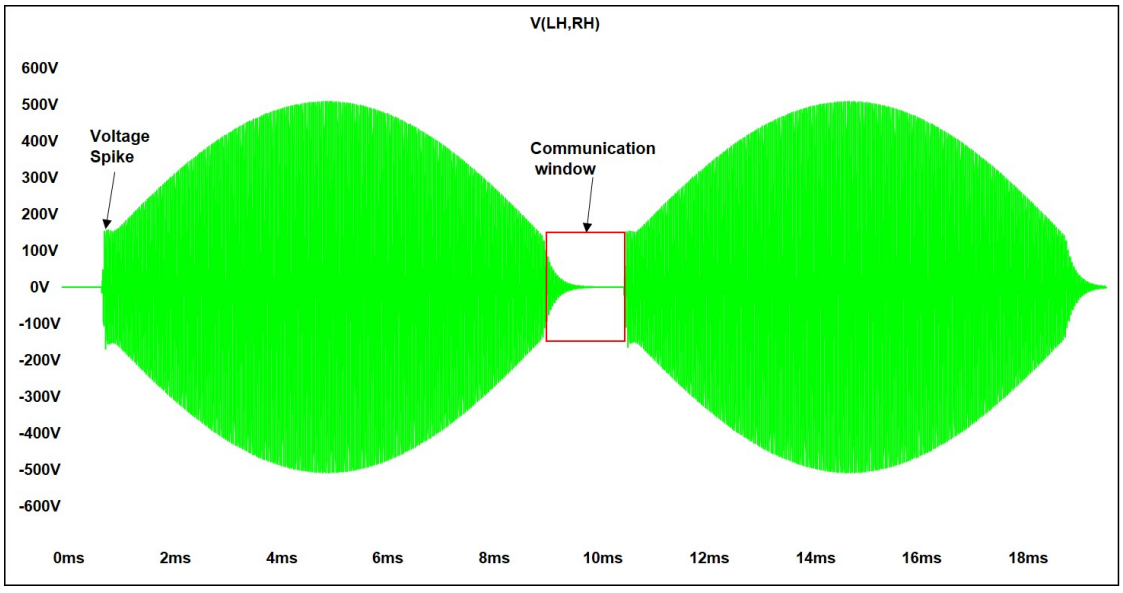

Figure 5-8: Transmitter coil voltage with a communication window, L_1=L_2=290uH, L_c=1mH,$C_1 = 1/(4\pi^2 f_{tx}^2 L_{res})$ F, $C_2 = 1/(4\pi^2 f_{rx}^2 L_2)$ F R_L= 10Ω, K=0.35, $V_{mains} = 325V50Hz$

By varying the duty cycle (D_{buck}) from 0 to 100% one can vary the input voltage for the inverter stage of the transmitter and hence can vary the power delivered to the load. From Figure 5-8 one can observe the voltage spikes when the communication channel is turned off and power channel is turned ON. To avoid these voltage spikes various techniques can be used but more research is required. Considering the scope of this thesis, these techniques are not described in this report.

5-4 Tuneability

The system shown in Figure 5-7 gives an added operational advantage of so called 'tuneability'. In practice, the load applied (R_L) can also change. A change in R_L changes the resonance frequencies (f_{rx} and hence f_{res}) of the system. The maximum efficiency of the power transfer can be achieved when f_{tx} and f_{rx} are equal [3]. Thus, f_{tx} has to be changed to keep the efficiency maximum. A circuit in which the resonant frequency can be controlled is called as a tuneable circuit. The series resonant topology is not inherently tuneable but, it can be made tuneable with the help of additional circuitry comprising diodes and the power switches[3]. The addition of these components can cause additional losses and therefore reduction in the efficiency, which is undesirable. As mentioned earlier, the proposed topology when operated at $f_{op} < f_{res1}$, has an event near the zero crossing of the sinewave, so called the 'freeze time' (T_{freeze}), where the voltage across the transmitter coil of the inductive coupler is almost zero. The relation between f_{op} and the freeze time (T_{freeze}) can be derived from the Figure 5-2 and is given by :

$$T_{freeze} = \frac{1}{2f_{op}} - \frac{1}{2f_{res1}}$$

This freeze time gives the this topology an added advantage of the so-called tuneability. Tuneability can be defined as the ability of the system to operate in resonance or near resonance, without causing significant losses. If the load (R_L) is changed, the resonant frequencies are changed. Due to high sampling time (10msec) of the communication channel, the control loop cannot recognize the load change instantly and f_{op} of the system remains the same for a while. As f_{res1} is changed but, f_{op} is the same, a change in T_{freeze} can be observed. Therefore, a change in R_L is reflected into a change in T_{freeze} without causing any high dV/dt's or loss of ZVS of the power switches. Thus, with the help of the freeze time, the transmitter can apparently be tuned with the receiver and hence to the load changes. Figure 5-9 shows the freeze time, the natural resonance frequency of the system (f_{res1}) and perceived resonant frequency by the receiver.

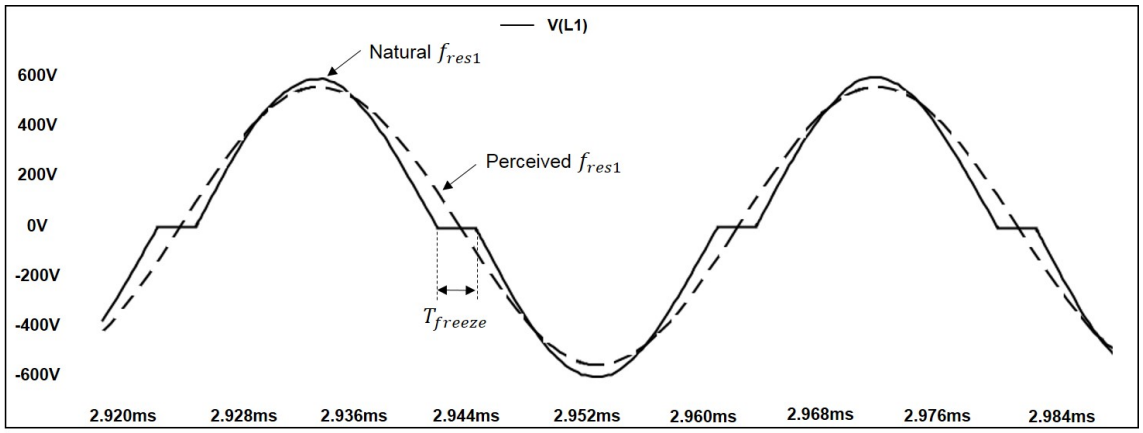

Figure 5-9: Conceptual representation for the perceived resonant frequency by the receiver

Therefore, it can be stated that this topology is inherently tuneable below the f_{res1}. It should also be noted that the increase in T_{freeze} increases the peak voltage across the switches

($V_{sw_{peak}}$) and reduces the efficiency. Thus, for this topology an operating region can be defined with the help of detailed mathematical analysis as shown in Appendix B-2 and Appendix D. Figure 5-10 shows the variation of the efficiency of the system (η) with the normalized operating frequency ($\hat{f}$). The simple equation for the efficiency of the system can be derived as shown in Equation 5-4 [Appendix B-2].

$$\eta = \frac{P_L}{P_P} \tag{5-4}$$

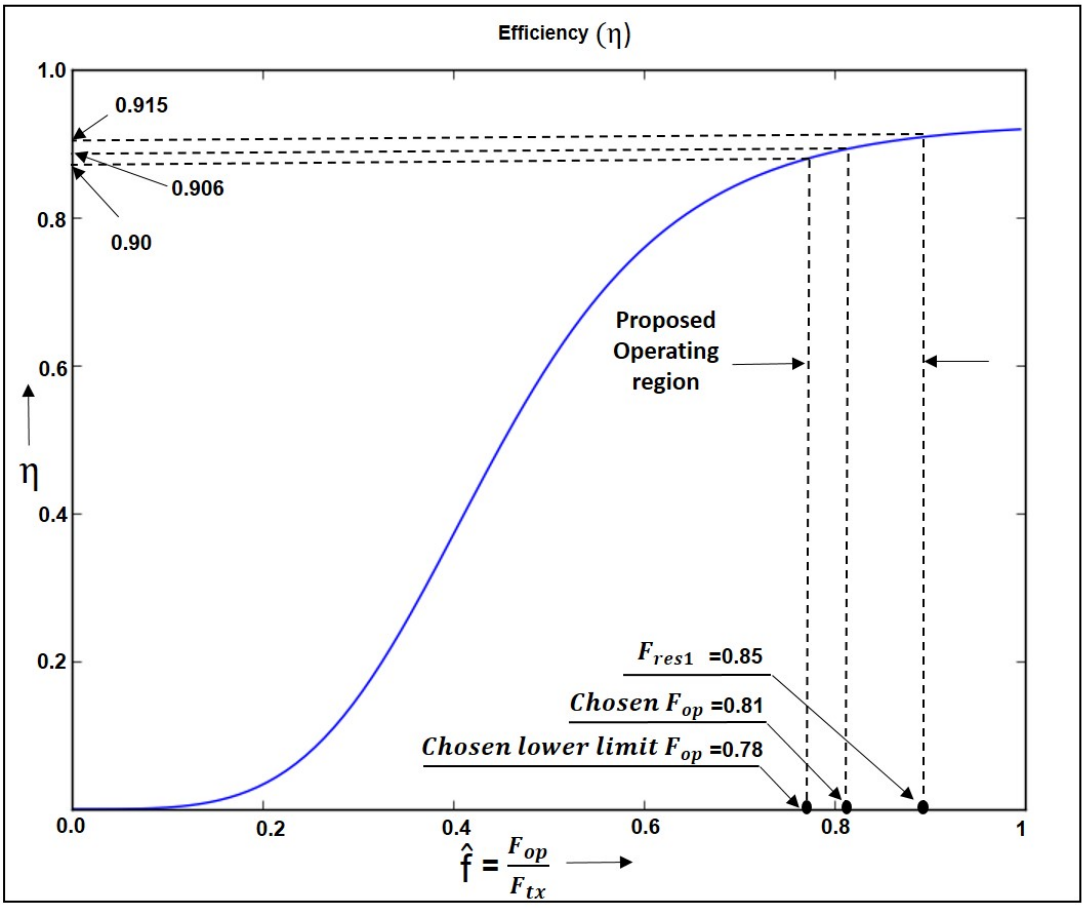

Figure 5-10: Efficiency variation of CS parallel resonant topology

It can be seen from Figure 5-10 that, as the $\hat{f}$ decreases below the f_{res1} the efficiency decreases drastically. Therefore, a lower limit for the operating frequency can be chosen such that at that operating point, the efficiency is 90 percent. In this case, the lower limit for operating frequency is found to be 26kHz. Thus, the proposed operating region for the CS parallel resonant topology is in between 26kHz to 29.2kHz.

Conclusion

The chapter *proposed* the CS parallel resonant topology for the cordless kitchen system, as it is simpler to meet all the non-functional requirements of the system. It explained why CS parallel resonant topology is suitable for the cordless kitchen system with the help of advantages and disadvantages of the topology over other resonant topologies. As explained in chapter 4, for the frequency domain analysis of the system equipped with the CS parallel resonant topology, the source ($\hat{V_{ac}}$) should be modeled accurately. This chapter derived a mathematical model for the source of the system using First Harmonic Approximation (FHA). However, due to confidentiality reasons the complete frequency domain analysis is provided in Appendix B-5 instead of this chapter. Furthermore, the chapter provided a solution to realize the communication window. An added operational advantage of so-called $'tuneability'$ is also described. At the end, the chapter proposed an operating region for the system, derived with the help of an efficiency plot.

Chapter 6

Experimental results

6-1 Introduction

The previous chapters described the cordless kitchen system, its requirements and various possible resonant topologies for the system. It is explained by mathematical analysis why the CS parallel resonant topology can be a good alternative for the presently used VS series resonant topology as the power stage of the transmitter. After proving it mathematically one can proceed with the experimental verification. This chapter provides the details about this experimental verification and shows measurements results regarding EMI. To make a good comparison between the EMI performance of the VS series resonant topology and CS parallel resonant topology, both topologies need to be built and tested. However due to time constraints, it was decided to build and test 60 W versions of the two transmitter topologies, making use of an existing transmitter prototype platform, available in Philips Drachten. With the help of this transmitter prototype platform, alternative designs can be implemented and control parameters can be modified as per the requirements.

6-2 Prototype platform

Figure 6-1 shows the block diagram of the transmitter prototype platform with the VS series resonant topology implemented, including the receiver part. It can be seen from Figure 6-1 that the full bridge VS series resonant topology makes use of a control circuit to manually adjust the operating frequency and the duty cycle. As explained in chapter 2, the frequency control block controls the operating frequency with the help of a phase observer as it is essential to operate the inverter stage of the transmitter in the inductive mode of operation. The duty cycle control block controls the phase shift between the power switches to vary the amount of power delivered to the load. Figure 6-2 shows the block diagram of the transmitter prototype platform with the CS parallel resonant topology implemented. As explained in chapter 5, in case of the CS parallel resonant topology, a pre-power stage can be used to control the power. The pre-power stage is not implemented on the transmitter prototype

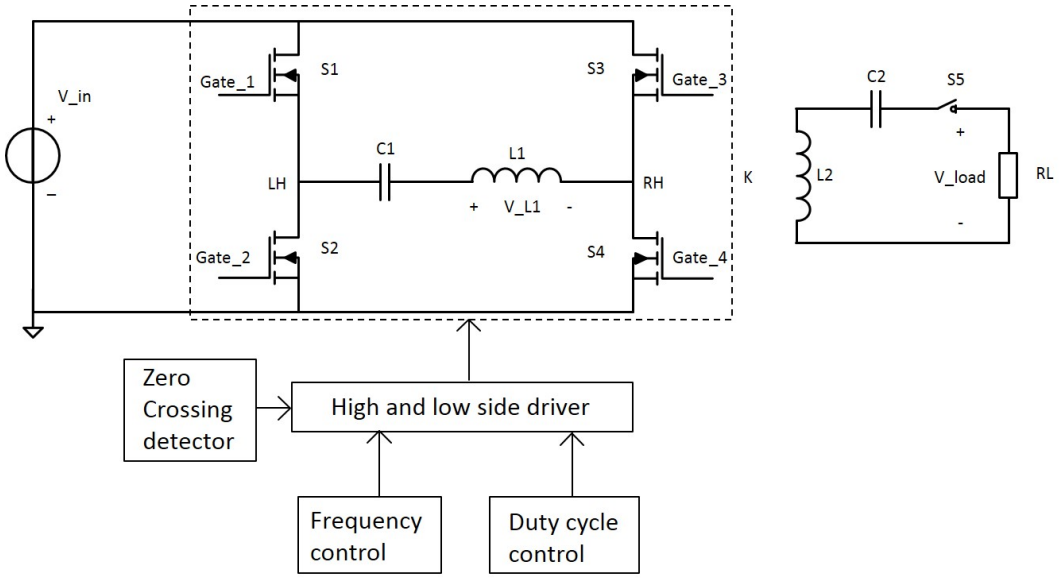

Figure 6-1: The prototype platform with the VS series resonant topology

platform. To control the power of the CS parallel resonant topology the voltage source (Vin) can be adjusted. This has the advantage that the switching noise of the pre-stage is not present in the EMI measurements. From Figure 6-1 and Figure 6-2 one can observe that the transmitter prototype platform also allows to check the system performance under load disconnection case. The load can either be disconnected completely or changed in a stepwise manner.

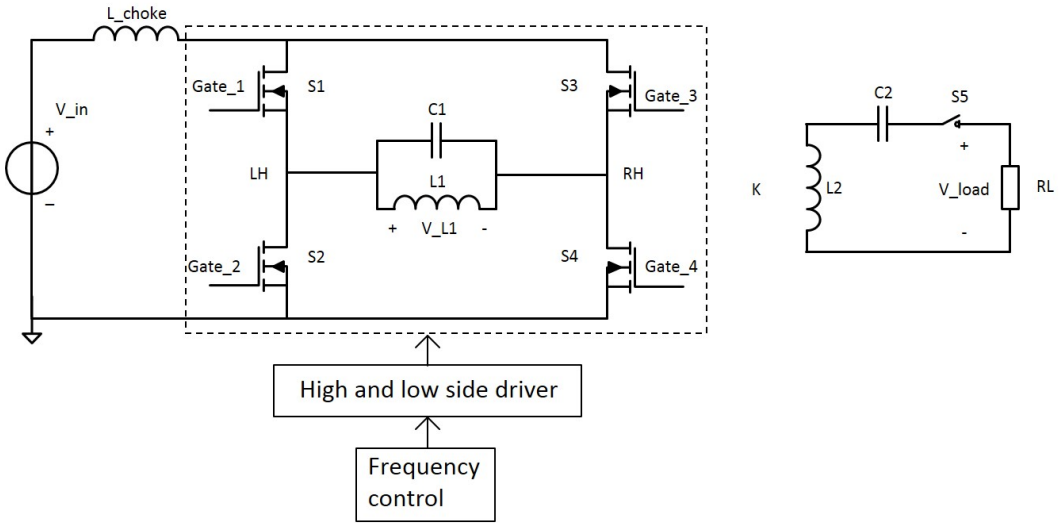

Figure 6-2: The prototype platform with the CS parallel resonant topology

The experimental setup of the CS parallel resonant topology is shown in Figure 6-7. The aim of this low power experimental set-up is to deliver 60 Watts of power to the load resistance (R_L) at a coupling factor of 0.35, in case there is no misalignment between the transmitter and the receiver coils. A standard A10 coil (according to Qi specifications) is used as both the transmitter and the receiver coil [12].

6-3 Measurement of coupling factor

Before proceeding to the tests, one must know the distance between the transmitter and the receiver coil in the experimental setup. As mentioned in the introduction, for the cordless kitchen system the power needs to be delivered to the load at a coil-to-coil distance of maximum 4cm, where the coupling factor equals 0.35. However, both the vertical distance between the coils and the horizontal misalignment between the coils affects the coupling factor, as shown in Figure 6-3[10].

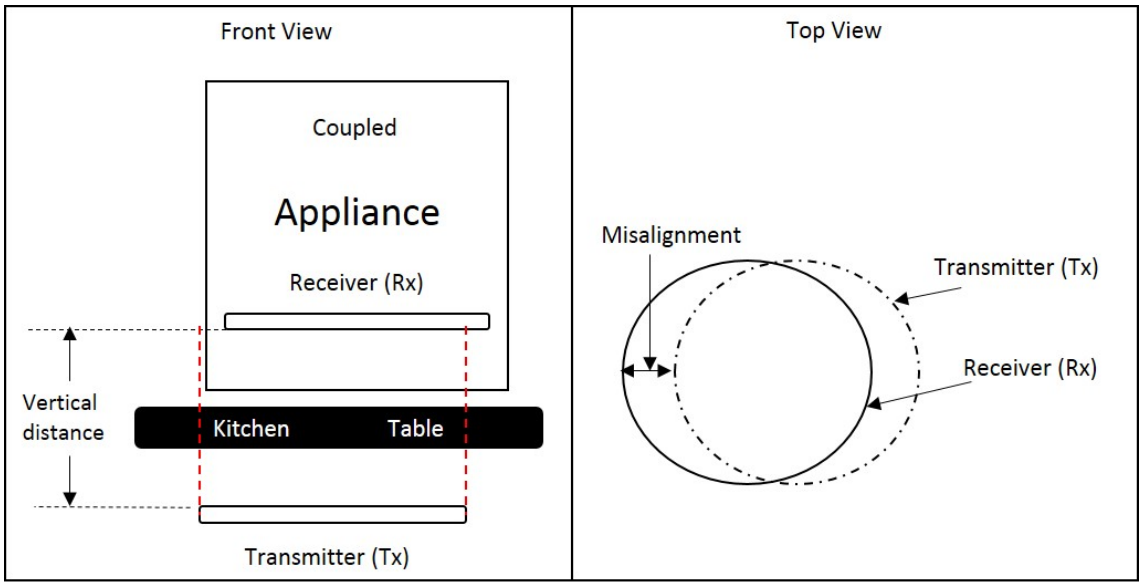

Figure 6-3: Horizontal misalignment of a transmitter coil and a receiver coil

This horizontal misalignment affects the coupling factor and hence the power transfer. One can study the effect of misalignment on the coupling factor as done in [12]. The graph in Figure 6-4 shows the effect of horizontal as well as vertical misalignment on the value of coupling factor. Figure 6-4 shows that to get the maximum coupling factor (i.e.say k=0.99) one should make sure that the vertical distance between the coils is as small as possible, there is no horizontal misalignment between the coils and the coils are of same type. One can observe that though there is no vertical misalignment between the coil, coupling factor (k) varies with the horizontal misalignment. Figure 6-4 shows that coupling factor decreases as the horizontal misalignment increases. It becomes zero at a particular distance, goes into the negative region and comes back to zero again. From the experimental measurements With the standard A10 coils the coupling factor (k) for this system was found out to be 0.35 at distance of 16mm.

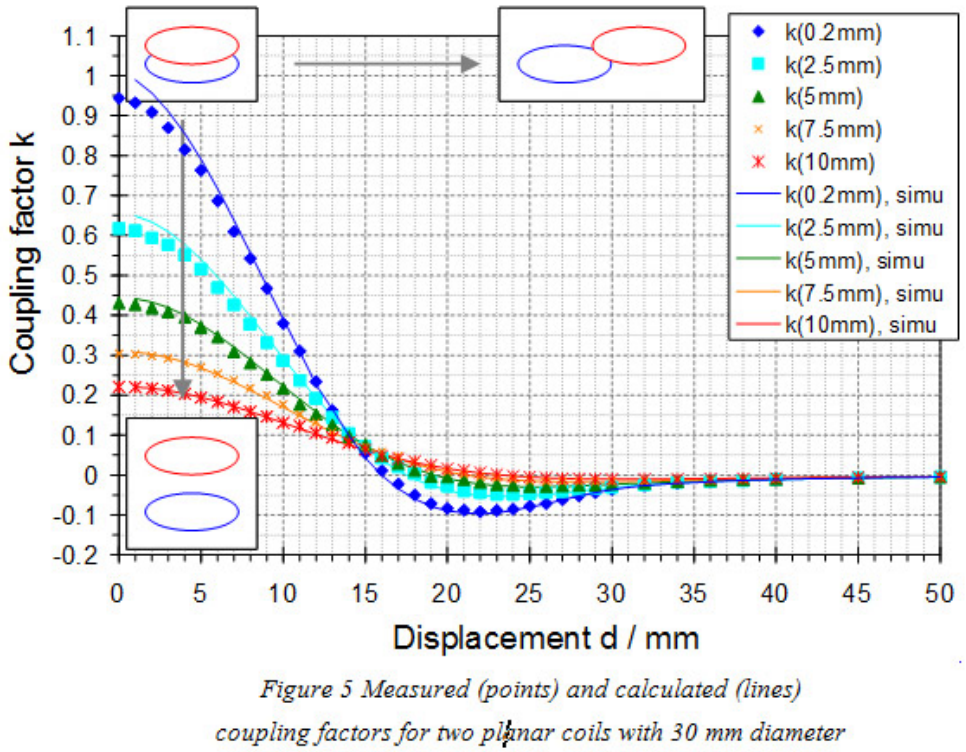

Figure 6-4: Effect of misalignment on the coupling factor[12]

6-4 Scaling the component values

As mentioned in the earlier section, due to time constraints it was decided to make use of the existing 60W transmitter prototype platform, to execute the experimental validations. The topology for the system remains the same however, as the power requirement is scaled down (from 2.4kW to 60 W), one should also scale down the circuit component values. To proceed with that one should decide a new load resistance ($R_{L_{new}}$) and a new operating frequency ($f_{op_{new}}$) for the inverter stage of the transmitter. After that one can make use of the scaling formulae to get the new component values [14]. The new chosen values of $R_{L_{new}}$ and $f_{op_{new}}$ along with the scaling formulae are given below:

$$\begin{aligned} R_{L_{new}} &= 4\Omega \\ f_{op_{new}} &= 135kHz \\ S_m &= \frac{R_{L_{new}}}{R_L} \\ S_f &= \frac{f_{op_{new}}}{f_{op}} \end{aligned} \tag{6-1}$$

where,

$$\begin{aligned} R_L &= 10\Omega \\ f_{op} &= 28kHz \end{aligned} \tag{6-2}$$

Resulting in,

$$\begin{aligned} L_{new} &= L_{old}\frac{S_m}{S_f} = 24uH \\ C_{new} &= \frac{C_{old}}{S_m S_f} = 41.6nF \end{aligned} \tag{6-3}$$

After scaling one can compare the behavior of the system against the behavior of the system with non-scaled component values as mentioned in previous chapters. An example of scaling down the CS parallel resonant system is shown in Figure 6-5. With the help of equivalent circuit shown in the Figure 4-5, one can observe the behaviour of the output voltage (V_{out}) with scaled down (low power version) as well as non-scaled down (high power version) parameters. Figure 6-5 shows the comparison between the output voltage (V_{out}) of the scaled down system (low power version) and non-scaled down system (high power version). One can observe that the scaled down system behaves exactly the same but at higher frequencies. However in this case, to meet the power requirements adjustment of the input voltage source (V_{in}) used. With

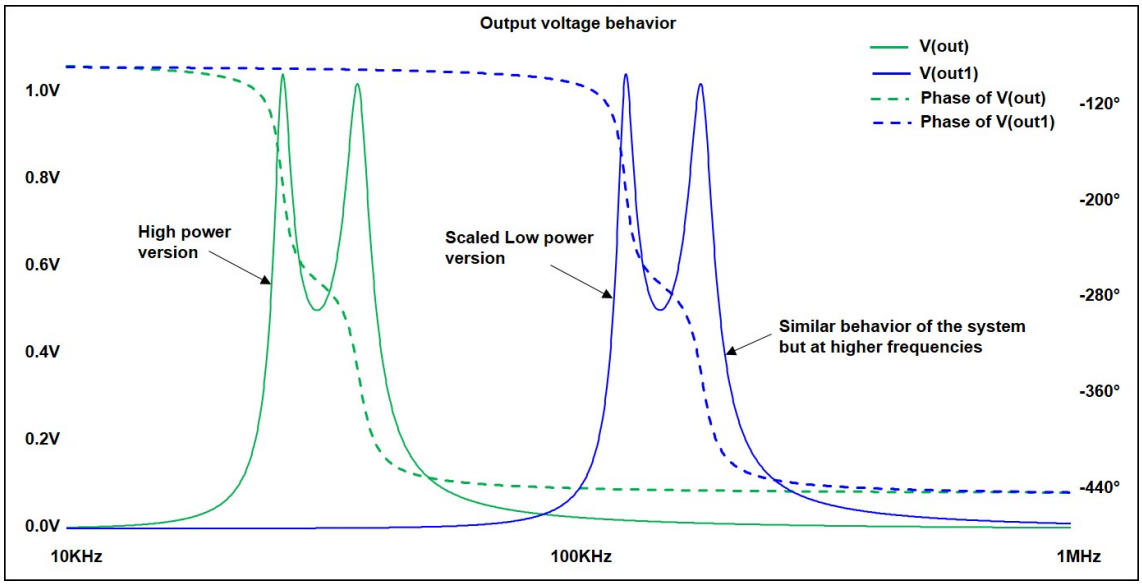

Figure 6-5: Effect of scaling down the component values for low power demo prototype

the help of scaled down circuit component values and the chosen topology shown in Figure 6-2 and Figure 6-1, the PCB of the transmitter prototype platform can be assembled. Figure 6-6 shows an image of the PCB with a transmitter prototype platform with a transmitter coil connected to it.

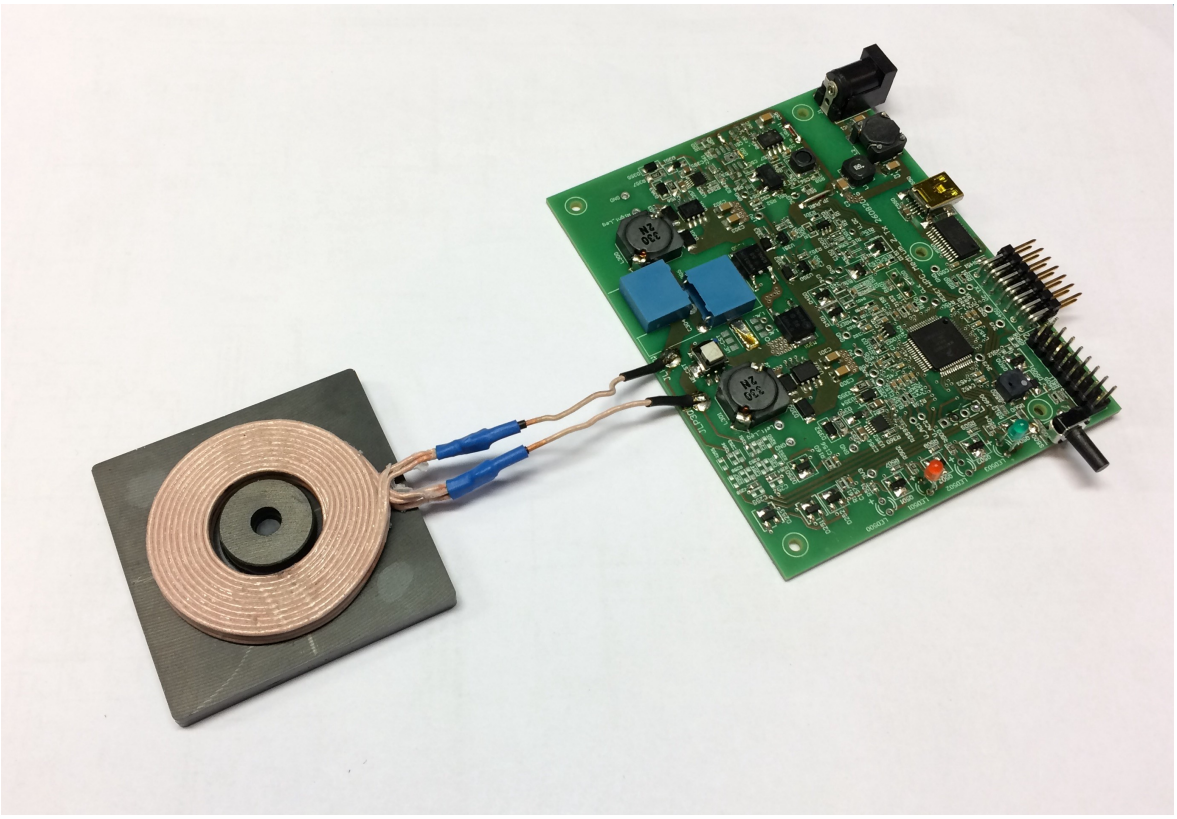

Figure 6-6: PCB-Transmitter prototype platform with CS parallel resonant topology,L_1=L_2=24u, C_1=C_2=41.6nF, f_{res1}=145kHz, $f_{op_{new}}$=135kHz, $R_{L_{new}}$=4 Ω, P_{out}=60W [10]

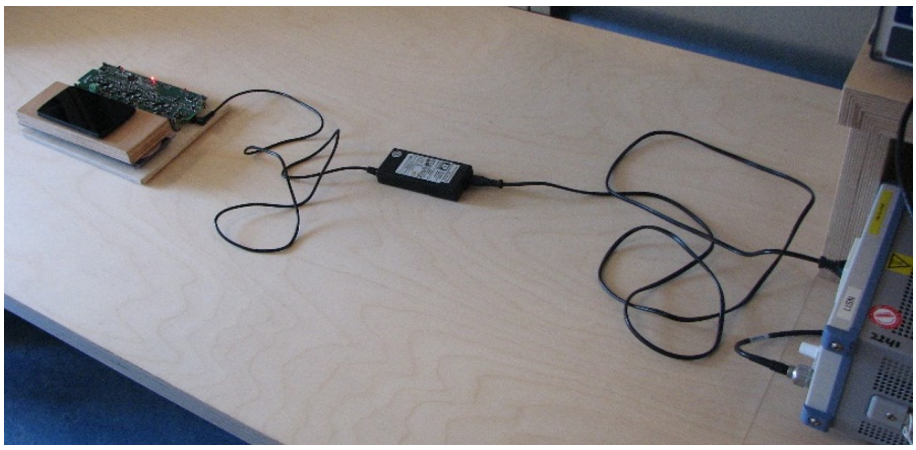

Figure 6-7: EMC Measurement setup- Transmitter prototype platform with CS parallel resonant topology[13]

6-5 EMI measurements

The 60 Watts low power experimental setup of both the VS series resonant topology and the CS parallel resonant topology have been tested according to the standard CISPR14-1

for EMC. Figure 6-7 shows the experimental set-up. Figure 6-8 and Figure 6-9 shows the EMC measurements recorded for the VS series resonant topology and the CS parallel resonant topology, respectively.

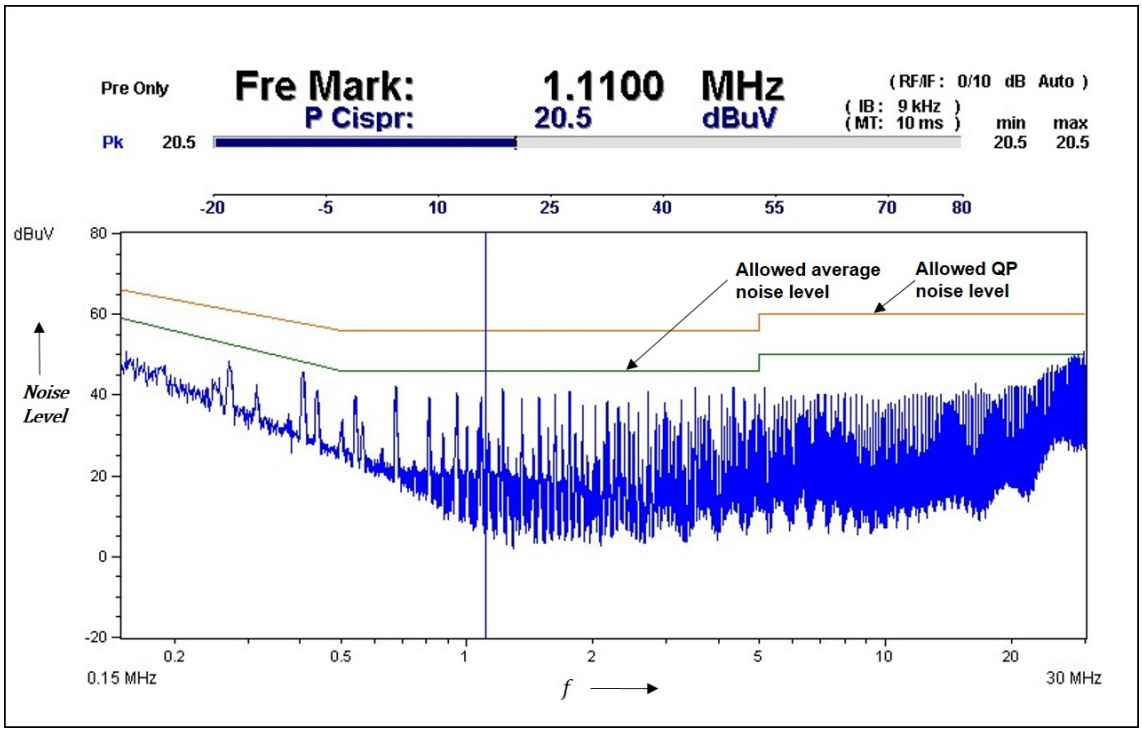

Figure 6-8: EMC measurements: Series resonant topology, f_{op}=135kHz, P_{out}=60W[10]

Both the figures shows the maximum allowed noise level for the quasi peak (QP) noise measurement according to CISPR14 (uppermost line) and maximum allowed noise level for the average noise measurements according to CISPR14 (middle line). As per expectations, one can observe from Figure 6-9 a considerable reduction (about 10dBuV) in the high frequency noise level in case of the proposed topology. It indicates that for the same amount of power transfer with the proposed topology, the size of the mains filter can be reduced.

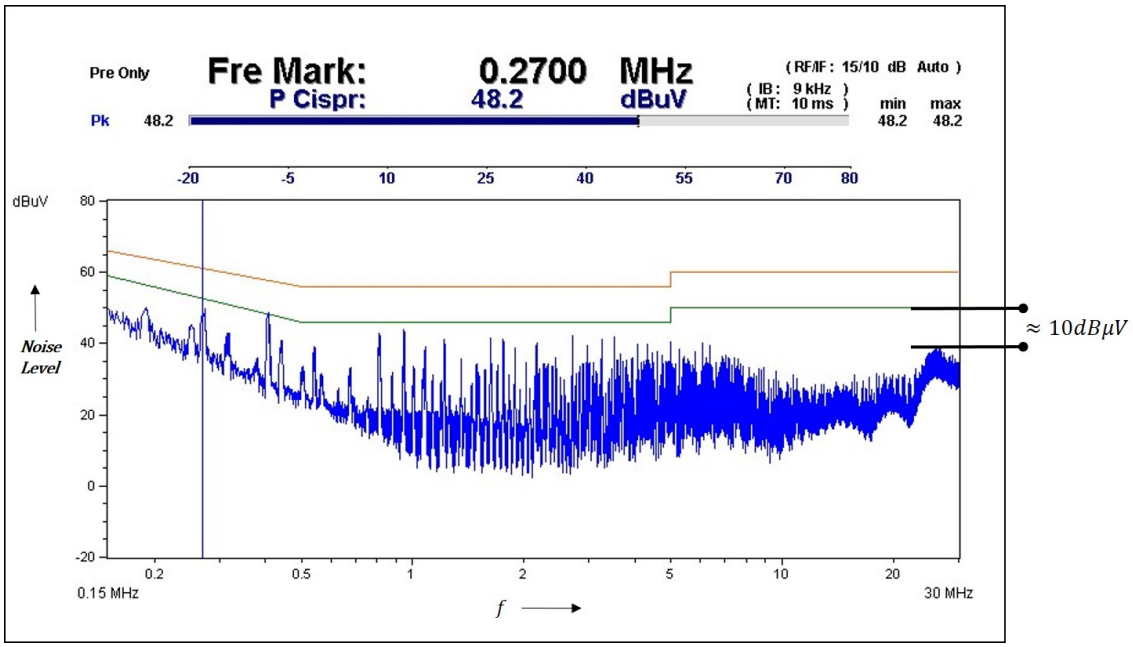

Figure 6-9: EMC measurements: CS parallel resonant topology, f_{op}=135kHz, P_{out}=60W[10]

Conclusion

The chapter describes the validation of the EMI performance of both the VS series resonant topology and the CS parallel resonant topology. The EMI measurements were executed in the EMC lab of Philips Drachten. For the measurements a low power (60 W) transmitter prototype platform was used to build a VS series resonant inverter and a CS parallel resonant inverter. With the help of scaling formulae, the circuit component values for the low power design (60 W) were derived from the high power design (2400 W). The measurements show that for the same output power, Tx and Rx coil types and coupling factor, the CS parallel resonant inverter has a lower noise level compared to the VS series resonant inverter. Furthermore, the chapter shows that the experimental measurements and analytical measurements can be related with each other and hence the mathematical model derived in previous chapter provides good results.

Chapter 7

Conclusion

The thesis explained the basic principle of the cordless kitchen system along with its requirements. There are functional as well as non-functional requirements. The present series resonant topology for the transmitter has the drawback that it is harder to meet the non-functional requirements. With the help of mathematical analysis as well as the simulations, the thesis proposed 'current source parallel resonant' topology which can meet the non-functional requirements more easily in the proposed operating region. From the mathematical analysis of all the topologies, voltage or current transfer functions can be derived [2], as shown in the Appendix A-2, A-4, B-1 and B-2. The order of characteristic equation is very important from the control point of view. The more poles in the system, the more difficult it is to control. It can be seen that, these transfer functions are of the order four, five and three for series, VS parallel and CS parallel (below f_{res1}) topologies, respectively. Thus, it is easier to control CS parallel topology when operated below f_{res1}. From the detailed analysis of all the topologies explained in Chapters 2 to 5, various other factors can be noted down, as shown in Table 7-1.

Table 7-1: Comparison of different topologies

	Series topology	VS parallel topology	CS parallel topology (in proposed region)
High dV/dt at choke coil	No Choke coil	Yes	No choke coil
High dV/dt at transmitter coil	Yes	No	No
Voltage across power switches	V_{in}	V_{in}	$(\pi/2)$*V_{in} or more
Over voltage on load removal	Considerable	Considerable	Not considerable
Use of duty cycle control	Possible	Possible	Not possible
Loss of ZVS	Possible	Not possible	Not possible
Control	Comparatively difficult	Comparatively difficult	Comparatively simpler
Intrinsic tuneablility	No	No	Yes

Table 7-1 shows that though the series resonant topology is easy to implement and widely used,

it possesses some drawbacks when applied in the cordless kitchen system. It has advantages like use of the low voltage switches, easy power control but, overvoltage and EMI are the undesired properties. These undesired properties can be overcome by using a fast frequency control loop and additional complex circuitry [3]. But as explained earlier, it is difficult to make a fast frequency control loop and the circuitry required to make the system tuneable, affects the efficiency of system.

The VS parallel resonant topology also possesses the advantages like use of duty cycle control to control the power delivered to the load, use of low voltage rating switches etc. However, it also possesses the drawback of high dV/dt's across the choke coil which offers relatively poor EMI performance.

The thesis showed that CS parallel topology can be the suitable topology for the cordless kitchen system, as it satisfies all of the non-functional requirements of the system more easily. The most important advantage of this topology is the intrinsic tuneability when operated at frequencies (f_{op}) below the system resonance frequency (f_{res1}). High dV/dt's do not occur, which offers good electromagnetic compatibility. From the experimental results it is evident that CS parallel resonant topology has better EMC than the present series resonant topology. In case of the load disconnection, the voltage across the transmitter does rise but the rise is not considerable. The topology offers inherent overvoltage protection which keeps the voltage rise within the safe limits. It eliminates the requirement of a complex control system. Also, an added operational advantage of the tuneability can help in meeting the functional requirements. The only disadvantages of the proposed topology are:

- Introduction of T_{freeze} increases the conduction losses in the power switches.
- Requirement of high voltage rating power switches (more than $2V_{in}$).
- Loss of control over the delivered power, as duty cycle control cannot be used.

For minimizing the conduction losses one can operate the inverter stage of the transmitter with the proposed topology close to the resonance frequency of the system (f_{res1}). This also reduces the peak voltage across the power switches. To control the amount of power delivered to the load, one can employ a pre-power stage on the transmitter side to vary the input voltage (V_{in}) or a post-power stage on the receiver side to vary the load voltage (V_{load}). Finally, the thesis presented a system model of current source parallel resonant topology equipped with a pre-power stage (buck converter) on the transmitter side. The time domain simulations of the proposed system model showed that with the help of the buck power stage, the power delivered to the load can be controlled and a communication window can be maintained. Therefore it can stated that, the proposed topology meets the non-functional requirements of the system without affecting the functional requirements of the system. Thus, it can be concluded that for the cordless kitchen system, the operation of the current source parallel resonant topology in the proposed operating region can be a good alternative to the present topology.

Chapter 8

Publication

Topology study for an Inductive Power Transmitter for Cordless Kitchen Appliances

Mahesh Itraj[1] and Will Ettes[2]

Abstract— **In a conventional kitchen an appliance may require over 2.4kW of power during normal operation. In a cordless kitchen the used appliances are cordless, so this power needs to be transferred over a distance of at least 4cm, at high efficiency. Therefore an inductive power system needs to be installed with an inductive power transmitter below the table countertop and an inductive power receiver inside the appliance. Next to the inductive power system the cordless appliance is also equipped with a communication channel. There are many transmitter topologies which can satisfy the functional requirements (like amount of power transferred, high efficiency, etc.) of the inductive power system. But satisfying the non-functional requirements (like EMI) most often takes several design iterations. Presently, a transmitter based on a series resonance principle will be the first choice of the designer because it is relatively simple to understand and can satisfy the functional requirements of the system easily. The aim of the paper is to describe the present choice for the transmitter and to explain a new transmitter topology that can intrinsically minimize the problems associated with the present choice. The paper proceeds with a brief introduction about the cordless kitchen concept, in section I. Section II gives the description and analysis of the presently used topology in the system. The requirements of a new transmitter topology are explained in section III and a new transmitter topology along with its analysis, is proposed in Section IV. Section V explains the experimental measurements and gives the comparison between the present and the proposed topologies. The conclusion is stated in section VI.**

I. INTRODUCTION

An alternating current flowing through a coil produces its own alternating magnetic field. If another coil is placed in the proximity of the first one then, this alternating magnetic field gets linked to it. Such an arrangement of the coils is called as an inductive coupler. In a cordless kitchen the inductive coupler consists of a transmitter coil and a mutually coupled receiver coil. The transmitter coil is located beneath the counter top of the kitchen table, whereas, the receiver coil is located inside an electrical appliance, as shown in Figure 1.

As shown in Figure 1, the system operates with the help of two channels: a power channel and a communication channel. The power transfer is executed by the power channel, whereas the information or data exchange is done using the communication channel. The power transfer and the communication is done at a coil to coil distance of 4cm. One of the operating principles for the power channel is Inductive Power Transfer (IPT). This principle is used in kitchen appliances which are equipped with a motor or a resistive heating element. A food processor or an oven are good examples of appliances working according to the IPT principle. The basic block diagram of the IPT power channel is shown in Figure 2. The IPT power channel consists of an AC source, an AC-AC conversion stage, a resonant inductive coupler, an AC-DC conversion stage (optional hence shown as dotted block) and a load. The AC-AC conversion stage along with the transmitter coil of the resonant inductive coupler is called the transmitter (Tx). The receiver coil of the resonant inductive coupler along with the AC-DC conversion stage (optional) and the load is called the receiver (Rx). The transmitter and the receiver coils are mutually coupled to each other with a certain coupling factor (k). The mains voltage is converted to a high frequency AC voltage by the AC-AC conversion stage. Due to the inductive coupling, the high frequency AC voltage is induced on the receiver side. This induced voltage can be converted to a DC voltage with the help of AC-DC conversion stage. The load can be a DC motor or simply a resistor.

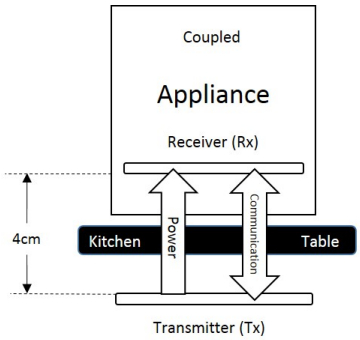

Fig. 1. Introduction to the cordless kitchen concept

In order to get the maximum system efficiency, the principle of resonance is used in the inductive coupler. To achieve this resonant nature, different combinations of interconnections of both the coils (L) and the capacitors (C) can be used. These different combinations are known as topologies. Each topology has its own operating principle with advantages as well as disadvantages, depending on the application.

*This work was supported by Philips Consumer Lifestyle B.V. and TU Delft

[1]Mahesh Itraj is with Faculty of Electrical Engineering, Mathematics and Computer Science, Delft University of technology, 2628 CD Delft, The Netherlands, Email: itraj.mahesh@gmail.com

[2]Will Ettes is with the Technical Expert Group, Philips Consumer Lifestyle B.V., 9206 AD, Drachten, The Netherlands, Email: w.ettes@philips.com

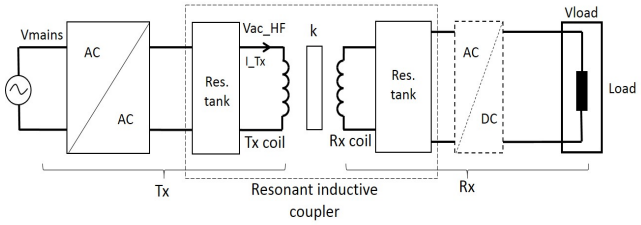

Fig. 2. IPT with motor

II. Present topology

Figure 3 shows the topology which is used in the present inductive power system. This system has the series resonance principle applied in the transmitter as well in the receiver side.

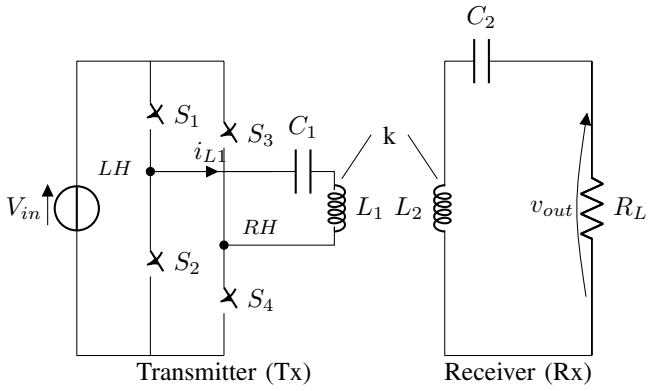

Fig. 3. Series resonant topology

A. Description of present topology

In Figure 3, V_{in} is the DC voltage obtained after rectifying the mains voltage. As mentioned earlier, the transmitter is nothing but the AC-AC conversion stage comprising V_{in}, an inverter stage and a resonant tank comprising of the series connection of the transmitter coil (L_1) and a capacitor (C_1). On the other hand, the receiver comprises of the receiver coil (L_2) and a capacitor (C_2) connected in series with the load (R_L).

If the transmitter (Tx) is powered, in the absence of the coupling (k), it has its natural resonant frequency (f_{tx}). Similarly, in the absence of the coupling (k), the receiver (Rx) has its natural resonant frequency (f_{rx}). In practice, the f_{tx} and f_{rx} are chosen to be equal [3] and the coupling factor (k) between the transmitter coil (L_1) and the receiver coil (L_2) is in the order of 0.1 to 0.35. Therefore, the whole inductive power system has its natural resonant frequency or frequencies (f_{res}). For low coupling factors the f_{tx} and f_{rx} are merged into a single resonant frequency f_{res}. For higher coupling factors the f_{tx} and f_{rx} frequencies are moved away from each other, resulting in f_{res1} and f_{res2}. The inverter stage of the transmitter can be operated at different operating points (f_{op}). Choosing the optimal f_{op} for the inverter is an important task because the high frequency AC voltage is applied to the transmitter coil, with the help of the power switches. Thus, one has to make sure that Zero Voltage Switching (ZVS) for the power switches is applied, avoiding high dV/dt's in the inverter stage. Therefore, in this case, the optimal f_{op} is chosen where the efficiency is maximum and input current (I_{L1}) is slightly lagging the inverter bridge voltage (V(LH,RH)). With the help of the mathematical analysis, one can determine the optimal operating frequency for the inverter stage of the transmitter, using the particular values of the circuit components shown in Figure 3 [2]. In the present topology, with the help of a frequency control loop the f_{op} can be varied to achieve the maximum efficiency for the power transfer. Furthermore, at a particular f_{op} the amount of power transfer can be controlled with the help of the duty (D) cycle control.

B. Analysis of present topology

The mathematical analysis along with time domain and frequency domain simulations of the series resonant topology is discussed in this section. The mathematical analysis can be used to derive the different transfer functions. The frequency domain simulations can be used to observe the bode plots of important parameters like impedance, input voltage (or current), output voltage (or current), etc. The time domain simulations can be used to observe the instantaneous voltages across and current through the different circuit components. For the time domain simulations, it should be noted that as the present topology is voltage source driven, there should be a 'dead time' between the switches of the same bridge leg. To proceed with the analysis following (realistic) values are chosen:

- f_{tx} = f_{rx} = 33 kHz
- L_1 = 290 uH
- L_2 = 290 uH
- C_1 = 1/$(4\pi^2 f_{tx}^2 L_1)$ F
- C_2 = 1/$(4\pi^2 f_{rx}^2 L_2)$ F
- k = 0.35
- R_L = 10 Ω
- V_{in} = 325 V DC (for time domain)
- V_{ac} = 1 V AC (for frequency domain)

1) Mathematical analysis: From Figure 3, a simplified equivalent circuit can be derived for the mathematical analysis as shown in Figure 4.

In the above circuit, R_1 represents the equivalent series resistance of the transmitter coil (L_1) along with the equivalent series resistance of the capacitor C_1. R_2 represents the load resistance along with the equivalent series resistance of the receiver coil (L_2) and the equivalent series resistance of the capacitor C_2. V_{12} represents the voltage induced in the transmitter coil due to the mutual inductance (say, M) and the current flowing through the receiver coil (i_2). V_{21} represents the voltage induced in the receiver coil due to the mutual inductance and current flowing through the transmitter coil (i_1).

With the help of Laplace transform and transformer theory, the voltage transfer function can be derived [2]. From the

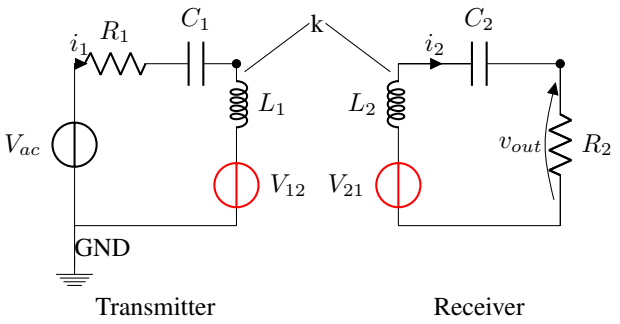

Fig. 4. Simplified equivalent circuit of present topology

$$\frac{V_{out}}{V_{ac}} = \frac{S^3(R_2C_2MC_1)}{S^4(-M^2C_1C_2 + L_1C_1L_2C_2) + S^3(L_1C_1R_2C_2 + R_1C_1L_2C_2) + S^2(R_1C_1R_2C_2 + L_2C_2 + L_1C_1) + S(R_2C_2 + R_1C_1) + 1}$$

above equation, it should be noted that the order of characteristic equation (denominator) is four. Consequently, it is called as 4^{th} order system. The roots of the characteristic equation converges to the resonance frequencies.

With the help of the derived transfer function, frequency domain simulations can be performed. Figure 5a shows the bode plot for the power delivered to R_2 whereas, Figure 5b shows the variation of the efficiency w.r.t. operating frequency. Figure 5a shows two resonant peaks. Thus, the transmitter can be operated at, or near two resonant frequencies for the maximum power transfer. There are two falling edges and two rising edges. The frequency control loop can operate either on the falling edge or on the rising edge. In any case, there are two operating points at which the gain is the same but the efficiency can be different.

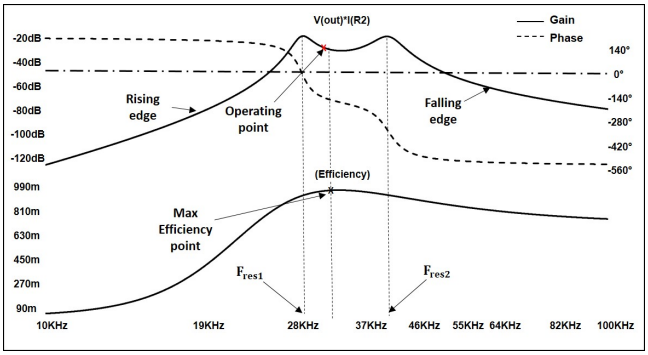

Fig. 5. Relation between output power and efficiency of power channel

From the marked crosses in Figure 5, it can be seen that the operating point for the maximum power gain and maximum efficiency is not the same. The maximum efficiency point lies in between the two resonant peaks.

2) Detailed analysis: As mentioned earlier, for this system the optimal operating point, where the efficiency is maximum and input current (I_{L1}) is slightly lagging the inverter bridge voltage (V(LH,RH)). can be calculated with the help of mathematical analysis as shown in [2]. For this topology and the calculated values of circuit components, the optimal operating point (f_{op}) can be calculated to be 32.7kHz[2] and the frequency control loop operates on the falling edge. At the calculated f_{op}, the time domain simulations can be performed.

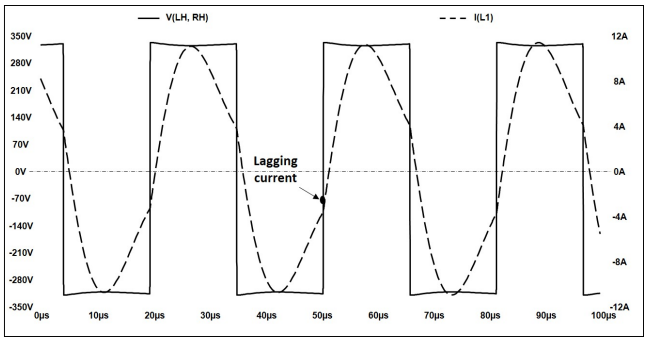

Fig. 6. Operation of the system at the calculated f_{op}, D=100%

Figure 6 shows the voltage across the inverter stage of the transmitter (V(LH,RH)) and the input current (I(L_1)). The lagging current indicates the system operating in an inductive mode. The inductive mode of operation is always preferred to get the advantage of Zero Voltage Switching (ZVS) of the power switches. ZVS of the power switches improves the efficiency of the system by minimizing the switching losses. Due to ZVS the voltage across the switches rises steadily, (i.e. no high dV/dt's) minimizing the EMI problem. As mentioned earlier, at a particular f_{op} the duty cycle (D) control is used to control the power delivered to the load. Figure 6 shows the waveforms for D=100%. Figure 7 shows the same waveforms but at D=50%. It can be observed from Figure 6 and Figure 7 that, introduction of duty cycle control results in loss of ZVS. The loss of ZVS causes high dV/dt on the corresponding node.

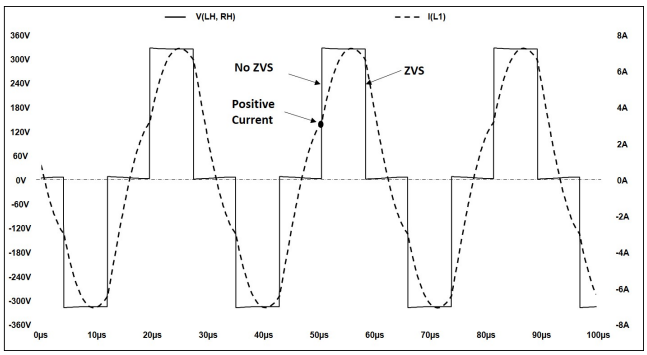

Fig. 7. Operation of the system at the calculated f_{op}, D=50%

Figure 8 shows the voltage across the transmitter coil, when f_{op}<f_{res1}, f_{op}=f_{res1} and f_{op}>f_{res1}. It can be clearly noted that high dV/dt's are observed in all the three cases.

These high dV/dt's may create a changing electric field between the node which carries the high dV/dt and surrounding conducting components, which has some kind of capacitive coupling to the environment. This can cause common mode currents to flow from the system to the environment and

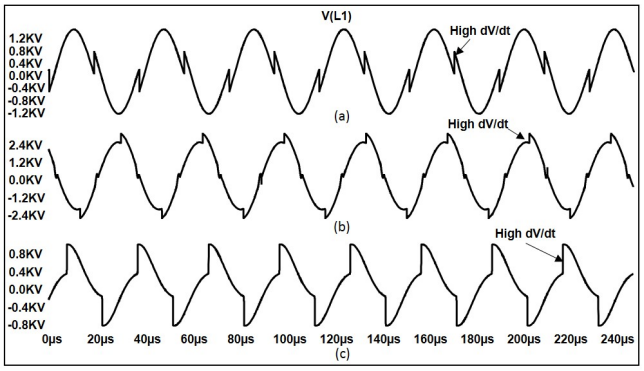

Fig. 8. Voltage across transmitter coil (a)f_{op}<f_{res1}, (b)f_{op}=f_{res1} and (c)f_{op}>f_{res1}, D=100%

back via the mains, causing common mode noise emission, as shown in Figure 9

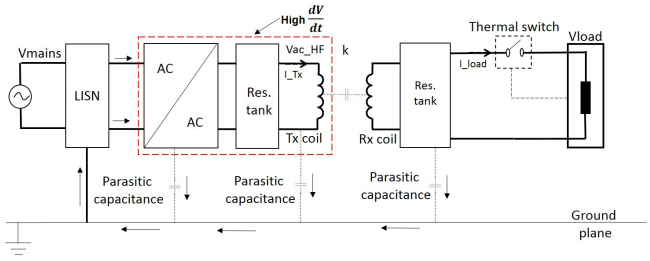

Fig. 9. Block diagram for the representation of common mode current flow

There are many protective means of reducing the common mode noise but, often these require additional and expensive components, like filters.

Another important point to note, is the voltage across the inverter power switches. From Figure 3, the peak amplitude of V_{in} can be expected and observed across the inverter power switches, irrespective of the load changes. Therefore, one can state that:

$$V_{sw_{peak}} = V_{mains_{peak}}$$

III. Requirements of the System

In the previous section, the presently used series resonant topology is discussed in detail. It is capable of transferring the power at high levels (kW) at high efficiency but it is difficult to meet the non-functional requirements of the inverter stage, i.e. EMI. In the cordless kitchen system, the transmitter (Tx) remains the same and the receiver (Rx) changes, depending on which appliance is located on the table top. Thus, it is beneficial if the drawback of the cordless kitchen system is minimized by modifying only the transmitter side. Thus, in the further studies different topologies for the transmitter are analyzed keeping the receiver part the same. The basic requirement from the new transmitter topology is to meet all the non-functional requirements intrinsically without compensating for the efficiency .

As mentioned earlier, the duty cycle control might result in the loss of ZVS of the power switches resulting in high dV/dt's at the bridge nodes. The change in the input current w.r.t. time (dI/dt) as well as the change in the voltage across the transmitter coil w.r.t. time (dV/dt) may create electromagnetic interference (EMI) problems. This gives rise to the first requirement of the system: having a low EMI.

Thus, one can summarize the requirements for the transmitter topology as, functional requirements:

- Power transfer upto 2.4kW
- Efficiency $> 90\%$
- Simple control system

and the most important non-functional requirement:

- Low EMI

Based on these requirements a new topology is identified and analyzed in further sections.

IV. Proposed Topology

Figure 10 shows the proposed topology which might be easier to meet the non-functional requirements. An attempt is made to meet the functional and non-functional requirements by modifying the transmitter side. And the best suitable topology is presented further in this section.

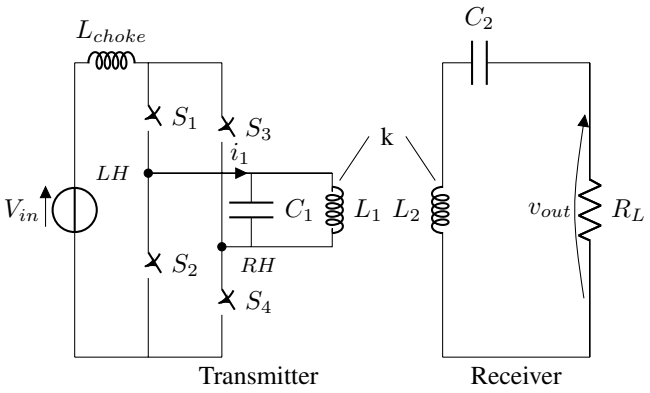

Fig. 10. Current source parallel resonant topology

A. Description of Current Source parallel resonant topology

Figure 10 shows the current source (CS) parallel resonant topology. L_{choke} is placed at the DC side of the inverter stage to realize a current source driven parallel resonant inductive coupler. It should be noted that, as it is a current source driven topology, there should be some 'overlap time' between the switches of the same bridge leg. Again, to analyze the properties of this topology, mathematical analysis together with the simulations in the time and frequency domain are performed. It can be observed that, due to the presence of L_{choke} it is harder to perform the frequency domain simulations for this topology. One can reduce the circuit with the proper mathematical analysis and proceed with the further evaluation. In this case, to proceed with the analysis following (realistic) values are chosen:

- f_{tx} = f_{rx} = 33 kHz
- L_1 = 290 uH

- L_2 = 290 uH
- C_1 = $1/(4\pi^2 f_{tx}^2 L_{res})$ F
- C_2 = $1/(4\pi^2 f_{rx}^2 L_2)$ F
- L_{choke} = 1 mH
- L_{res} = $L_1||2L_{choke}$
- k = 0.35
- R_L = 10 Ω
- V_{in} = 325 V DC (for time domain)

B. Analysis of CS parallel resonant topology

1) Mathematical analysis: The topology is based on the principle of parallel resonance in which the circuit offers maximum impedance at the resonant frequencies.

For this topology and calculated circuit component values, the resonant frequency of the whole system (f_{res1}) is observed to be 28.2kHz. With the help of these calculated circuit component values, the time domain simulations of the circuit shown in Figure 10 can be performed. Figure 11 shows the voltage across the transmitter coil of the resonant inductive coupler when the inverter stage is operated at f_{op}<f_{res1}, f_{op}=f_{res1} and f_{op}>f_{res1}.

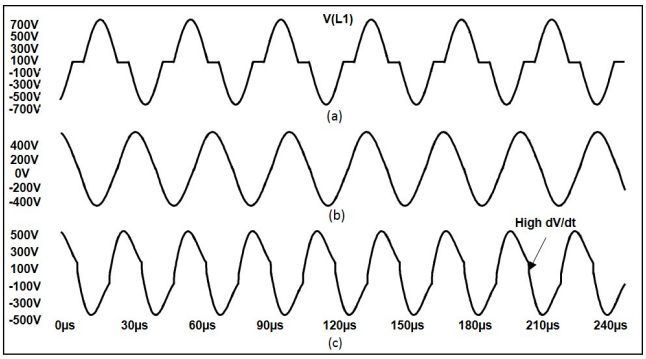

Fig. 11. Voltage across transmitter coil (a)f_{op}<f_{res1}, (b)f_{op}=f_{res1} and (c)f_{op}>f_{res1}

Interestingly from Figure 11, it can be seen that when the inverter stage of the transmitter is operated at or below the f_{res1}, high dV/dt's are not observed. On the other hand, when the inverter stage is operated above the f_{res1}, high dV/dt's are observed. Therefore, based upon the requirements stated in the earlier section, the operation of this topology at or below f_{res1} is preferred. When the system is operated below f_{res1}, the transmitter coil voltage waveform is almost a sine wave. It has an event near the zero crossing of the sinewave where the voltage is almost zero (say T_{freeze}). Thus, for the analysis of the system operating at or below f_{res1}, First Harmonic Approximation (FHA) can be used [1]. With the help of FHA, a simplified equivalent circuit of the system can be derived as shown in the Figure 12.

The FHA allows to replace the current source (I_{ac}) and the capacitor (C_1) with an AC voltage source ($\hat{V_{ac}}$). The transmitter capacitor (C_1) does not influence the receiver coil voltage gain but it does affect the phase of the input current (I_1). Thus, the capacitor (C_1) can be regarded as a phase compensator for the input current drawn from the AC voltage

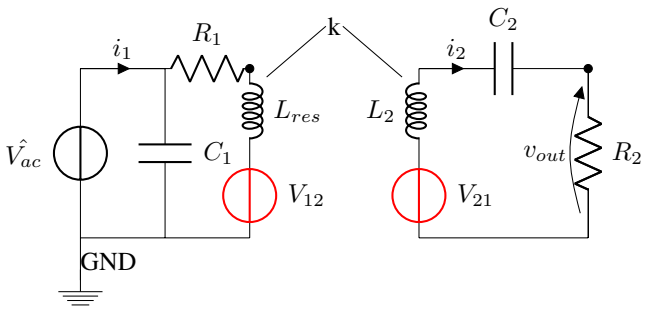

Fig. 12. Simplified equivalent circuit for CS parallel resonant topology operated below f_{res1}

source ($\hat{V_{ac}}$). In the equivalent circuit shown in Figure 12, R_1 represents the equivalent series resistance of the transmitter coil (L_1), equivalent series resistance of the choke coil (L_{choke}) along with the equivalent series resistance of the capacitor (C_1). R_2 represents the load resistance along with the equivalent series resistance of the receiver coil (L_2) and the equivalent series resistance of the capacitor (C_2). V_{12} represents voltage induced in the transmitter coil due to the mutual inductance (say, M) and the current flowing through the receiver coil (i_2). V_{21} represents the voltage induced in the receiver coil due to the mutual inductance and the current flowing through the transmitter coil. By applying the Laplace transformation and the transformer theory, a voltage transfer function can be derived as shown below.

$$\frac{V_{L_2}}{\hat{V_{ac}}} = \frac{s^2(R_2MC_2) + sM}{s^3(L_{res}L_2C_2 - M^2C_2) + s^2(L_2R_1C_2 + L_{res}C_2R_2) + s(R_1R_2C_2 + L_{res}) + R_1} \quad (1)$$

The above equation shows that the order of the characteristic equation (denominator) is 3. The more poles in the system, the more difficult it is to control. Again interestingly, it implies that the proposed topology is simpler to control than the present topology. Therefore, in the further analysis, the operation of the current source parallel resonant topology above the f_{res1} is discarded and the operation at or below the f_{res1} is considered.

2) Detailed analysis: As mentioned earlier, for this topology and calculated circuit component values, the resonant frequency (f_{res1}) is observed to be 28.2kHz where T_{freeze} is zero. Therefore the system is operated at or below 28.2kHz, and other parameters like the voltage across switches, behaviour on load disconnection etc. are examined in this section.

With the help of time domain simulations of the circuit shown in Figure 10, at f_{op} say 27kHz, the voltage across all the circuit components, in steady state conditions can be observed.

Figure 13 shows the voltage observed across the choke coil (L_{choke}) and the transmitter coil. It shows that there are no high dV/dt's present in any of the coils on transmitter side, under normal operating conditions. This is beneficial from the EMI point of view.

As shown in Figure 11a, when the inverter stage of the transmitter is operated below f_{res1}, the voltage across the

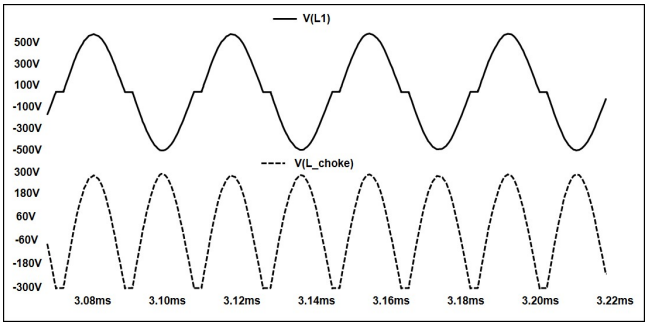

Fig. 13. Voltage across L_1 and L_{choke} at f_{op}=27kHz

transmitter coil appears to be a discontinuous function. With the help of time domain simulations, it can be observed that the peak voltage across the transmitter coil (V_{tx}) and T_{freeze} increases with decrease in operating frequency. Therefore, it can be stated that the amplitude of the first harmonic also changes with the change in operating frequency (f_{op}). And thus, it is comparatively difficult to perform the frequency domain simulations for the equivalent circuit shown in Figure 12. For better results from the frequency domain simulations, one has to model the source $\hat{v}$ such that the amplitude of the first harmonic changes according to the operating frequency. The relation between the amplitude of the first harmonic ($V_{ac_{FHA}}$) and the operating frequency (f_{op}) can be derived with the help Fourier analysis of the transmitter coil voltage waveform shown in Figure 14.

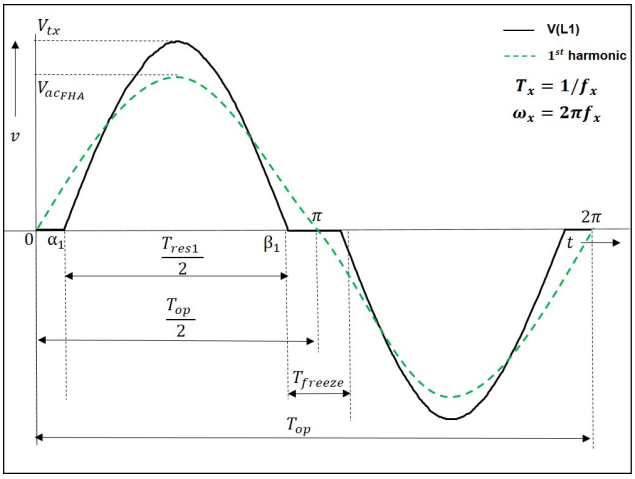

Fig. 14. Transmitter coil voltage waveform for detailed analysis

From Figure 14 the relation between the peak amplitude (V_{tx}) and operating frequency (f_{op}) can be derived and is as shown in the equation below:

$$V_{tx} = f(f_{op}, f_{res}) \tag{2}$$

And, at $f_{op} = f_{res}$, the peak amplitude can be given by:

$$V_{tx_{res}} = \frac{V_{in}\pi}{2} \tag{3}$$

And with the help of Equation 2, the amplitude of the first harmonic (V_{ac}) can be given by:

$$V_{ac_{FHA}} = f(V_{tx}, f_{op}, f_{res}) \tag{4}$$

$$\hat{V_{ac_{FHA}}} = \frac{V_{ac_{FHA}}}{V_{tx_{res}}} \tag{5}$$

The normalized value ($\hat{V_{ac_{FHA}}}$) can be used in Equation 1 for the frequency domain simulations. Figure 15 shows the variation in normalized V_{ac} with respect to operating frequency.

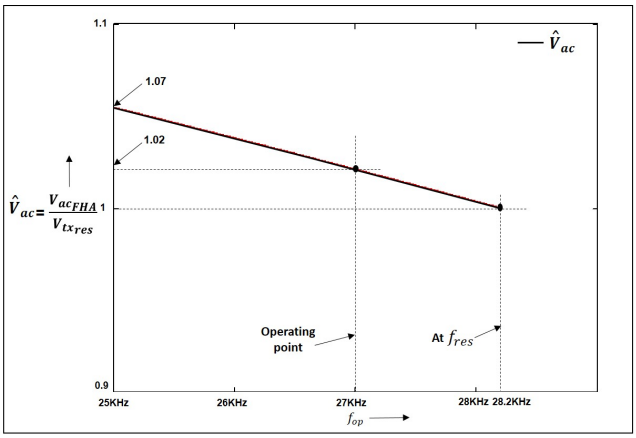

Fig. 15. Variation of normalized fundamental harmonic with respect to f_{op}

It should be noted that the FHA is valid only at or below f_{res1}. Therefore, the whole mathematical model for the frequency domain analysis is valid only at or below f_{res1}.

Another important point to observe is the switch voltage. It can be seen from Figure 16 that, the peak voltage ($V_{sw_{peak}}$) appearing across the switches is more than V_{in}. With the help of previously derived relation of the peak amplitude (V_{tx}), it can be calculated that $V_{sw_{peak}}$ is $\pi/2$ times the V_{in} at resonance, and it increases further with decrease in the f_{op}, as shown in Figure 16.

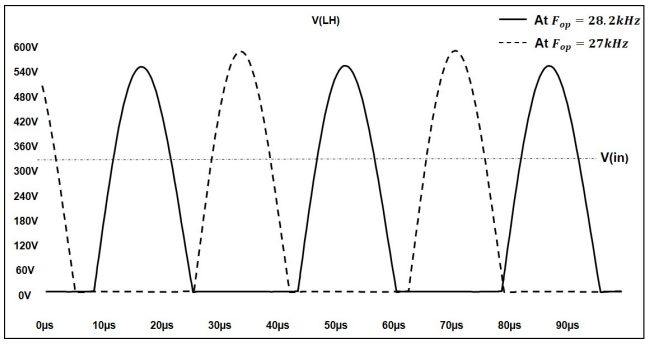

Fig. 16. Voltage across the switch S_2

V. Experimental Measurements and Comparison

To verify the calculated and simulated results, a new prototype with the proposed topology was built. The EMC

tests according to the standard CISPR14 were performed on the present system (series resonant topology) as well as the new prototype (CS parallel resonant topology). Figure 17 and Figure 18 shows the EMC measurements recorded for the present system and new prototype, respectively.

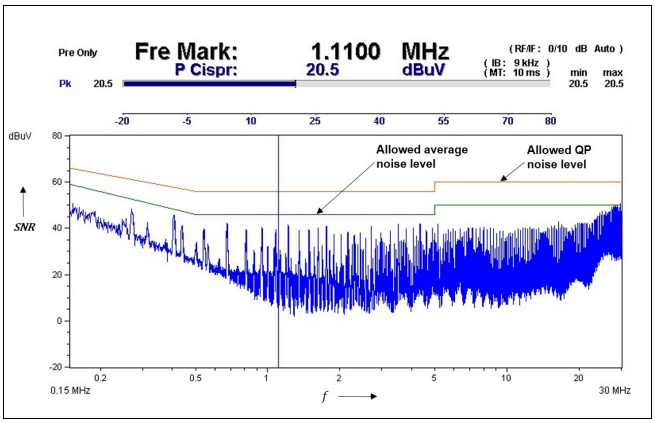

Fig. 17. Series resonant topology- EMC measurements, f_{op}=135kHz, P_{out}=2.4kW

Both the figures shows the maximum allowed noise level for the Quasi Peak (QP) noise measurement according CISPR14 (uppermost line) and maximum allowed noise level for the average noise measurement according CISPR14 (middle line).

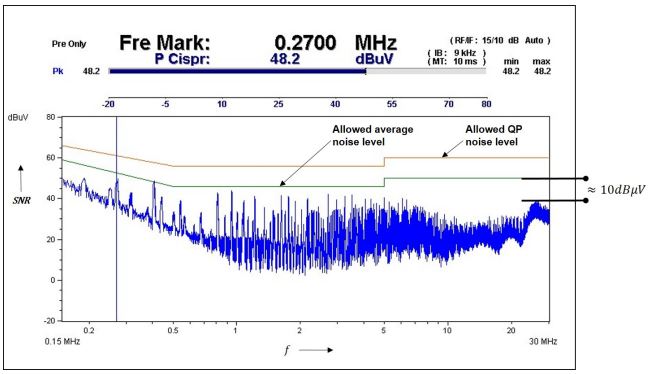

Fig. 18. CS parallel resonant topology- EMC measurements, f_{op}=135kHz, P_{out}=2.4kW

As per expectations, from Figure 18 a considerable reduction (10 dBuV) in the high frequency noise level can be observed in case of the CS parallel resonant topology. Therefore, the size of the mains filter can reduced.

From the detailed analysis explained in section II and experimental results, various factors can be noted down, as shown in table I.

Table I shows that, though the series resonant topology is easy to implement and widely used, it possesses some drawbacks when applied in the cordless kitchen system. It has advantages like the use of the low voltage switches, easy power control but, the EMI performance is relatively poor.

It can be observed that CS parallel topology is more suitable topology for the cordless kitchen system, when it comes

TABLE I
COMPARISON OF DIFFERENT TOPOLOGIES

	Series topology	CS parallel topology (in proposed region)
High dV/dt in transmitter coil	Yes	No
Voltage across power switches	V_{in}	(π/2)*V_{in} or more
Use of duty cycle control	Possible	Not possible
Loss of ZVS	Possible	Not possible
Control	Comparatively difficult	Comparatively simpler

to saitsfy the non-functional requirements. High dV/dt's do not occur, which offers good electromagnetic compatibility. The only disadvantages of the proposed topology are the high voltage rating of the power switches (more than $2V_{in}$) and the loss of control over the delivered power, as duty cycle control cannot be used. One can make use of the varying input voltage (V_{in}) to control the delivered power.

VI. CONCLUSION

The paper explained the basic principle of cordless kitchen system along with its requirements. There are functional as well as non-functional requirements. The present series resonant topology for the transmitter has the drawback that it is harder to meet the non-functional requirements. With the help of mathematical analysis, simulations as well as the experimental results, the paper suggested the 'current source parallel resonant' topology for the cordless kitchen system which can meet the non-functional requirements more easily. To achieve the control over the delivered power to the load, one can employ a pre-power stage on the transmitter side or a post-power stage on the receiver side. Thus, it can be concluded that for the cordless kitchen system, the operation of the current source parallel resonant topology at or below resonant frequency of the system is a good alternative.

REFERENCES

[1] R.Steigerwald, "A comparison of half-bridge resonant converter topologies", *IEEE Transactions on Power Electronics*, vol. 3, no. 2, pp. 174-182, 1988.

[2] M.Itraj, "Mathematical modeling of cordless kitchen appliances", unpublished.

[3] S.Wassenaar, "Tunable wireless Power Transmitter", unpublished.

Appendix A

Appendix

A-1 Cordless kitchen system operation- Flow chart

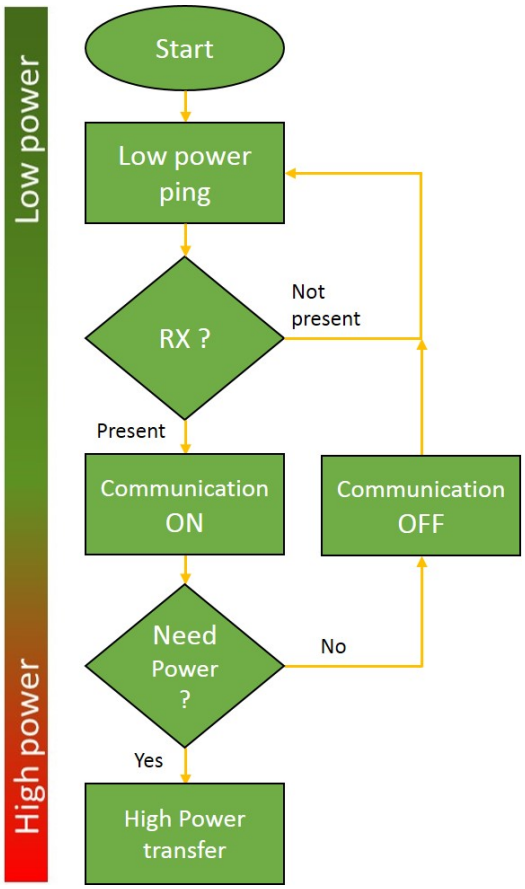

Figure A-1: Cordless kitchen system-Flowchart

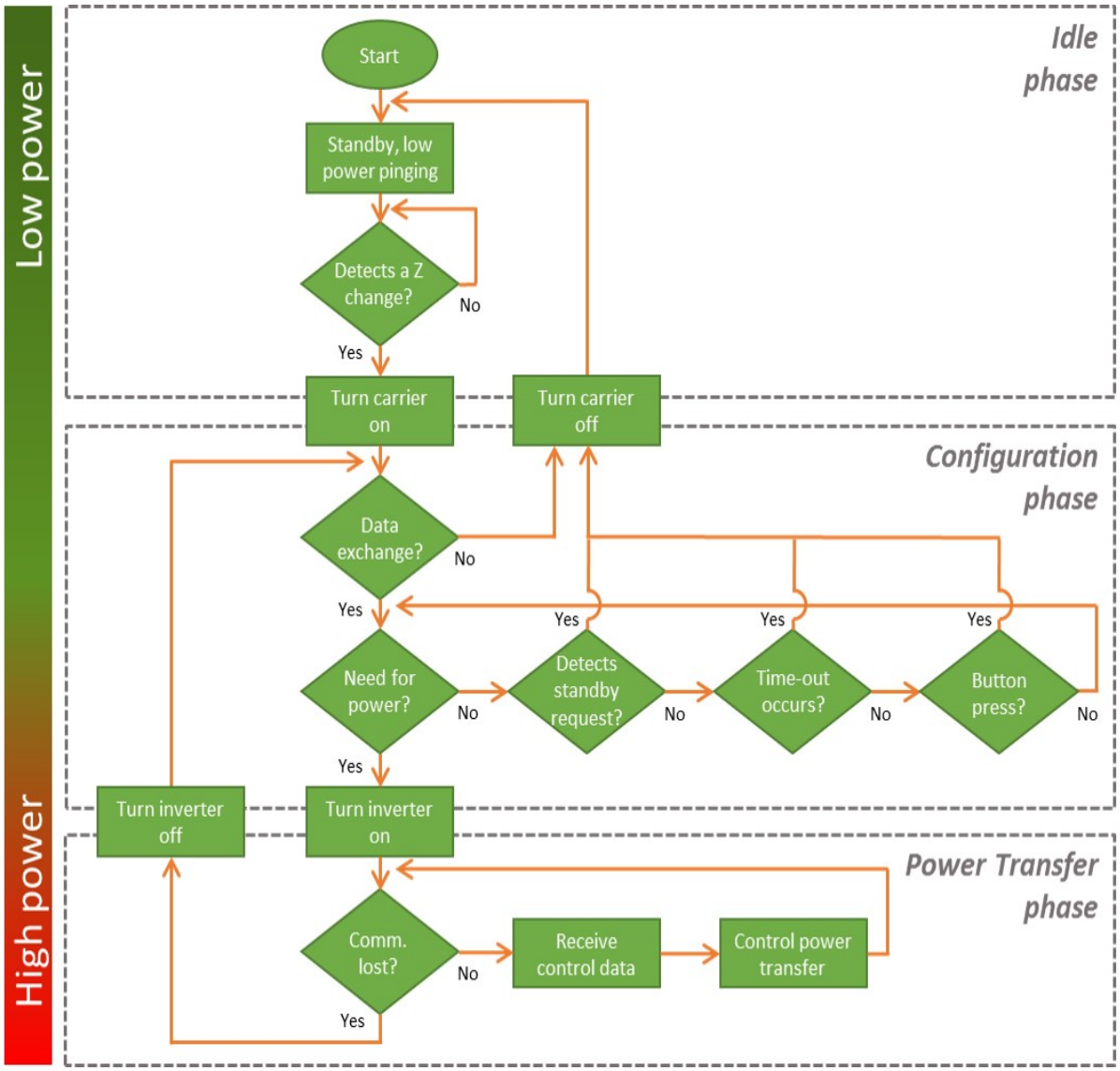

Figure A-2: Cordless kitchen system-Detailed Flowchart [1]

A-2 Voltage transfer function for series resonant cordless kitchen system

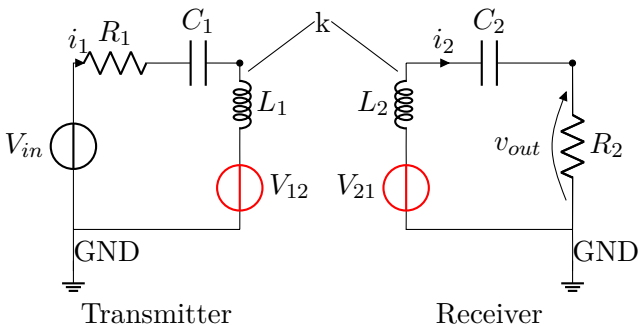

Figure A-3: Simplified equivalent circuit of present topology

By applying Kirchoff's voltage law to A-3, we can get following equations:

$$V_{in} = V_{12} + I_1 Z_1 \tag{A-1}$$

where :

$$V_{12} = I_2(j\omega)M \tag{A-2}$$
$$V_{21} = -I_2 Z_2 = I_1(j\omega)M \tag{A-3}$$

$$\therefore I_2 = \frac{-I_1(j\omega)M}{Z_2} \tag{A-4}$$

where,

$$M = k\sqrt{L_1 L_2} \tag{A-5}$$

and

$$K = \sqrt{k_{12}k_{21}} \tag{A-6}$$

Putting this I_2 in second and hence the first equation, we get:

$$V_{in} = I_1 Z_1 - \frac{-I_1(j\omega)M}{Z_2}(j\omega)M \tag{A-7}$$
$$\therefore V_{in} = (Z_1 - \frac{s^2M^2}{Z_2})I_1 \tag{A-8}$$

Therefore, one can say,

$$V_{in} = Z_{total} I_1 \tag{A-9}$$

where,

$$Z_{total} = (Z_1 - \frac{s^2M^2}{Z_2}) \tag{A-10}$$

or,

$$Z_{total} = (Z_1 + Z_{reflected}) \tag{A-11}$$

where,

$$Z_{reflected} = -\frac{s^2M^2}{Z_2} \tag{A-12}$$

By applying voltage divider rule, voltage across $Z_{reflected}$ is :

$$V_t = \frac{Z_{reflected}}{Z_{total}} V_{in} \tag{A-13}$$

or

$$V_t = Z_{reflected} I_1 \tag{A-14}$$

One must take this voltage in term of secondary winding parameters.
Thus, using relation from (A.4) in (A.12)

$$V_t = \frac{Z_{reflected}}{Z_{total}} \frac{(V_{in} Z_2)}{(-j\omega)M} \tag{A-15}$$

Now for the output voltage (V_{out}), we can again apply voltage divider rule, to get voltage across R_2 (i.e. load)

$$V_{out} = \frac{R_2}{Z_2} V_t \tag{A-16}$$

Using (A.13) in (A.14), one can get,

$$V_{out} = \frac{R_2}{Z_2} \frac{Z_{reflected}}{Z_{total}} \frac{(V_{in} Z_2)}{(-s)M} \tag{A-17}$$

Using (A.10) in (A.15),

$$\frac{V_{out}}{V_{in}} = R_2 \frac{-\frac{s^2M^2}{Z_2}}{Z_{total}} \frac{1}{(-s)M} \tag{A-18}$$

$$\therefore \frac{V_{out}}{V_{in}} = R_2 \frac{\frac{sM}{Z_2}}{Z_{total}} \tag{A-19}$$

Now from (A.8) Z_{total} is :

$$\frac{Z_1 Z_2 - s^2M^2}{Z_2} \tag{A-20}$$

Thus,

$$\frac{V_{out}}{V_{in}} = \frac{R_2 sM}{(Z_1 Z_2 - s^2M^2)} \tag{A-21}$$

Solving it, gives us the required transfer function:

$$\frac{V_{out}}{V_{in}} = \frac{s^3(C_1C_2MR_2)}{s^4(L_1L_2C_1C_2 - M^2C_1C_2) + s^3(R_2L_1C_1C_2 + R_1L_2C_1C_2) + s^2(L_2C_2 + L_1C_1 + R_1R_2C_1C_2) + s(R_1C_1 + R_2C_2) + 1} \tag{A-22}$$

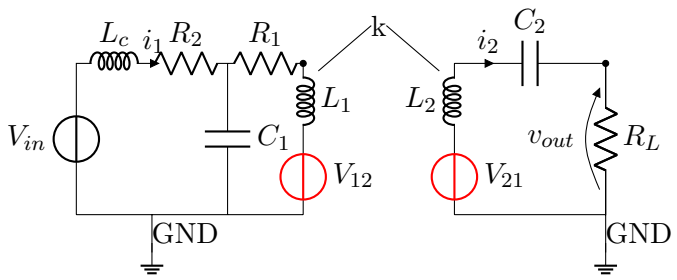

Figure A-4: Simplified equivalent circuit for VS parallel resonant topology

A-3 Voltage TF for the equivalent circuit of VS parallel resonant topology

By applying Kirchoff's voltage law to Figure A-4, we can get following equations:

$$V_{in} = V_{12} + I_1 Z_1 \tag{A-23}$$

where :

$$V_{12} = I_2(j\omega)M \tag{A-24}$$

$$Z_1 = R_1 + sL_c + [\frac{1}{sC_1}||(R_2 + sL_1)] \tag{A-25}$$

$$V_{21} = -I_2 Z_2 = I_1(j\omega)M \tag{A-26}$$

$$\therefore I_2 = \frac{-I_1 * (j\omega) * M}{Z_2} \tag{A-27}$$

where,

$$M = k\sqrt{L_1 L_2} \tag{A-28}$$

$$Z_2 = R_L + sL_2 + \frac{1}{sC_2} \tag{A-29}$$

and

$$k = \sqrt{k_{12}k_{21}} \tag{A-30}$$

Putting this I_2 in second and hence the first equation, we get:

$$V_{in} = I_1 Z_1 - \frac{-I_1(j\omega)M}{Z_2}(j\omega)M \tag{A-31}$$

$$\therefore V_{in} = (Z_1 - \frac{s^2M^2}{Z_2})I_1 \tag{A-32}$$

Therefore, one can say,

$$V_{in} = Z_{total} I_1 \tag{A-33}$$

where,

$$Z_{total} = (Z_1 - \frac{s^2M^2}{Z_2}) \tag{A-34}$$

or,

$$Z_{total} = (Z_1 + Z_{reflected}) \tag{A-35}$$

where,

$$Z_{reflected} = -\frac{s^2M^2}{Z_2} \tag{A-36}$$

By applying voltage divider rule, voltage across $Z_{reflected}$ is :

$$V_t = \frac{Z_{reflected}}{Z_{total}} V_{in} \tag{A-37}$$

or

$$V_t = Z_{reflected} I_1 \tag{A-38}$$

One must take this voltage in term of secondary winding parameters.
Thus, using relation from (A.4) in (A.12)

$$V_t = \frac{Z_{reflected}}{Z_{total}} \frac{(V_{in} Z_2)}{(-j\omega)M} \tag{A-39}$$

Now for the output voltage (V_{out}), we can again apply voltage divider rule, to get voltage across R_L (i.e. load)

$$V_{out} = \frac{R_L}{Z_2} V_t \tag{A-40}$$

Using (A.13) in (A.14), one can get,

$$V_{out} = \frac{R_L}{Z_2} \frac{Z_{reflected}}{Z_{total}} \frac{(V_{in} Z_2)}{(-s)M} \tag{A-41}$$

Using (A.10) in (A.15),

$$\frac{V_{out}}{V_{in}} = R_L \frac{-\frac{s^2M^2}{Z_2}}{Z_{total}} \frac{1}{(-s)M} \tag{A-42}$$

$$\therefore \frac{V_{out}}{V_{in}} = R_L \frac{\frac{sM}{Z_2}}{Z_{total}} \tag{A-43}$$

Now from (A.8) Z_{total} is :

$$\frac{Z_1 Z_2 - s^2 M^2}{Z_2} \tag{A-44}$$

Thus,

$$\frac{V_{out}}{V_{in}} = \frac{R_L sM}{(Z_1 Z_2 - s^2 M^2)} \tag{A-45}$$

Solving it, gives us the required transfer function:

$$\frac{V_{out}}{V_{ac}} = \frac{sMR_L(s^3L_1C_1C_2 + s^2R_2C_1C_2 + sC_2)}{\begin{array}{c} s^5(L_1L_2C_1C_2L_c - L_1C_1M^2C_2) + s^4(R_1L_1L_2C_1C_2 + R_2L_2C_2L_cC_1 + L_1C_1L_cR_LC_2 - R_2C_1C_2M^2) \\ +s^3(R_1R_2C_1L_2C_2 + L_cL_2C_2 + L_1L_2C_2 + R_LC_2L_1C_1R_1 + R_2L_cC_1R_LC_2 + L_1C_1L_c - M^2C_2) \\ +s^2(L_2C_2R_1 + L_2C_2R_2 + R_1R_2R_LC_1C_2 + R_LL_cC_2 + R_LL_1C_2 + L_1C_1R_1 + R_2L_cC_1) \\ +s(R_1R_LC_2 + R_2R_LC_2 + R_1R_2C_1 + L_c + L_1) + (R_1 + R_2) \end{array}}$$

A-4 Normalized current TF of series resonant cordless kitchen system

Defining $V_{in} = u_p$

1. Basic equations for figure A-3 are:

$$u_p = (\frac{1}{j\omega C_1} + j\omega L_1 + R_1)i_1 - j\omega M_{12}i_2 \tag{A-46}$$

$$0 = (\frac{1}{j\omega C_2} + j\omega L_2 + R_2)i_2 - j\omega M_{21}i_1 \tag{A-47}$$

2. Putting

$$\frac{1}{C_x} = \omega_x^2 L_x,\ R_x = \frac{\omega_x L_x}{Q_x},\ M_{xy} = K_{xy}\sqrt{L_xL_y} \tag{A-48}$$

one can get,

$$u_p = (\frac{\omega_1^2 L_1}{j\omega} + j\omega L_1 + \frac{\omega_1 L_1}{Q_1})i_1 - j\omega K_{12}\sqrt{L_1L_2}i_2 \tag{A-49}$$

$$0 = (\frac{\omega_2^2 L_2}{j\omega} + j\omega L_2 + \frac{\omega_2 L_2}{Q_2})i_2 - j\omega K_{12}\sqrt{L_1L_2}i_1 \tag{A-50}$$

3. Now let us define,

$$n_{21} = \sqrt{\frac{L_2}{L_1}} \tag{A-51}$$

$$\therefore \sqrt{L_1L_2} = L_1n_{21}, \tag{A-52}$$

thus one can obtain:

$$u_p = (\frac{\omega_1^2 L_1}{j\omega} + j\omega L_1 + \frac{\omega_1 L_1}{Q_1})i_1 - j\omega K_{12}L_1n_{21}i_2 \tag{A-53}$$

$$0 = (\frac{\omega_2^2 L_2}{j\omega} + j\omega L_2 + \frac{\omega_2 L_2}{Q_2})i_2 - j\omega K_{12}\frac{L_2}{n_{21}}i_1 \tag{A-54}$$

4. Dividing each equation by $j\omega L_x$

$$\frac{u_p}{j\omega L_1} = [\frac{-\omega_1^2}{\omega^2} + 1 + \frac{\omega_1}{j\omega Q_1}]i_1 - K_{12}n_{21}i_2 \tag{A-55}$$

$$0 = [\frac{-\omega_2^2}{\omega^2} + 1 + \frac{\omega_2}{j\omega Q_2}]i_2 - \frac{K_{12}}{n_{21}}i_1 \tag{A-56}$$

5. From (B.14):

$$i_2 = [\frac{(\frac{K_{12}}{n_{21}})i_1}{[\frac{-\omega_2^2}{\omega^2} + 1 + \frac{\omega_2}{j\omega Q_2}]}] \tag{A-57}$$

6. Putting (B.12) in (B.10)

$$\frac{u_p}{j\omega L_1} = [\frac{-\omega_1^2}{\omega^2} + 1 + \frac{\omega_1}{j\omega Q_1}]i_1 - K_{12}n_{21}[\frac{(\frac{K_{12}}{n_{21}})i_1}{[\frac{-\omega_2^2}{\omega^2} + 1 + \frac{\omega_2}{j\omega Q_2}]}] \tag{A-58}$$

7. Simplifying:

$$\frac{u_p}{j\omega L_1} = [\frac{-\omega_1^2}{\omega^2} + 1 + \frac{\omega_1}{j\omega Q_1} - K_{12}^2([\frac{-\omega_2^2}{\omega^2} + 1 + \frac{\omega_2}{j\omega Q_2}]^{-1})]i_1$$

8. Simplifying:

$$i_1 = \frac{\frac{u_p}{j\omega L_1}}{\frac{-\omega_1^2}{\omega^2} + 1 + \frac{\omega_1}{j\omega Q_1} - K_{12}^2([\frac{-\omega_2^2}{\omega^2} + 1 + \frac{\omega_2}{j\omega Q_2}]^{-1})} \tag{A-59}$$

9. Now using some more definitions:

$$\beta = \frac{\omega_2}{\omega_1},\ \gamma = \frac{Z_L}{\omega_2 L_2},\ f = \frac{\omega}{\omega_1},\ u = \frac{u_{op}}{u_{op,max}},\ i = \frac{u_p}{\omega_1 L_1} \tag{A-60}$$

one can get:

$$i_1 = \frac{\frac{u_p}{j\omega L_1}}{(\frac{1}{jf})^2 + 1 + \frac{1}{jfQ_1} - K_{12}^2([(\frac{\beta}{jf})^2 + 1 + \frac{\beta}{jfQ_2}]^{-1})} \tag{A-61}$$

10. Simplifying:

$$i_1 = \frac{(jf)ui}{(jf)^2 + 1 + \frac{jf}{Q_1} - K_{12}^2(jf)^4([\beta^2 + (jf)^2 + \frac{jf\beta}{Q_2}]^{-1})} \tag{A-62}$$

$$\therefore i_1 = \frac{(jf)ui}{1 - f^2 + \frac{jf}{Q_1} - K_{12}^2 f^4([\beta^2 - f^2 + \frac{jf\beta}{Q_2}]^{-1})} \tag{A-63}$$

Now From equation (B.19) one can write as:

$$i_2 = \frac{-\frac{K_{12}}{n_{12}}f^2 i_1}{(\beta^2 - f^2 + \frac{\beta}{jf}(\frac{1}{Q_2} + \gamma))} \tag{A-64}$$

Thus, equation (B.25) and (B.27) represents the final expressions for the input and output currents of a 3 winding transformer.
Therefore, other formulas can be derived, as shown below:
Dimensionless Load voltage, say u_L:

$$u_L = i_2 \gamma \beta n_{12}^2 \tag{A-65}$$

Dimensionless Load power, say P_L:

$$P_L = i_2^2 \gamma \beta n_{12}^2 \tag{A-66}$$

Dimensionless received power, say P_r:

$$P_r = \frac{i_2^2}{Q2} \beta n_{12}^2 + P_L \tag{A-67}$$

Dimensionless transmitted power, say P_t:

$$P_t = P_r \tag{A-68}$$

Dimensionless input power, say P_p

$$P_p = \frac{i_1^2}{Q1} + P_t \tag{A-69}$$

Efficiency, say η

$$\eta = \frac{P_L}{P_p} \tag{A-70}$$

A-5 Communication channel- Time Division Multiplexing [1]

The communication channel between the inductive power source and cordless appliance makes use of a standard NFC protocol. This type of wireless communication allows data transfer only at close proximity between the transmitter and appliance. When wireless power transfer and data communication happen simultaneously, interference from the power transfer will occur and will disturb the data communication channel. To eliminate this problem, Time Division Multiplexing (TDM) is implemented. TDM is a method where the data communication and power are transferred over the same channel but alternated in time. In case of the cordless kitchen concept this channel is 4 cm of air. To have less interference from the wireless power transfer during data communications, a time-slot of 2ms is chosen. During this time-slot the power channel is turned off. In order to minimize power transfer loss the 2ms time-slot is activated during the mains (50 Hz) zero crossings of the mains. A zero crossing detector as shown in Chapter-6, can be used to detect the mains zero crossings.

Figure A-5 shows an overview of the TDM principle and the communication protocol package format. $Ucarrier$ is the signal that represents the communication signal. The On_Off signal indicates the moments in time whenever the power transfer is enabled or disabled. Iac_Tx represents the current through the Tx coil modulated with the power carrier from the Tx inverter. The transmitter and the receiver are equipped with a control unit which modulate or demodulate the communication signal and provide an input to the power channel, if required.

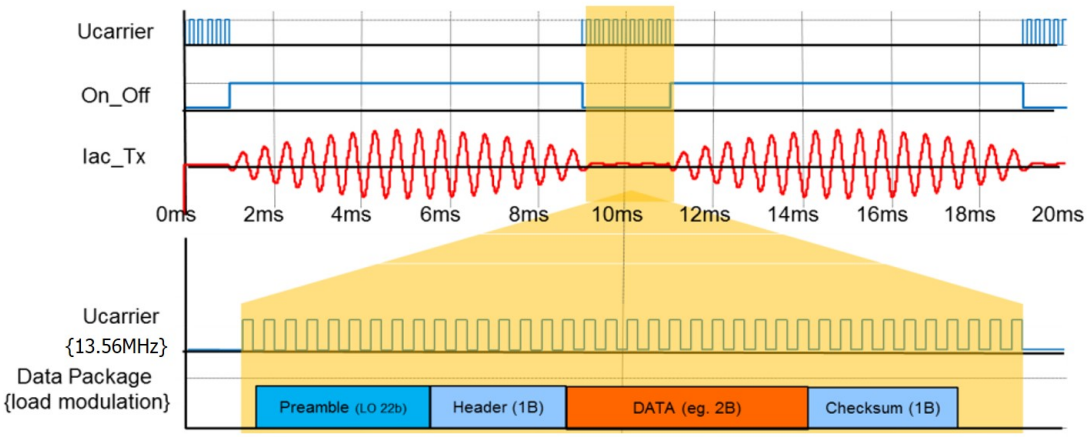

Figure A-5: Conceptual representation of Time Division Multiplexing (TDM)[1]

A-6 Simulation model for proposed topology

This section explains the development of the practical model which can be built. For the time domain simulations, LTSpice is used. A basic simulation model without any control mechanism as shown in Figure A-6 can be simulated in LTSpice.

Figure A-6 shows the circuit along with the calculations required to calculate the circuit components. L_1 represents the transmitter coil whereas, L_2 represents the receiver coil. To realize the resonant tanks, capacitors C_1 and C_2 are used on the transmitter and the receiver side, respectively. The sources represents the gate drive circuitry required for the inverter power switches (S_1 to S_4). With the aid of LTSpice simulator, in-built MOSFET's can also be used as power switches instead of these normal switches. L_3 represents the choke coil. Capacitor C_4, diode D_{mains1} and power supplies (V_{10} and $B1$) together represent the diode bridge rectifier. To control the power delivered to the load and introduce a communication window, buck converter as a pre-power stage can be used. The details about PWM signal given to the buck power stage are given in next section.

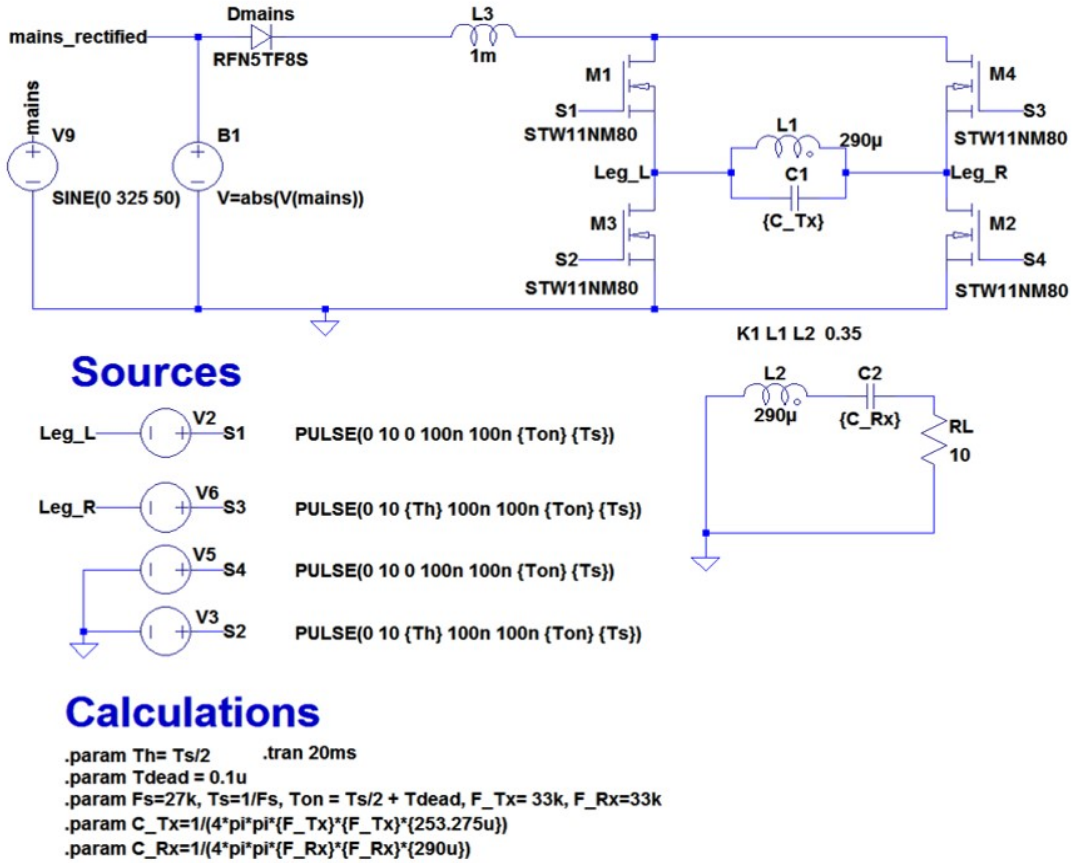

Figure A-6: LTSpice model for CS parallel resonant topology

A-7 PWM block schematic

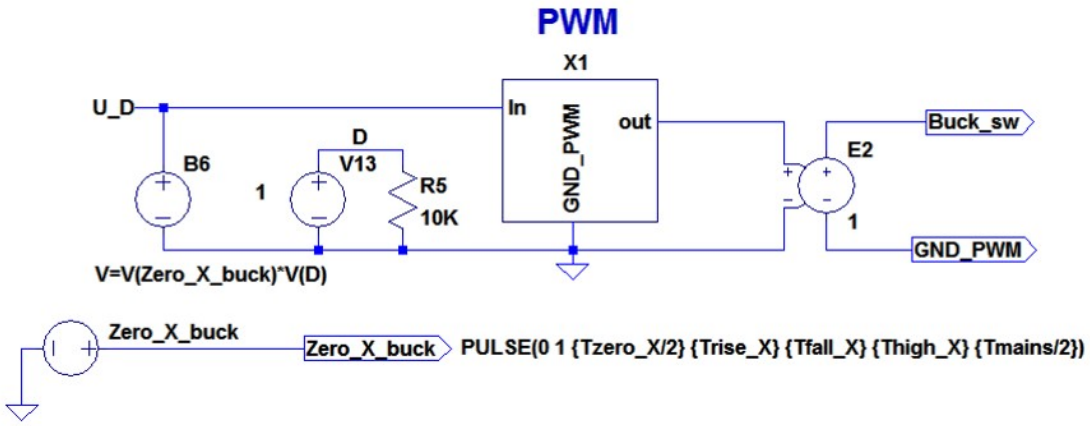

Figure A-7: Duty cycle control for the buck stage of the transmitter

Figure A-7 shows an example of such PWM generator required for the buck power stage. It can be seen from Figure A-7 that by varying V(D) in the schematic, the duty cycle can be

varied. To detect the mains zero crossings, a zero crossing detector ($zero\_x\_buck$) is used. It can be defined with the help of different constants like zero crossing time $Tzero_{X/2}$, rise time (T_{riseX}), fall time (T_{fallX}), On time (T_{highX}). In this case, the duty cycle signal (U_D) changes from 0 to the desired value (say 100%) in the time period defined by T_{riseX}, stays at the desired value for the time period defined by T_{highX} and goes back to 0 in the time period defined by T_{fallX}.

The detailed schematic of the PWM generation block (X_1) is shown in Figure A-8. The generation takes place by comparing the duty cycle signal (U_D) with a triangular waveform of twice the inverter operating frequency (f_{op}). Using such a system one can observe the transmitter coil voltage at a particular operating frequency. Figure 5-8 shows us the transmitter coil voltage with a communication window, at operating frequency 28.2kHz and duty cycle (D_{buck}) equal to 100% .

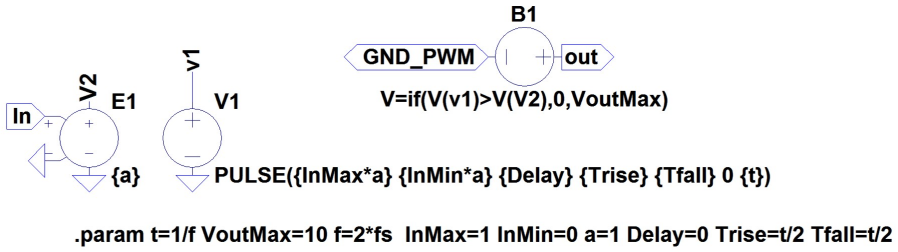

Figure A-8: Detailed schematic of PWM generation block

A-8 Advanced zero crossing signal

To reduce the higher harmonic content one can reduce the slope of zero crossing signals ($V(Zero\_X\_buck)$) used by the PWM generation circuit. This can be done by increasing the T_{rise_X} and T_{fall_X} in the schematic[4]. Thus, the duty cycle signal (U_D) can slowly increase from 0 to the desired value (say 100%) instead of a sudden change. Figure A-9 shows the original and advanced zero crossing signals supplied to the PWM generation circuit.

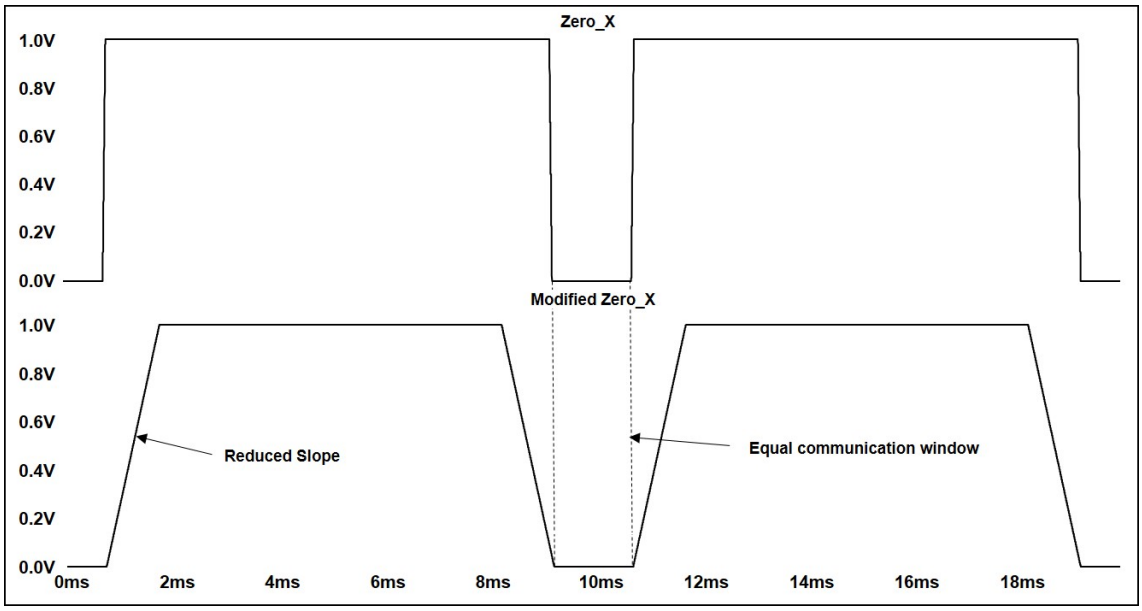

Figure A-9: Advanced zero crossing signal for reduction in mains current harmonics

A-9 Loss of Zero Voltage Switching at low duty cycles

A-9-1 Hard switching

In any power converter, power switches do contribute to the losses in the system. In the power switches, there are two types of losses: Conduction losses and Switching losses. The conduction losses are the losses caused by on-resistance (R_{on}) of the switch and current flowing through the switch (I_L). R_{on} is the resistance offered by the switch while it is in the conduction state. Figure A-10 shows the conceptual representation for hard switching indicating different types of losses in the switches.

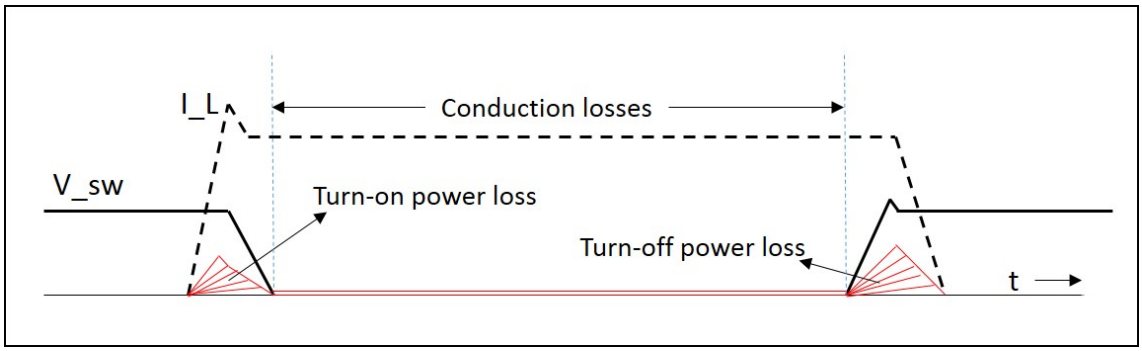

Figure A-10: Conceptual representation of hard switching[8]

Apart from that, it can be seen from Figure A-10 that during turn-on (closing the switch) and turn-off (opening the switch) presence of voltage across and current through the switch can also contribute the power dissipation in the switch. Therefore, switching losses are the losses in a switch caused due to the presence of voltage across (V_{sw}) and current (I_L) through the

switch. More the power dissipation in the power switches, lesser the efficiency of the system. The conduction losses can be considered as constant losses, for a given load, as R_{on} of the power switches cannot be varied. But one can reduce the switching losses. Therefore, some switching techniques are applied where the switch is turned-ON or turned-OFF or both at zero voltage (ZV) or at zero current (ZC) or both (ZV-ZC). For the power switches, Zero Voltage Switching (ZVS) technique is most commonly used, to avoid the losses the internal capacitances of the switches[ref of book]. Implementation of ZVS helps us in two ways:

- It minimizes the switching losses.
- It reduces the dV/dt's (rate of change of voltage with respect to time) across the switches and hence it improves the EMC performance of the system.

A-9-2 Loss of ZVS

One can make sure that ZVS is applied to avoid high dV/dt's and minimize the switching losses, however, in some cases (as explained in Chapter 3) the system might lose the ZVS technique. The detailed decription of loss of ZVS at low duty cycles is given in this section.

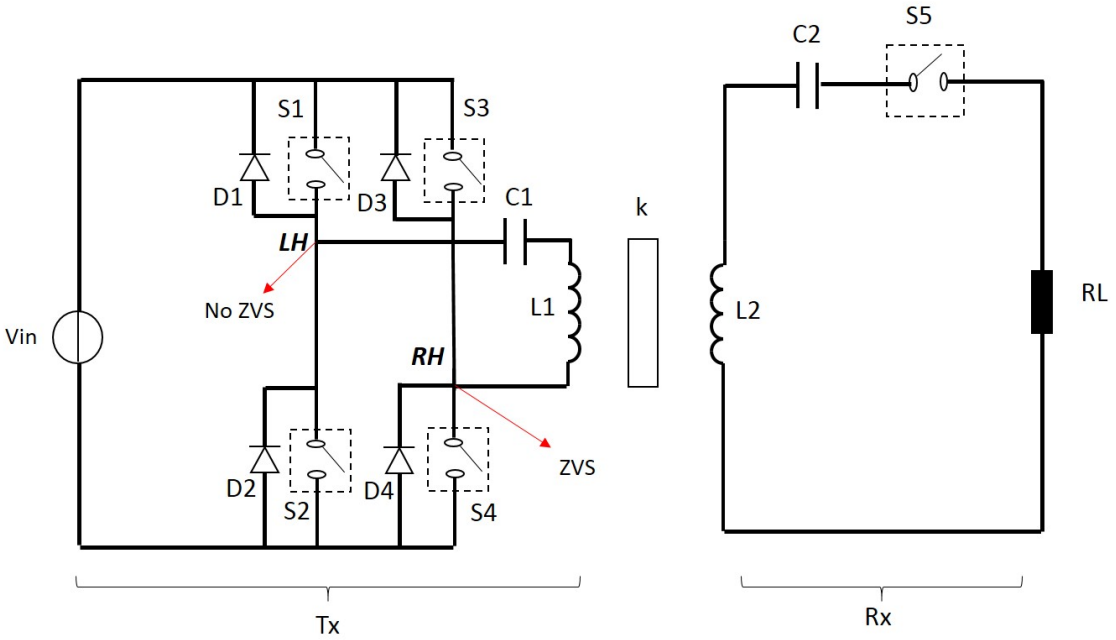

Figure A-11: Series resonant topology at L_1=L_2 =290uH, C_1=C_2 =80.278nF, k=0.35, V_{in} =325V, R_L =10 Ω, f_{op} =32.7kHz, D=50%

In case of series resonant topology at low duty cycles, loss of ZVS switching is observed. As shown in Figure A-11, at low duty cycles one of the inverter bridge legs operates with ZVS technique whereas, another leg loses its ability to operate with ZVS technique. Figure A-12 shows the details of the voltage across the inverter bridge (V(LH,RH)) and current through the transmitter coil (I_{L1}). Figure A-12 also shows the conducting devices and ZVS instances.

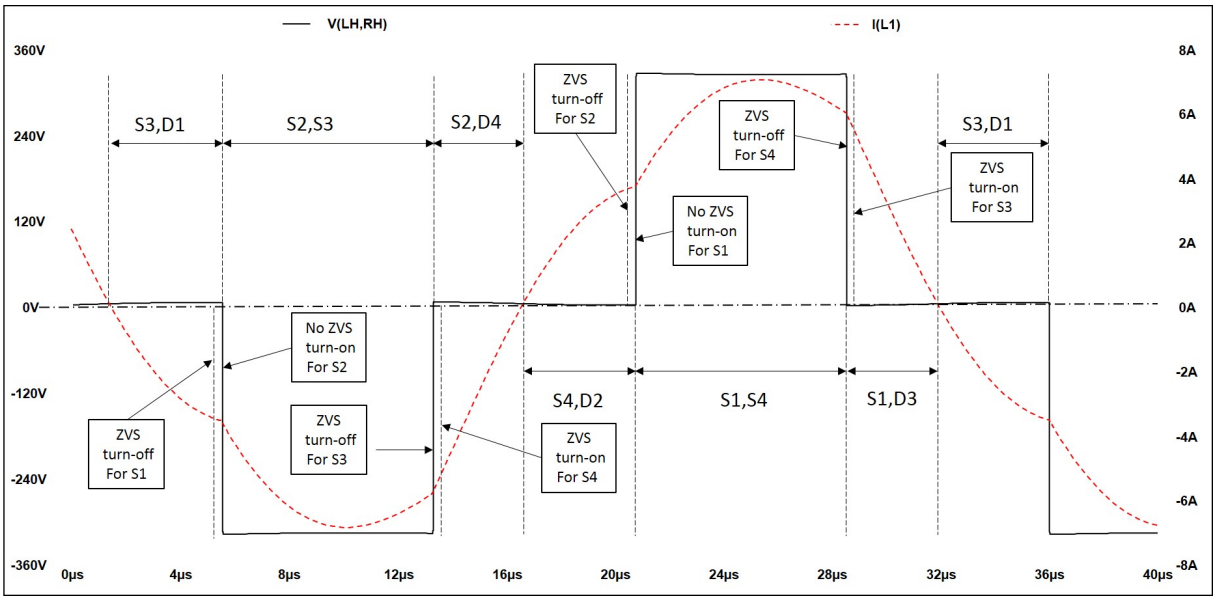

Figure A-12: Series resonant topology at low duty cycles- inverter bridge voltage and current waveforms

Explanation: For instance one can observe the positive rising edge of the inverter bridge voltage (V(LH,RH)). Just before the rising edge, switch S_2 is turned-OFF. As the current (I_{L1}) is flowing through the diode (D_2) of the switch (S_2), the switch is turned-OFF with ZVS technique. At the rising edge, switch S_4 is already ON and switch S_1 is turned-ON (closed). Therefore, one can observe that switch S_1 is turned-ON without ZVS technique. For some period of time, switch S_1 and S_4 conducts and delivers the power to the load. On the falling edge of the inverter bridge voltage (V(LH,RH)) switch S_4 is turned-OFF while current is still flowing through it and thus switch S_4 is turned-OFF with ZVS technique. Similarly, during the negative half of the inverter bridge voltage (V(LH,RH)) turn-ON of the switch S_2 is observed to be with ZVS technique and turn-OFF of the switch S_3 is observed to be without ZVS technique.

Appendix B

Appendix

B-1 Voltage TF for reduced equivalent circuit of CS parallel resonant topology

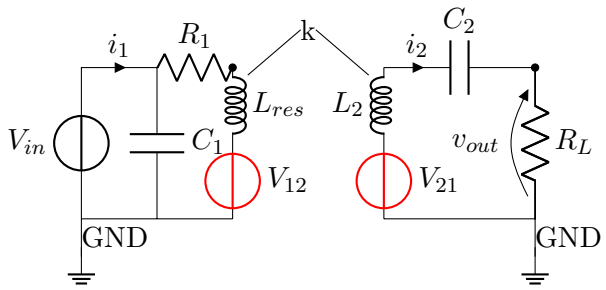

Figure B-1: Simplified equivalent circuit for CS parallel resonant topology operated below f_{res1}

By applying Kirchoff's voltage law to Figure B-1, we can get following equations:

$$V_{in} = V_{12} + I_1 Z_1 \tag{B-1}$$

where :

$$V_{12} = I_2(j\omega)M \tag{B-2}$$
$$Z_1 = R_1 + sL_{res} \tag{B-3}$$
$$V_{21} = -I_2 Z_2 = I_1(j\omega)M \tag{B-4}$$
$$\therefore I_2 = \frac{-I_1(j\omega)M}{Z_2} \tag{B-5}$$

where,

$$M = k\sqrt{L_1 L_2} \tag{B-6}$$
$$Z_2 = R_L + sL_2 + \frac{1}{sC_2} \tag{B-7}$$

and

$$k = \sqrt{k_{12}k_{21}} \tag{B-8}$$

Putting this I_2 in second and hence the first equation, we get:

$$V_{in} = I_1 Z_1 - \frac{-I_1(j\omega)M}{Z_2}(j\omega)M \tag{B-9}$$

$$\therefore V_{in} = (Z_1 - \frac{s^2M^2}{Z_2})I_1 \tag{B-10}$$

Therefore, one can say,

$$V_{in} = Z_{total}I_1 \tag{B-11}$$

where,

$$Z_{total} = (Z_1 - \frac{s^2M^2}{Z_2}) \tag{B-12}$$

or,

$$Z_{total} = (Z_1 + Z_{reflected}) \tag{B-13}$$

where,

$$Z_{reflected} = -\frac{s^2M^2}{Z_2} \tag{B-14}$$

By applying voltage divider rule, voltage across $Z_{reflected}$ is :

$$V_t = \frac{Z_{reflected}}{Z_{total}}V_{in} \tag{B-15}$$

or

$$V_t = Z_{reflected}I_1 \tag{B-16}$$

One must take this voltage in term of secondary winding parameters.
Thus, using relation from (A.4) in (A.12)

$$V_t = \frac{Z_{reflected}}{Z_{total}}\frac{(V_{in}Z_2)}{(-j\omega)M} \tag{B-17}$$

Now for the output voltage (V_{out}), we can again apply voltage divider rule, to get voltage across R_L (i.e. load)

$$V_{out} = \frac{R_L}{Z_2}V_t \tag{B-18}$$

Using (A.13) in (A.14), one can get,

$$V_{out} = \frac{R_L}{Z_2}\frac{Z_{reflected}}{Z_{total}}\frac{(V_{in}Z_2)}{(-s)M} \tag{B-19}$$

Using (A.10) in (A.15),

$$\frac{V_{out}}{V_{in}} = R_L\frac{-\frac{s^2M^2}{Z_2}}{Z_{total}}\frac{1}{(-s)M} \tag{B-20}$$

$$\therefore \frac{V_{out}}{V_{in}} = R_L\frac{\frac{sM}{Z_2}}{Z_{total}} \tag{B-21}$$

Now from (A.8) Z_{total} is :

$$\frac{Z_1 Z_2 - s^2 M^2}{Z_2} \tag{B-22}$$

Thus,

$$\frac{V_{out}}{V_{in}} = \frac{R_L s M}{(Z_1 Z_2 - s^2 M^2)} \tag{B-23}$$

Solving it, gives us the required transfer function:

$$\frac{V_{out}}{V_{in}} = \frac{s^2 C_2 M R_L}{s^3(L_{res} L_2 C_2 - M^2 C_2) + s^2(R_L L_{res} C_2 + R_1 L_2 C_2) + s(R_1 R_L C_2 + L_{res}) + R_1} \tag{B-24}$$

B-2 Normalized current TF for simplified CS parallel resonant topology

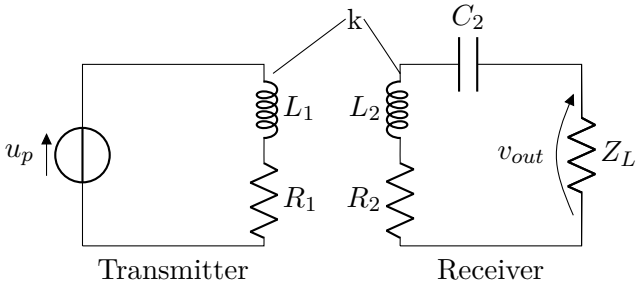

1. Basic 2 equations are:

$$u_p = [(j\omega L_1 + R_1) i_1 - j\omega M i_2 \tag{B-25}$$

$$0 = (\frac{1}{j\omega C_2} + j\omega L_2 + R_2 + Z_L) i_2 - j\omega M i_1 \tag{B-26}$$

2. Putting

$$\frac{1}{C_2} = \omega_2^2 L_2,\ R_x = \frac{\omega_x L_x}{Q_x},\ M = K\sqrt{L_1 L_2} \tag{B-27}$$

one can get,

$$u_p = [(j\omega L_1 + \frac{\omega_1 L_1}{Q_1}) i_1 - j\omega K\sqrt{L_1 L_2} i_2] \tag{B-28}$$

$$0 = (\frac{\omega_2^2 L_2}{j\omega} + j\omega L_2 + \frac{\omega_2 L_2}{Q_2} + Z_L) i_2 - j\omega K\sqrt{L_1 L_2} i_1 \tag{B-29}$$

3. Now let us define,

$$n = \sqrt{\frac{L_2}{L_1}} \tag{B-30}$$

$$\therefore \sqrt{L_1 L_2} = L_1 n = \frac{L_2}{n} \tag{B-31}$$

thus one can obtain:

$$u_p = [(j\omega L_1 + \frac{\omega_1 L_1}{Q_1})i_1 - j\omega K L_1 n i_2] \tag{B-32}$$

$$0 = (\frac{\omega_2^2 L_2}{j\omega} + j\omega L_2 + \frac{\omega_2 L_2}{Q_2} + Z_L)i_2 - j\omega K \frac{L_2}{n} i_1 \tag{B-33}$$

4. Dividing each equation by $j\omega L_x$

$$\frac{u_p}{j\omega L_1} = [(1 + \frac{\omega_1}{j\omega Q_1})i_1 - K n i_2] \tag{B-34}$$

$$0 = [\frac{-\omega_2^2}{\omega^2} + 1 + \frac{\omega_2}{j\omega}(\frac{1}{Q_2} + \frac{Z_L}{L_2})]i_2 - \frac{K}{n} i_1 \tag{B-35}$$

5. From (B.11):

$$i_2 = [\frac{(\frac{K}{n})i_1}{[\frac{-\omega_2^2}{\omega^2} + 1 + \frac{\omega_2}{j\omega Q_2} + \frac{Z_L}{j\omega L_2}]}] \tag{B-36}$$

6. Putting (B.12) in (B.10)

$$\frac{u_p}{j\omega L_1} = [1 + \frac{\omega_1}{j\omega Q_1} - K^2[\frac{-\omega_2^2}{\omega^2} + 1 + \frac{\omega_2}{j\omega Q_2} + \frac{Z_L}{j\omega L_2}]^{-1}]i_1 \tag{B-37}$$

7. Further simplifying for i_1:

$$i_1 = \frac{\frac{u_p}{j\omega L_P}}{1 + \frac{\omega_1}{j\omega Q_1} - K^2[\frac{-\omega_2^2}{\omega^2} + 1 + \frac{\omega_2}{j\omega Q_2} + \frac{Z_L}{j\omega L_2}]^{-1}} \tag{B-38}$$

$$i_1 = \frac{\frac{u_p}{j\omega L_P}}{1 + \frac{\omega_1}{j\omega Q_1} + K^2[\frac{-\omega_2^2}{\omega^2} + 1 + \frac{\omega_2}{j\omega}(\frac{1}{Q_2} + \frac{Z_L}{\omega_2 L_2})]^{-1}} \tag{B-39}$$

8. Now using some more definitions:

$$\beta = \frac{\omega_2}{\omega_1},\ \gamma = \frac{Z_L}{\omega_2 L_2},\ f = \frac{\omega}{\omega_1},\ u = \frac{u_{op}}{u_{op,max}},\ i = \frac{u_p}{\omega_1 L_1} \tag{B-40}$$

one can get:

$$i_1 = \frac{\frac{ui}{jf}}{1 + \frac{1}{jfQ_1} - K^2[1 + (\frac{\beta}{jf})^2 + \frac{\beta}{jf}(\frac{1}{Q_2} + \gamma)]^{-1}} \tag{B-41}$$

12. Simplifying:

$$i_1 = \frac{ui}{jf + \frac{1}{jfQ_1} - K^2(jf)^3\ [(jf)^2 + \beta^2 + jf\beta(\frac{1}{Q_2} + \gamma)]^{-1}} \tag{B-42}$$

$$i_1 = \frac{ui}{jf + \frac{1}{jfQ_1} + K^2 jf^3\ [-f^2 + \beta^2 + jf\beta(\frac{1}{Q_2} + \gamma)]^{-1}} \tag{B-43}$$

Now From equation (B.12) one can write as:

$$i_2 = \frac{-K}{n} f^2[\beta^2 - f^2 + jf\beta(\frac{1}{Q2} + \gamma)]^{-1} i_1 \tag{B-44}$$

Thus, equation (B-43) and (B-44) represents the final expressions for the input and output currents of a CS parallel resonant system.
Therefore, other formulas can be derived, as shown below:
Dimensionless Load voltage, say u_L:

$$u_L = i_2 \gamma \beta n^2 \tag{B-45}$$

Dimensionless Load power, say P_L:

$$P_L = i_2^2 \gamma \beta n^2 \tag{B-46}$$

Dimensionless received power, say P_r:

$$P_r = \frac{i_2^2}{Q2} \beta n^2 + P_L \tag{B-47}$$

Dimensionless transmitted power, say P_t:

$$P_t = P_r \tag{B-48}$$

Dimensionless input power, say P_p

$$P_p = \frac{i_1^2}{Q1} + P_t \tag{B-49}$$

Efficiency, say η

$$\eta = \frac{P_L}{P_p} \tag{B-50}$$

B-3 Fourier analysis

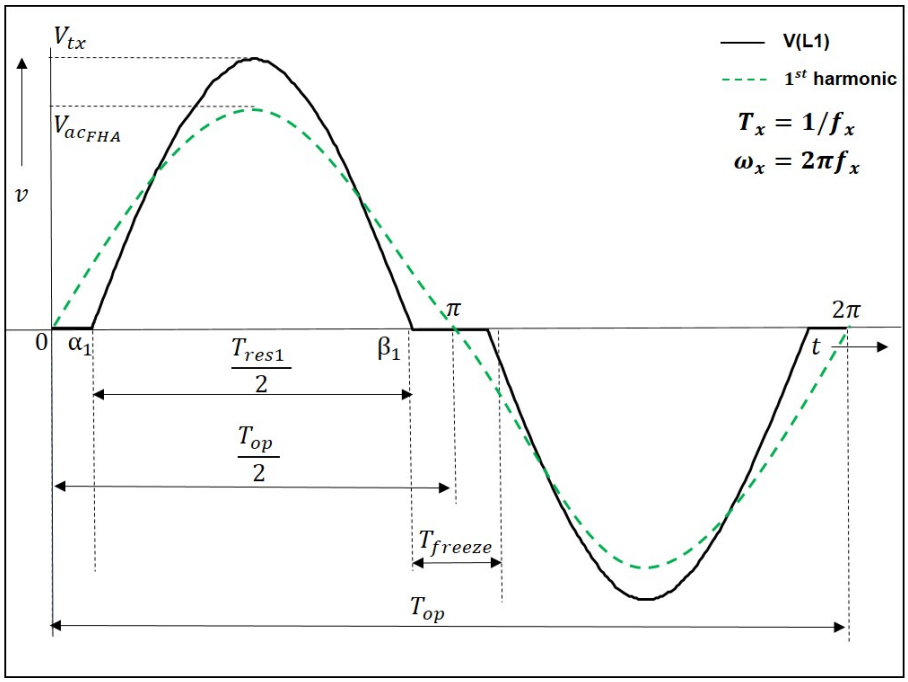

Figure B-2: Transmitter coil voltage waveform for detailed analysis

The waveform can be defined by:

$$\begin{aligned} f(t) &= 0 && 0 \leqslant t \leqslant \alpha_1 \\ &= V_{tx} sin\omega_{res}(t-\alpha_1) && \alpha_1 \leqslant t \leqslant \beta_1 \\ &= 0 && \beta_1 \leqslant t \leqslant \frac{T_{op}}{2} \end{aligned} \tag{B-51}$$

The waveform is symmetrical, therefore a_n=0 .

$$b_n = \frac{2V_{tx}}{\frac{T_{op}}{2}} \int_0^{\frac{T_{op}}{2}} f(t) sin\ n\omega_{op} t\ dt \tag{B-52}$$

$$= \frac{4V_{tx}}{T_{op}} \int_{\alpha_1}^{\beta_1} sin\omega_{res}(t-\alpha_1) sin\ n\omega_{op} t\ dt \tag{B-53}$$

$$= \frac{4V_{tx}}{T_{op}} \int_{\alpha_1}^{\beta_1} \frac{1}{2} cos(\omega_{res} t - \omega_{res}\alpha_1 - n\omega_{op} t) - \frac{1}{2} cos(\omega_{res} t - \omega_{res}\alpha_1 + n\omega_{op} t)\ dt \tag{B-54}$$

for the first harmonic, n=1.

$$b_1 = \frac{4V_{tx}}{T_{op}} \int_{\alpha_1}^{\beta_1} \frac{1}{2} cos(\omega_{res}t - \omega_{res}\alpha_1 - \omega_{op}t) - \frac{1}{2} cos(\omega_{res} - \omega_{res}\alpha_1 + \omega_{op}t)\ dt \tag{B-55}$$

$$= \frac{2V_{tx}}{T_{op}} [\frac{sin(\omega_{res}t - \omega_{res}\alpha_1 - \omega_{op}t)}{(\omega_{res} - \omega_{op})} - \frac{sin(\omega_{res}t - \omega_{res}\alpha_1 + \omega_{op}t)}{(\omega_{res} + \omega_{op})}]_{\alpha_1}^{\beta_1} \tag{B-56}$$

$$= \frac{2V_{tx}}{T_{op}} [\frac{sin(\omega_{res}\beta_1 - \omega_{res}\alpha_1 - \omega_{op}\beta_1)}{(\omega_{res} - \omega_{op})} - \frac{sin(\omega_{res}\beta_1 - \omega_{res}\alpha_1 + \omega_{op}\beta_1)}{(\omega_{res} + \omega_{op})} - \frac{sin(-\omega_{op}\alpha_1)}{(\omega_{res} - \omega_{op})} + \frac{sin(\omega_{op}\alpha_1)}{(\omega_{res} + \omega_{op})}] \tag{B-57}$$

To simplify the above equation one can define and substitute α_1 and β_1 where,

$$\alpha_1 = \frac{1}{2}(\frac{\pi}{\omega_{op}} - \frac{\pi}{\omega_{res}}) \tag{B-58}$$

$$\beta_1 = \frac{1}{2}(\frac{\pi}{\omega_{op}} + \frac{\pi}{\omega_{res}}) \tag{B-59}$$

to get,

$$b_1 = V_{ac_{FHA}} = \frac{-8V_{tx}}{T_{op}} cos(\frac{\pi}{2}\frac{\omega_{op}}{\omega_{res}}) \frac{\omega_{res}}{\omega_{op}^2 - \omega_{res}^2} \tag{B-60}$$

Equation (B-62), gives the amplitude of first harmonic of the waveform shown in Figure(3). Using this equation, it can be seen that, when converter is operated at frequencies $0.9f_{res} < f_{op} < f_{res}$, amplitude of first harmonic is more than 0.94. Thus, for an AC analysis a suitable model can be derived using first harmonic approximation. Also the amplitude of the third harmonic can be given as:

$$b_3 = \frac{2V_{tx}}{T_{op}} [\frac{sin(\omega_{res}\beta_1 - \omega_{res}\alpha_1 - 3\omega_{op}\beta_1)}{(\omega_{res} - 3\omega_{op})} - \frac{sin(\omega_{res}\beta_1 - \omega_{res}\alpha_1 + 3\omega_{op}\beta_1)}{(\omega_{res} + 3\omega_{op})} - \frac{sin(-3\omega_{op}\alpha_1)}{(\omega_{res} - 3\omega_{op})} + \frac{sin(3\omega_{op}\alpha_1)}{(\omega_{res} + 3\omega_{op})}] \tag{B-61}$$

B-4 Relation between peak amplitude and operating frequency

For a waveform as shown in Figure B-2, one can write :

$$V_{in} = \frac{2}{T_{op}} \int_0^{\frac{T_{res}}{2}} V_{tx} sin\omega_{res} t \; dt \tag{B-62}$$

$$\begin{aligned} &= \frac{2V_{tx}}{T_{op}} [\frac{-cos\omega_{res} t}{\omega_{res}}]_0^{\frac{T_{res}}{2}} \\ &= \frac{2V_{tx}}{T_{op}\omega_{res}} [-cos\frac{T_{res}\omega_{res}}{2} - cos\ 0] \\ &= \frac{4V_{tx}}{T_{op}\omega_{res}} \\ &= \frac{2V_{tx}}{\pi}(\frac{T_{res}}{T_{op}}) \end{aligned} \tag{B-63}$$

$\therefore At\ \omega_{op} = \omega_{res}$

$$V_{tx} = \frac{V_{in}\pi}{2} \tag{B-64}$$

B-5 Frequency domain analysis

With the help of equivalent circuit derived in Figure 5-3, one can perform the frequency domain analysis. It should be noted that, the mathematical model for $\hat{V_{ac}}$ is valid only below f_{res1}, therefore the frequency domain analysis can be performed only till f_{res1}.

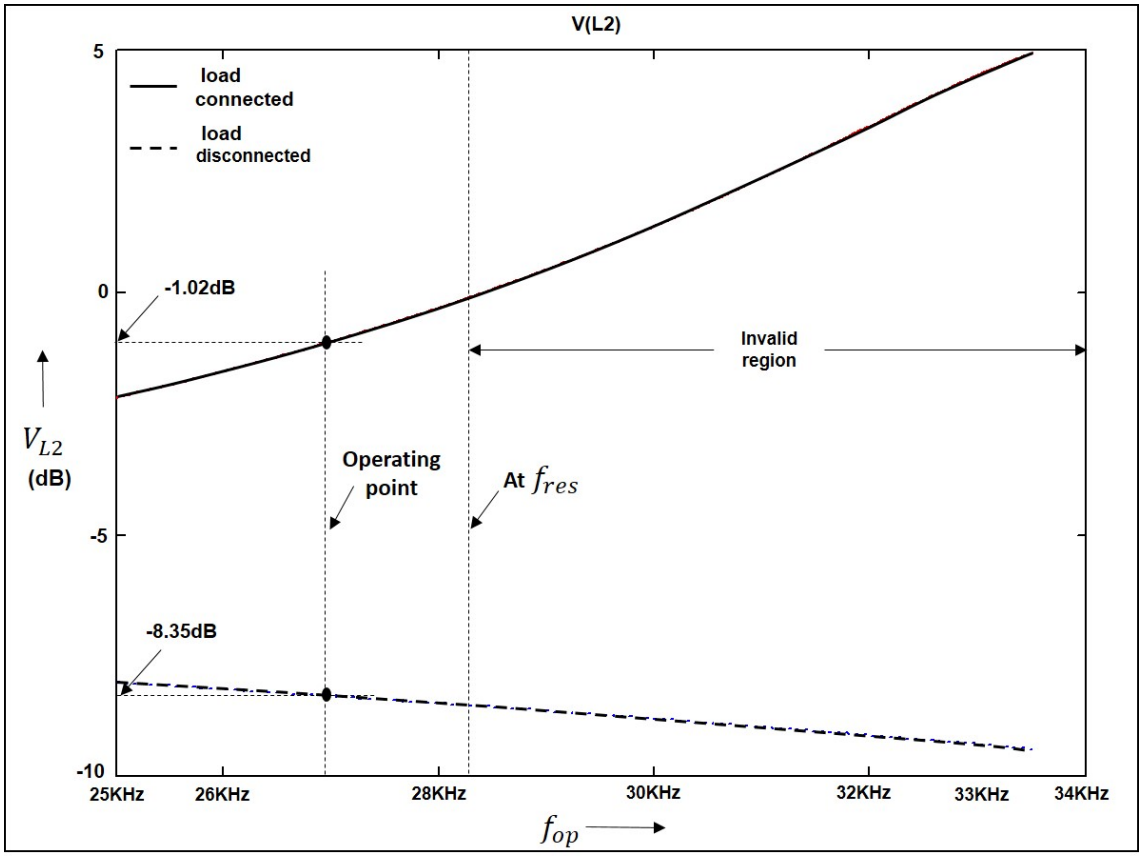

Figure B-3: Frequency domain analysis of CS parallel topology: receiver coil voltage below f_{res}

Figure B-3 shows the receiver coil voltage gain (V_{L2}) when operated below f_{res1}. As discussed in case of the series resonant topology, the load disconnection can result in severe overvoltages across the transmitter and the receiver coil. However, the behaviour of the CS parallel resonant topology on load disconnection is observed to be different. From Figure B-3 it can be observed that the receiver coil voltage decreases on the load disconnection. It implies that the transmitter acts like an inductive voltage source and offers intrinsic overvoltage protection. As explained earlier, the capacitor (C_1) does not influence the receiver coil voltage gain but it does affect the phase of the input current (I_1). Therefore, for analyzing the behaviour of the input current on load disconnection, one should take into account the transmitter capacitor (C_1). Figure B-4a shows the frequency domain analysis of the input current (I_1) when the load is connected. It can be observed that at the operating point, the phase of the input current is negative.

Figure B-4b shows the same current on load disconnection. It can be observed that the phase of the input current remains the negative. Therefore with this topology, the load disconnection

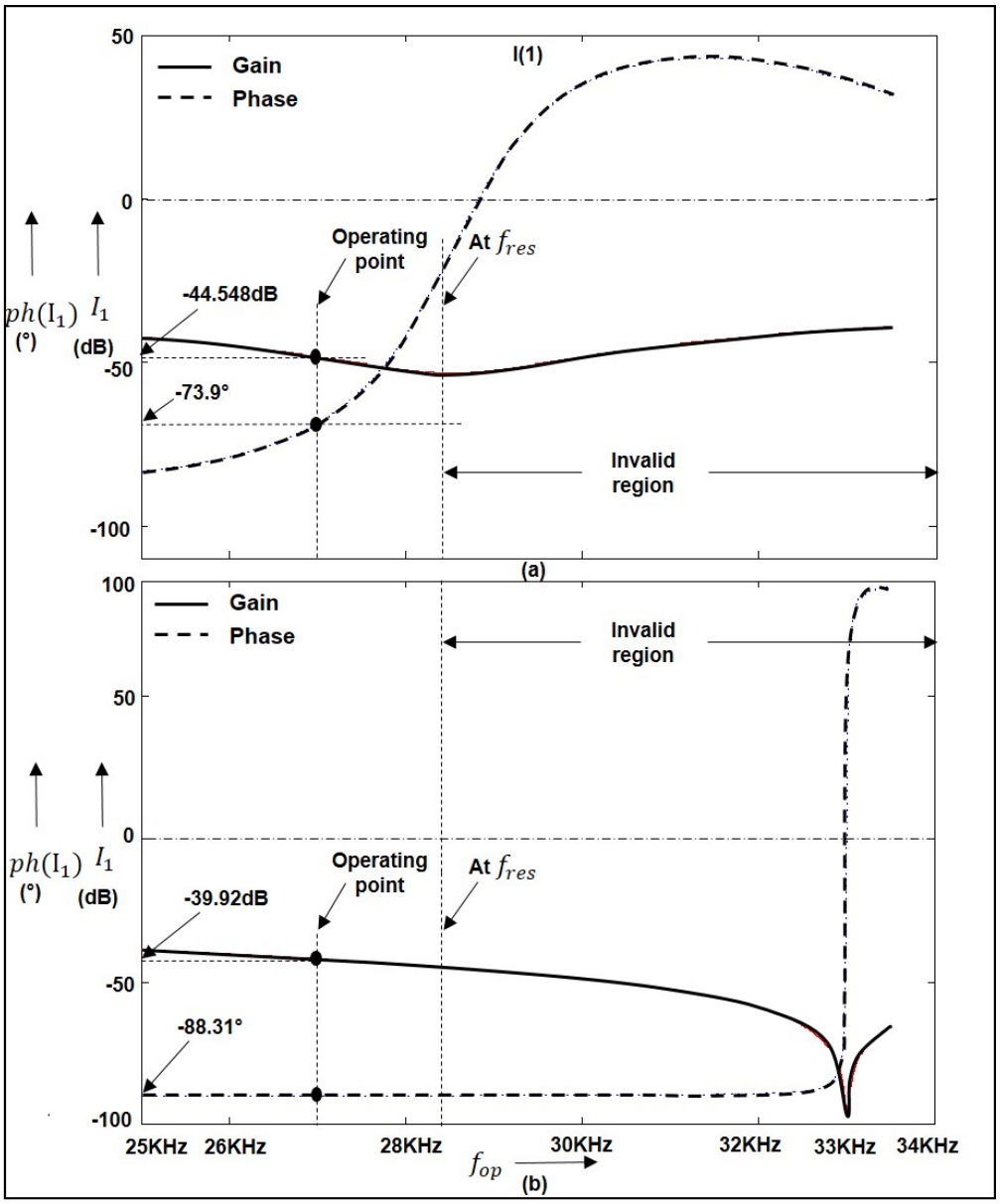

Figure B-4: Input current at f_{op}=27kHz when (a) load connected and (b) load disconnected

does not result in the capacitive mode of operation of the system. Thus, high dV/dt's and the overvoltages across the transmitter coil will not be observed. The input current will always lag the transmitter coil voltage.

Appendix C

Appendix

C-1 Mathematical model: MathCAD

To calculate the amplitude of fundamental harmonic one has to define the components:

$U := 325$ $\quad R1 := 0.01$ $\quad RL := 10$ $\quad RL1 := 1000$

$Lchoke := 1 \cdot 10^{-3}$ $\quad C2 := 80.278 \times 10^{-9}$ $\quad L2 := 2.90 \times 10^{-4}$

$f\_res := 28200$

$L1 := \dfrac{Lchoke \cdot 2 \cdot 290 \cdot 10^{-6}}{2Lchoke + 290 \cdot 10^{-6}}$ $\quad i := \sqrt{-1}$

$f\_op := 25000 25001.33500$

$t(f\_op) := \dfrac{1}{f\_op}$ $\quad C1 := \dfrac{1}{4 \cdot \pi^2 \cdot 33000^2 \cdot L1}$

$t\_res := \dfrac{1}{f\_res}$ $\quad M := 0.35\sqrt{L1 \cdot L2}$

$\omega\_res := 2 \cdot \pi \cdot f\_res$

$\omega(f\_op) := 2 \cdot \pi \cdot f\_op$

$\beta(f\_op) := \dfrac{1}{2} \cdot \left(\dfrac{\pi}{\omega(f\_op)} + \dfrac{\pi}{\omega\_res} \right)$ $\quad s(f\_op) := \omega(f\_op)\, i$

$\alpha(f\_op) := \dfrac{1}{2} \cdot \left(\dfrac{\pi}{\omega(f\_op)} - \dfrac{\pi}{\omega\_res} \right)$

$\omega\_op(f\_op) := 2 \cdot \pi \cdot f\_op$

$$Vpeak(f\_op) := \frac{U \cdot \pi \cdot \left(\dfrac{t(f\_op)}{t\_res} \right)}{2}$$

$$fundamental\ (f\_op) := -8 \frac{Vpeak(f\_op)}{t(f\_op)} \cdot \cos\left(\frac{\pi}{2} \cdot \frac{\omega(f\_op)}{\omega\_res} \right) \cdot \frac{\omega\_res}{\omega(f\_op)^2 - \omega\_res^2}$$

To observe the behaviour of the input current and its phase, when the load is connected one can use the following script:

$$Vin1(f\_op) := \frac{fundamental\ (f\_op)}{U \cdot \dfrac{\pi}{2}}$$

$$Iin(f\_op) := \frac{s(f\_op)^4 \cdot \left(L1 \cdot L2 \cdot C1 \cdot C2 - M^2 \cdot C1 \cdot C2 \right) + s(f\_op)^3 (RL \cdot L1 \cdot C1 \cdot C2 + R1 \cdot C1 \cdot C2 \cdot L2) + s(f\_op)^2 (L2 \cdot C2 + L1 \cdot C1 + R1 \cdot RL \cdot C1 \cdot C2) + s(f\_op) \cdot (RL \cdot C2 + R1 \cdot C1) + 1}{s(f\_op)^3 \left(L1 \cdot L2 \cdot C2 - M^2 \cdot C2 \right) + s(f\_op)^2 (RL \cdot L1 \cdot C2 + R1 \cdot L2 \cdot C2) + s(f\_op) \cdot (L1 + R1 \cdot RL \cdot C2) + R1} \cdot Vin1(f\_op)$$

$$x1(f\_op) := 20\log\left(\left|Iin(f\_op)\right|\right)\left|\right.$$

$$x2(f\_op) := \arg(Iin(f\_op))\cdot\frac{180}{\pi}$$

To observe the behaviour of the input current and its phase, when the load is disconnected one can use the following script:

$$Iin\_dis(f\_op) := \frac{s(f\_op)^4\cdot\left(L1\cdot L2\cdot C1\cdot C2 - M^2\cdot C1\cdot C2\right) + s(f\_op)^3(RL1\cdot L1\cdot C1\cdot C2 + R1\cdot C1\cdot C2\cdot L2) + s(f\_op)^2(L2\cdot C2 + L1\cdot C1 + R1\cdot RL1\cdot C1\cdot C2) + s(f\_op)\cdot(RL1\cdot C2 + R1\cdot C1) + 1}{s(f\_op)^3\left(L1\cdot L2\cdot C2 - M^2\cdot C2\right) + s(f\_op)^2(RL1\cdot L1\cdot C2 + R1\cdot L2\cdot C2) + s(f\_op)\cdot(L1 + R1\cdot RL1\cdot C2) + R1}\cdot Vin1(f\_op)\left|\right.$$

$$x3(f\_op) := 20\log\left(\left|Iin\_dis(f\_op)\right|\right)\left|\right.$$

$$x4(f\_op) := \arg(Iin\_dis(f\_op))\cdot\frac{180}{\pi}$$

To observe the behaviour of the receiver coil voltage, when the load is connected and disconnected one can use the following script:

$$vout(f\_op) := \frac{s(f\_op)^2\cdot RL\cdot C2\cdot M + s(f\_op)\cdot M}{s(f\_op)^3\left(L1\cdot L2\cdot C2 - M^2\cdot C2\right) + s(f\_op)^2\cdot(R1\cdot L2\cdot C2 + RL\cdot L1\cdot C2) + s(f\_op)\cdot(R1\cdot RL\cdot C2 + L1) + R1}\cdot Vin1(f\_op)\left|\right.$$

$$vout\_dis(f\_op) := \frac{s(f\_op)^2\cdot RL1\cdot C2\cdot M + s(f\_op)\cdot M}{s(f\_op)^3\left(L1\cdot L2\cdot C2 - M^2\cdot C2\right) + s(f\_op)^2\cdot(R1\cdot L2\cdot C2 + RL1\cdot L1\cdot C2) + s(f\_op)\cdot(R1\cdot RL1\cdot C2 + L1) + R1}\cdot Vin1(f\_op)\left|\right.$$

$$x(f\_op) := 20\log\left(\left|vout(f\_op)\right|\right)\left|\right.$$

$$y(f\_op) := 20\log\left(\left|vout\_dis(f\_op)\right|\right)\left|\right.$$

To observe the behaviour of RMS value, freeze time (t_{freeze}) with respect to operating frequency, one can use the following formulae:

$$\text{RMS}(\text{f\_op}) := \frac{\text{Vpeak}(\text{f\_op})}{\sqrt{2}} \cdot \sqrt{\frac{\text{f\_op}}{\text{f\_res}}} \Bigg|$$

$$\text{t\_freeze}(\text{f\_op}) := 2 \cdot \alpha(\text{f\_op}) \Big|$$

Appendix D

Appendix

D-1 Mathematical model: Python script for normalized current transfer functions

```
from __future__ import division
import matplotlib.pyplot as plt
import numpy as np
import numpy.matlib
#import control as c
from pylab import *
from cmath import *
from operator import truediv
from mpl_toolkits.mplot3d import Axes3D
R1=0.05
R2=0.05
R3=0.05
ZL=10
L1=253.275*10**-6
L2=290*10**-6
L3=290*10**-6
f_tx=33000
f_rx=33000
C1=(1/4*np.pi**2*f_tx**2*L1)
C2=(1/4*np.pi**2*f_rx**2*L2)
C3=80.278*10**-9
K=0.35
K12=0
K13=0.35
K23=0
M12=K12*(L1*L2)**0.5
M13=K13*(L1*L3)**0.5
M23=K23*(L2*L3)**0.5
omega1=1/((L1*C1)**0.5)
```

```
30 omega2=1/((L2*C2)**0.5)
31 omega3=1/((L3*C3)**0.5)
32 Q1=100
33 Q2=100
34 Q3=100
35 beta= omega2/omega1
36 #beta2 = omega2/omega1
37 beta3 = omega3/omega1
38
39 n = (L2/L1)**0.5
40 n31 = (L3/L1)**0.5
41 n32 = (L3/L2)**0.5
42 up=1
43 up_max=1
44 u=up/up_max
45 i = up_max/(omega1*L1)
46
47
48 def my_range(start, end, step):
49     while start <= end:
50         yield start
51         start += step
52 def R2P(x):
53     return abs(x), angle(x)
54 f,i1,i2,i3,Pl,Pin,Pt,eff = [],[],[],[],[],[],[],[]
55 f= np.linspace(0.1,1,200)
56 gamma =1
57 for f in my_range(0.005,1.005,0.005):
58
59         i1.append (u/(1j*f + (1/1j*f*Q1)+K**2*1j*f**3*(-f**2+beta**2+1j*f
               *beta*(1/Q2 + gamma))**-1))
60         angle(i1)
61         i2.append ((-K/n)*f**2*(-f**2+beta**2+1j*f*beta*(1/Q2 + gamma))
               **-1* (u/(1j*f + (1/1j*f*Q1)+K**2*1j*f**3*(-f**2+beta**2+1j*f*
               beta*(1/Q2 + gamma))**-1)))
62         np.absolute(i1)
63         np.absolute(i2)
64         f = np.linspace (0,1,200,endpoint=False, dtype = np.float)
65         Pl.append ((np.absolute(i2))**2*gamma*beta*n**2)
66         Pt.append (((np.absolute(i2))**2/Q2)*beta*n**2 + ((np.absolute(i2
               ))**2*gamma*beta*n**2))
67         Pin.append (((np.absolute(i1))**2/Q1) + (((np.absolute(i2))**2/Q2
               )*beta*n**2 + ((np.absolute(i2))**2*gamma*beta*n**2)))
68         eff= Pl[-1]/Pin[-1]
69 #for plotting input current
70 fig = plt.figure()
71 plt.plot(f,np.absolute(i1))
72 fig.suptitle('Input current transfer function', fontsize = 20)
73 plt.xlabel('frequency  (dimensionless)', fontsize = 10)
74 plt.ylabel('Input current (dimensionless)', fontsize = 10)
75 fig.show()
76
77 #for plotting output current
```

```
78 fig1 = plt.figure()
79 plt.plot(f,np.absolute(i2))
80 fig1.suptitle('Output current transfer function', fontsize = 20)
81 plt.xlabel('frequency (dimensionless)', fontsize = 10)
82 plt.ylabel('Output current (dimensionless)', fontsize = 10)
83 fig1.show()
84
85 #for plotting efficiency
86 fig2 = plt.figure()
87 plt.plot(f,np.absolute(eff))
88 fig2.suptitle('Efficiency variation', fontsize = 20)
89 plt.xlabel('frequency (dimensionless)', fontsize = 10)
90 plt.ylabel('Efficiency', fontsize = 10)
91 fig2.show()
92
93 #for plotting input current phase
94 fig3 = plt.figure()
95 plt.plot(f,(angle(i1)*180/(np.pi)))
96 fig3.suptitle('Phase variation', fontsize = 20)
97 plt.xlabel('frequency (dimensionless)', fontsize = 10)
98 plt.ylabel('Phase angle', fontsize = 10)
99 fig3.show()
100 plt.show()
```

Appendix E

Appendix

E-1 Schematic for the CS parallel resonant topology with buck power stage

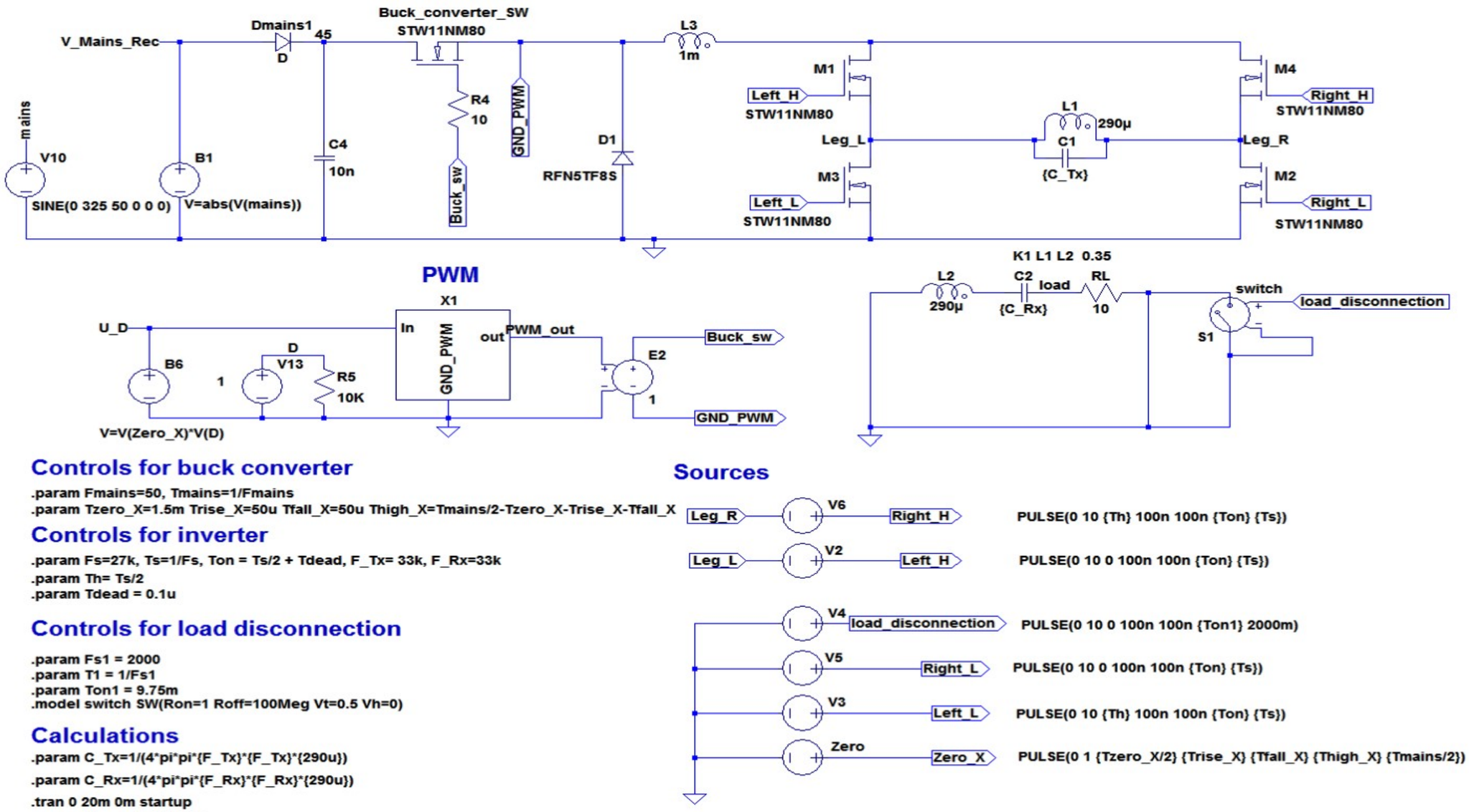

E-2 Schematic for the CS parallel resonant topology with advanced control buck power stage

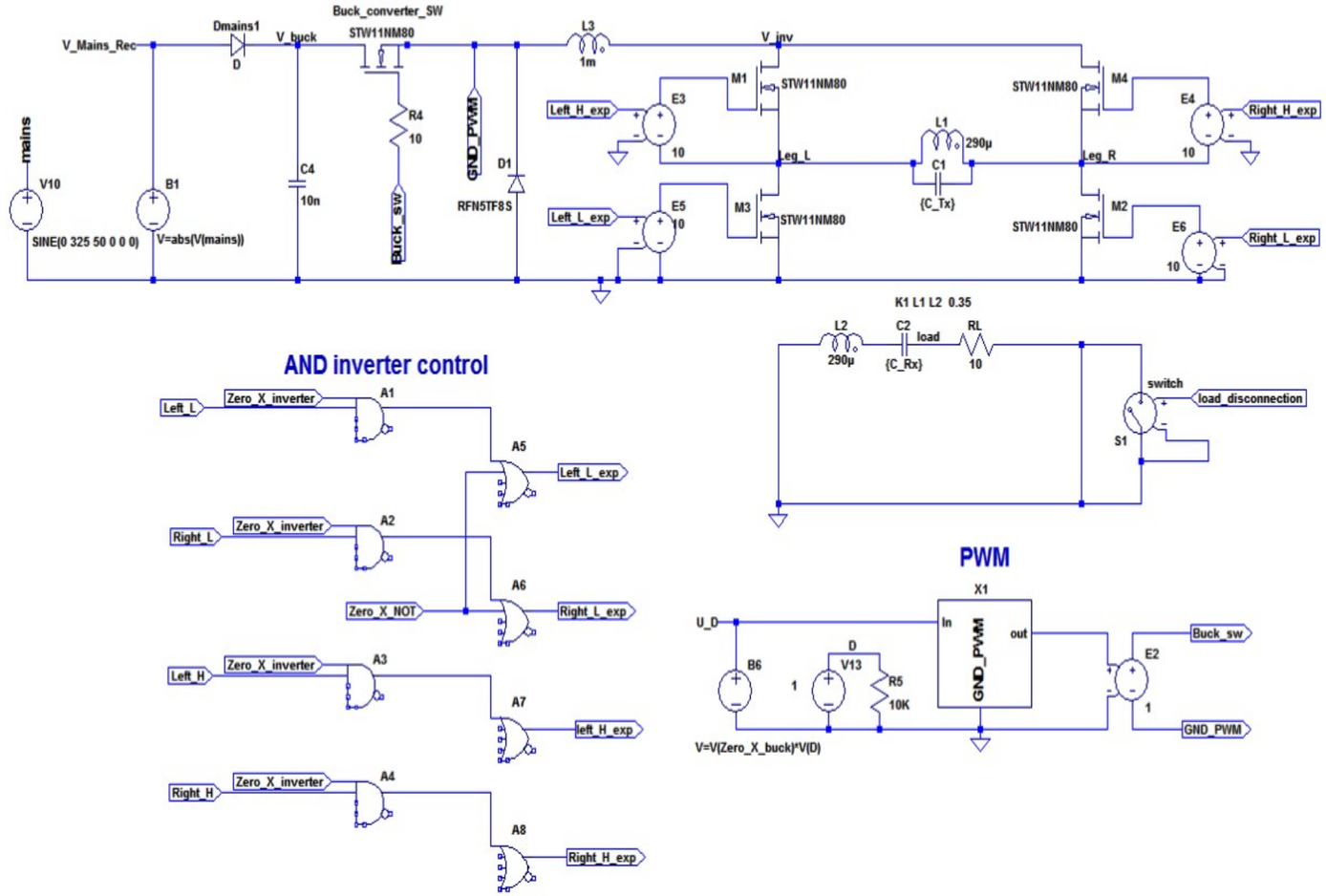

Controls for buck converter

.param Fmains=50, Tmains=1/Fmains

.param Tzero_X=1.5m Trise_X=0.25m Tfall_X=0.25m Thigh_X=Tmains/2-Tzero_X-Trise_X-Tfall_X-1.5m

.param Thigh_X_not=Tmains/2-Tzero_X/2-Trise_X_not-Tfall_X_not

.param Trise_X_not=1u Tfall_X_not=1u

Controls for inverter

.param Fs=28.2k, Ts=1/Fs, Ton=Ts/2+Tdead, F_Tx=33k F_Rx =33k

.param Th= Ts/2

.param Tdead=0.1u

.param Trise_X1=0.01m Tfall_X1=0.25m Thigh_X1=Tmains/2-Tzero_X-Trise_X1-Tfall_X1

Controls for load disconnection

.param Fs1 = 2000

.param T1 = 1/Fs1

.param Ton1=6.75m

.model switch SW(Ron=1 Roff=100Meg Vt=0.5 Vh=0)

Calculations

.param C_Tx=1/(4*pi*pi*{F_Tx}*{F_Tx}*{253.275u})

.param C_Rx=1/(4*pi*pi*{F_Rx}*{F_Rx}*{290u})

.param Phaseshift=(Ts/2)

.tran 0 20m 0m startup

Sources

V6 Right_H PULSE(0 10 {Th} 100n 100n {Ton} {Ts})

V2 Left_H PULSE(0 10 0 100n 100n {Ton} {Ts})

V4 load_disconnection PULSE(0 10 0 100n 100n {Ton1} 2000m)

V5 Right_L PULSE(0 10 0 100n 100n {Ton} {Ts})

V3 Left_L PULSE(0 10 {Th} 100n 100n {Ton} {Ts})

Zero_X_buck Zero_X_buck PULSE(0 1 {Tzero_X/2} {Trise_X} {Tfall_X} {Thigh_X} {Tmains/2})

Zero_opposite Zero_X_NOT PULSE(1 0 1u {Trise_X_not} {Tfall_X_not} {Thigh_X_not} {Tmains/2})

Zero_X_inverter Zero_X_inverter PULSE(0 1 {Tzero_X/2} {Trise_X1} {Tfall_X1} {Thigh_X1} {Tmains/2})

Bibliography

[1] R.Steigerwald, "A comparison of half-bridge resonant converter topologies", *IEEE Transactions on Power Electronics*, vol. 3, no. 2, pp. 174-182, 1988.

[2] Philips Consumer Lifestyle B.V., "Mathematical modeling of cordless kitchen appliances", unpublished.

[3] Philips Consumer Lifestyle B.V., "Tunable wireless Power Transmitter", unpublished.

[4] Philips Consumer Lifestyle B.V., "Reduction of mains harmonic distortion for wireless kitchen appliances", unpublished.

[5] Philips Consumer Lifestyle B.V., "Cordless power transmission: Feasibility and applicability study of the repeater coil", unpublished.

[6] Philips Consumer Lifestyle B.V., "Cordless kitchen: inductive power sources", unpublished.

[7] D. Voglitsis, "3-Coil Configuration Analysis", Master's Thesis, Delft University of Technology, 2017.

[8] Power Electronics: Converters, Applications and Design, 1st ed. John Wiley and Sons, Inc., 1989, pp. 154-197.

[9] M. Kazimierczuk and D. Czarkowski, Resonant Power converters, 1st ed. John Wiley and Sons, Inc., 1995.

[10] Philips Consumer Lifestyle B.V., "EMI emission reduction for Large & Medium Z transmitters", unpublished.

[11] [Online]. Available: https://www.wirelesspowerconsortium.com/data/images/2/1/figure5.jpg. [Accessed: 17- Jul- 2017].

[12] [Online]. Available: http://www.farnell.com/datasheets/1736772.pdf. [Accessed: 17- Jul- 2017].

[13] Philips Consumer Lifestyle B.V., "EMC of Qi large-z transmitter", unpublished.

[14] [Online]. Available: http://doc.lijun.li/analog-scaling.html. [Accessed: 17- Jul- 2017].

Glossary

Table E-1: List of abbreviations and symbols

EMI	Electromagnetic Interference
ZVS	Zero Voltage Switching
WPC	Wireless Power Consortium
NFC	Near Field Communication
IPT	Inductive Power Transfer
IH	Induction Heating
Tx	Transmitter
Rx	Receiver
TDM	Time Division Multiplexing
VS	Voltage Source
CS	Current Source
FHA	First Harmonic Approximation
PWM	Pulse Width Modulation
EMF	Electromotive Force
f_{tx}	Natural resonant frequency of the transmitter
f_{rx}	Natural resonant frequency of the receiver
f_{res}	Natural resonant frequency of the whole system
f_{op}	Operating frequency of the transmitter inverter stage